Analysis and Order Reduction of an Autonomous Lunar Lander Navigation System

by

Clark Patrick Newman, B.S.

THESIS

Presented to the Faculty of the Graduate School of

The University of Texas at Austin

in Partial Fulfillment

of the Requirements

for the Degree of

MASTER OF SCIENCE IN ENGINEERING

THE UNIVERSITY OF TEXAS AT AUSTIN

August 2009

Analysis and Order Reduction of an Autonomous Lunar Lander Navigation System

APPROVED BY

SUPERVISING COMMITTEE:

Robert H. Bishop, Supervisor

Maruthi R. Akella

Dedicated to my mother and father.

Acknowledgments

I would like to thank everyone in general who helped me accomplish this task. I would like to thank my advisor, Dr. Robert Bishop, for giving me the opportunity to enter graduate studies within his organization. I would like to thank Kyle J. DeMars for his assistance throughout my studies, his input has been invaluable and has made my studies possible. I would also like to thank the organization and donor behind the Thrust 2000 Graduate Fellowship in the College of Engineering. Their financial support of me has allowed me to focus on my studies, and their gifts will continue to assist me beyond my graduate studies.

Analysis and Order Reduction of an Autonomous Lunar Lander Navigation System

Clark Patrick Newman, M.S.E.
The University of Texas at Austin, 2009

Supervisor: Robert H. Bishop

A navigation system for precision lunar descent and landing is presented and analyzed. The navigation algorithm is based upon the extended Kalman Filter and employs measurements from an inertial measurement unit to propagate the vehicle's position, velocity, and attitude forward in time. External measurements from an altimeter, star camera, terrain camera, and velocimeter are utilized in state estimate updates. The navigation algorithm also attempts to estimate the values of corrupting parameters which introduce errors into the measurements from the preceding instruments. Finally, the navigation algorithm estimates the map-tie angle of the landing site, which is a measure of the misalignment of the actual landing site location on the surface of the Moon versus the estimated position of the landing site.

The navigation algorithm is subject to a sensitivity analysis which investigates the contribution of each error source to the total estimation performance of the navigation system. Per the results of the sensitivity analysis, it

is found that certain error sources need not be actively estimated to achieve similar estimation performance at a reduced computational burden. A new, reduced-order system is presented and tested through covariance analysis and a monte carlo analysis. The new system is shown to have comparable estimation performance at a fraction of the computer run-time, making it more suitable for a real-time implementation.

Table of Contents

List of Tables

List of Figures

Chapter 1

Introduction

1.1 Motivation

It is published upon the website of the National Air and Space Administration (NASA) that "[at] the core of NASA's future space exploration is a return to the moon, where we will build a sustainable long term human presence." [1] As an essential component of that mission statement, it will be necessary to again land on the moon as it had been done in the Apollo days of the 1960's and 1970's. Computer technology has advanced to the point now that the guidance, navigation, and control of the lunar lander system will require minimal human input for a successful descent-to-landing execution. This thesis will address the navigation algorithm for lunar landing. To successfully execute a descent-to-landing task, the lunar lander system will need to be able to discern its physical state over the Moon, so that it may execute the proper maneuvers required to bring the system safely to the surface so that it may deliver robotics, supplies, or human astronauts.

The navigation system to be investigated is built around the extended Kalman filter (EKF), which is the de-facto standard for space-borne navigation. The EKF fuses measurements from various sensor sources to return an

estimated state of the vehicle and an associated estimation error covariance, which may be interpreted as the level of certainty of that state estimate. The EKF requires a mathematical model of i) the environment in which the system is operating, ii) the sensor measurements and iii) the sensitivity of the sensor measurement to deviations of the system state. The EKF is derived and analyzed in detail in Gelb [2], Maybeck [14], Tapley [3], Crassidis and Junkins [4] and many other publications.

The design flow of a navigation is presented in Fig. 1.1. The design begins (as written in the upper left corner of the diagram) with the definitions of the dynamical systems and definitions of the sensor models. These models are framed around an extended Kalman filter with all the relevant states and uncertainty parameters being actively estimated to produce a comprehensive navigation filter design. The comprehensive filter design for the lunar landing problem is tuned and proven through monte carlo analysis. The monte carlo analysis which proves that the system is properly tuned is performed by DeMars [9]. With the tuned comprehensive navigation system at our disposal, we create an error budget to catalog the estimation performance as contributions from error groups. A sensitivity analysis is then performed, to quantify the expected impact on the state estimation error as a result of off-nominal values of the various error groups. The error budget and sensitivity analysis is outlined in Demars and Bishop [8]. The sensitivity analysis results will show that while an off-nominal value of some error sources will result in a great increase in estimation error (for example, an inflated initial uncertainty of velocity will

likely result in greater estimation error of position during the navigation simulation), there are error sources which do not contribute significantly to the estimation errors of the navigation system. These insensitive states need not be actively estimated by the navigation algorithm and their removal should not result in increased estimation error. This thesis will focus on developing a reduced-order navigation algorithm based on the comprehensive EKF presented by DeMars and Bishop [9]. The state reduction and re-tuning of the navigation system and a comparison of the estimation and computation performance of the reduced order system to the comprehensive system will show that a more computationally tractable solution exists with approximately the same state estimation performance.

Should the new system prove to be accurate and its computational burden is considered significantly less, it serves as a basis for the actual navigation algorithm to support lunar landing.

1.2 Organization

The navigation system dynamical model is described in Chapter 2. The linear acceleration is derived, and the vehicular angular velocity is derived. The accelerometer and gyroscope measurement models are found, and the error between the interpreted measurements and the true acceleration/angular velocity are found. The landing site location dynamics are described, and the pertinent reference frames of the navigation system are described. In Chapter 3, the navigation algorithm is derived, as well as the external sensor mathe-

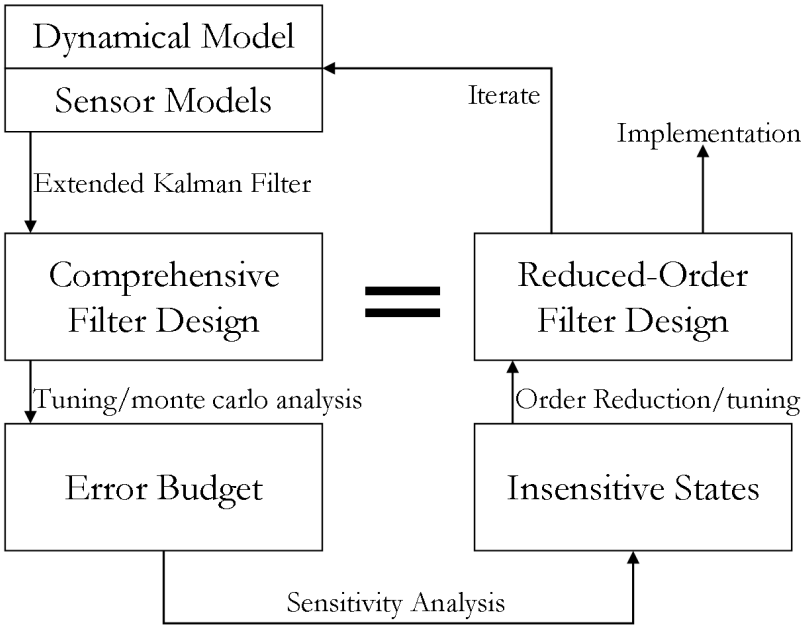

Figure 1.1: Design flow of the navigation algorithm

matical models. The EKF algorithm is derived, and the sensor measurement values are described. The sensitivity of the external sensor measurement values to deviations in the state are found, and the mathematical aids which create a more robust system are derived. Chapter 4 deals with the sensitivity analysis of the navigation system and subsequent model order reduction. The components of the navigation system which are found to not contribute to the estimation performance of the navigation system are removed, and the new system is described and re-tuned. A monte-carlo analysis of both the comprehensive system and the reduced-order system is executed and the results are compared for estimation performance and computation run-time. Recommendations are then made for further refinement of the design of the navigation

system. Finally, some mathematical notations used within the thesis are described in Appendix A.

Chapter 2

Dynamics Model

The navigation system requires a detailed dynamics mathematical model to accurately interpret the measurements from the accelerometer and gyroscope package within the inertial measurement unit (IMU). The translational and rotational dynamics of the spacecraft are derived, and the model which returns the non-gravitational acceleration and vehicle angular velocity are found. The IMU is corrupted by sensor noise and manufacturing imperfections, which results in an error between the interpreted non-gravitational acceleration or angular velocity and the true vehicular non-gravitational acceleration and angular velocity. The dynamics of the IMU are explored, as they are used in propagating the uncertainty of the spacecraft state estimate. Also of interest is the modeling of the location of the landing site which is corrupted by a map-tie error.

2.1 Reference Frames

It is important to first discuss the different reference frames and their respective importance to the system and simulation. There are five general reference frames utilized in the simulation: the celestial inertial frame, the

celestial planet-fixed frame, the vehicle body frame, and sensor/case reference frames. Table 2.1 lists the reference frames used in the simulation and their designations.

Table 2.1: Reference Frame Designations

Designation	Description
i	celestial inertial frame
f	celestial planet-fixed frame
b	vehicle body frame
c	IMU case frame
v	velocimeter frame
sc	star camera frame
tc	terrain camera frame

The celestial inertial frame is the J2000 reference frame with its origin anchored at the center of mass of the planet. It is fixed for all time and is used as the navigation reference frame.

The planet-fixed reference frame is anchored at the center of the planet and rotates about its z-axis (which is defined to be colinear with the inertial frame z-axis) to remain fixed to the planet. The fixed-to-inertial transformation matrix takes the form

$$\mathbf{T}_f^i = \begin{bmatrix} \cos\omega_{L,z}\Delta t & \sin\omega_{L,z}\Delta t & 0 \\ -\sin\omega_{L,z}\Delta t & \cos\omega_{L,z}\Delta t & 0 \\ 0 & 0 & 1 \end{bmatrix}, \tag{2.1}$$

where $\omega_{L,z}$ is the angular velocity of the Moon, and has the value $\omega_{L,z} = 2.661695727807125 \times 10^{-6}\,[\text{rad}]\,[\text{s}]^{-1}$. The term Δt is the time span from the initial time t_0 to the current time t.

The vehicle body reference frame is fixed to the vehicle. The axes of the vehicle body reference frame lie along the structure of the spacecraft so that each axis points along the roll, pitch, and yaw directions. It is defined by the inertial-to-body quaternion of rotation, given by

$$\bar{\mathbf{q}} = \begin{bmatrix} q \\ \mathbf{q} \end{bmatrix} = \begin{bmatrix} \sin\frac{\theta}{2}\mathbf{e} \\ \cos\frac{\theta}{2} \end{bmatrix}. \tag{2.2}$$

where θ is the angle of rotation, and $\mathbf{e} \in \Re^{3\times 1}$ is the axis of rotation. More information on quaternion mathematics may be found in Appendix A.2.

Each sensor has its respective sensor reference frame which is fixed to the sensor. For each sensor reference frame, the $+z$-axis points along the line-of-sight of the sensor, while the x- and y- axes define the perpendicular plane to the sensor boresight and complete the orthonormal triad which defines the sensor reference frame. This orientation is defined by a body-to-sensor rotation quaternion. In Fig. 2.1, the axes which define the vehicle body reference frame, and a set of axes which define a sensor reference frame are depicted. The position and orientation of each sensor reference frame with respect to the body reference frame is fixed and assumed to be perfectly known through preflight calibration.

2.2 Translational Dynamics

The translational dynamics would naturally describe the motion of the center-of-gravity (CG) of the vehicle. However, the non-gravitational accelerations are measured by the IMU which is (generally) not located at the CG.

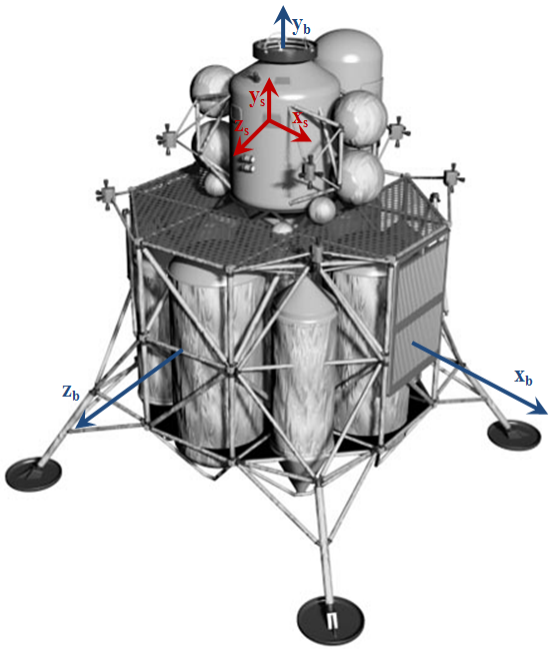

Figure 2.1: Body and sensor coordinate frames fixed to the Altair Lunar Lander

We will argue that the best navigation performance with simplest computational complexity is achieved when the navigation system utilizes equations of motion describing the position of the IMU rather than the position of the CG. The position of the IMU can thus be represented as

$$\mathbf{r}_{imu} = \mathbf{r}_{cg} + \mathbf{r}_{imu/cg}\,. \tag{2.3}$$

The translational dynamics as described at the IMU can be shown to be [9]

$$\mathbf{a}_{imu} = \mathbf{a}_g(\mathbf{r}_{cg}) + \mathbf{a}_{ng} \tag{2.4}$$

where $\mathbf{a}_g(\mathbf{r}_{cg})$ is the gravitational acceleration and is a function of the CG alone and $\mathbf{a}_{ng}$ is the non-gravitational acceleration, which is

$$\begin{aligned}\mathbf{a}_{ng} = \mathbf{a}_{cg,nc} + \mathbf{a}_{imu/cg} + 2\boldsymbol{\omega} \times \mathbf{v}_{imu/cg} \\ + \dot{\boldsymbol{\omega}} \times \mathbf{r}_{imu/cg} + \boldsymbol{\omega} \times (\boldsymbol{\omega} \times \mathbf{r}_{imu/cg}) \,.\end{aligned} \tag{2.5}$$

In Eq. (2.5), $\mathbf{a}_{cg,nc}$ is the non-conservative acceleration at the CG, $\mathbf{a}_{imu/cg}$ is the acceleration of the IMU with respect to the CG, $\boldsymbol{\omega}$ is the angular velocity of the vehicle, $\mathbf{v}_{imu/cg}$ is the velocity of the IMU with respect to the CG, $\dot{\boldsymbol{\omega}}$ is the angular acceleration of the vehicle, and $\mathbf{r}_{imu/cg}$ is the position of the IMU with respect to the CG. The gravitational acceleration is a function of the position of the CG, which is given by Eq. (2.3). Conversely, the translational acceleration of the CG can be shown to be represented by [9]

$$\begin{aligned}\mathbf{a}_{cg} = \mathbf{a}_g + \mathbf{a}_{ng} - \mathbf{a}_{imu/cg} - 2\boldsymbol{\omega} \times \mathbf{v}_{imu/cg} \\ - \dot{\boldsymbol{\omega}} \times \mathbf{r}_{imu/cg} - \boldsymbol{\omega} \times (\boldsymbol{\omega} \times \mathbf{r}_{imu/cg}) \,.\end{aligned} \tag{2.6}$$

Knowledge of the position of the CG with respect to the IMU is required in both circumstances in Eq. (2.4) and Eq. (2.6). The position of the CG with respect to the IMU can be modeled as

$$\mathbf{r}_{cg} = \mathbf{r}_{imu} - \mathbf{r}^{o}_{cg/imu} + \Delta\mathbf{r}_{cg/imu} \,, \tag{2.7}$$

where $\mathbf{r}^{o}_{cg/imu}$ is the nominal position of the IMU with respect to the CG, and $\Delta\mathbf{r}_{cg_imu}$ is the displacement of the position of the CG with respect to the IMU. The displacement of the CG can be the result of fuel depletion or slosh during the duration of the mission and is modeled as a zero-mean Gaussian distributed random constant with

$$\mathrm{E}\left\{\Delta\mathbf{r}_{cg/imu}\right\} = 0 \qquad \text{and} \qquad \mathrm{E}\left\{\Delta\mathbf{r}_{cg/imu}\Delta\mathbf{r}^{\mathrm{T}}_{cg/imu}\right\} = \mathbf{P}_{\Delta\mathbf{r}}$$

If we analyze the dynamics of the CG we will find that its formulation leads to possibly compounding integration errors. The center of gravity and IMU are moving very slowly with respect to each other, so the $\mathbf{a}_{imu/cg}$ term may be neglected, as well as the $\mathbf{v}_{imu/cg}$ term. The time rate of change of the angular velocity and the position of the IMU with respect to the CG however are not negligible and must be considered for further analysis. The angular acceleration is not directly measured, and must be found through numerical differentiation of the angular velocity, which can lead to erroneous values, especially during periods of highly non-linear actions affecting the angular velocity such as vehicle maneuvers. Secondly, the position of the IMU with respect to the CG in Eq. (2.7) contains the unknown displacement of the IMU. Uncertainty in the position of the IMU with respect to the CG will further compound integration errors from angular velocity and angular acceleration.

Due to the increased propensity for compounding unwanted integration errors, that we choose to evaluate the translational dynamics of the vehicle at the location of the IMU.

2.2.1 Gravity Model

The gravity model can take one of many configurations, ranging from simplistic and easily implemented to complex and computationally intensive but with higher fidelity of results. The three major choices when determining a gravity model are point-mass gravitating body, spherical harmonics represented gravity field, and a numerical gravity map interpolated from a map.

Here, a point-mass gravity approach is taken. The gravitational potential under this model is

$$U = \frac{\mu}{r}\,,$$

where μ is the gravitational parameter of the body in question and r is the is the distance between the vehicle CG and the center of the gravitating body. For the Moon, the gravitational parameter is $\mu = 4902.8 \times 10^9\,[\mathrm{m}^3/\mathrm{s}^2]$. From this, the gravitational acceleration is thus given by

$$\mathbf{a}_g = -\frac{\mu}{r^3}\mathbf{r}\,. \tag{2.8}$$

Also of interest is the gravity gradient matrix which is the second spatial derivative of the gravitational potential. For a point-mass gravitating body, the gravity gradient matrix is found to be [3, 11, 15]

$$\mathbf{G} = \frac{\mu}{r^5}\left(3\mathbf{r}\mathbf{r}^{\mathrm{T}} - r^2\mathbf{I}^{3\times 3}\right)\,. \tag{2.9}$$

The gravity gradient matrix is used in the propagation of the state estimate error covariance, specifically in the integration of the state estimate error equations, discussed in Section 2.6.

2.3 Rotational Dynamics

The rotational dynamics presented in this section describe the equations of motion involving rotation through the use of rotation quaternions. More information about quaternion mathematics and usefulness is presented in Appendix A. Recall that the quaternion of rotation includes an angle of

rotation (θ) and an axis of rotation ($\mathbf{e}$) to describe the rotation as [16]

$$\bar{\mathbf{q}} = \begin{bmatrix} q \\ \mathbf{q} \end{bmatrix} = \begin{bmatrix} \cos\frac{\theta}{2} \\ \sin\frac{\theta}{2}\mathbf{e} \end{bmatrix} . \tag{2.10}$$

The time rate of change of the quaternion is thus

$$\dot{\bar{\mathbf{q}}} = \begin{bmatrix} -\frac{1}{2}\sin\frac{\theta}{2}\dot{\theta} \\ \frac{1}{2}\cos\frac{\theta}{2}\mathbf{e}\dot{\theta} + \sin\frac{\theta}{2}\dot{\mathbf{e}} \end{bmatrix} . \tag{2.11}$$

The time rate of change of the axis of rotation and the time rate of change of the rotation angle may be found to be [12]

$$\begin{aligned} \dot{\mathbf{e}} &= \frac{1}{2}\left[[\mathbf{e}\times] - \cot\frac{\theta}{2}[\mathbf{e}\times]^2\right]\boldsymbol{\omega} \\ \dot{\theta} &= \mathbf{e}^{\mathrm{T}}\boldsymbol{\omega} . \end{aligned} \tag{2.12}$$

Substituting Eq. (2.12) into the time rate of change of the quaternion in Eq. (2.11) yields

$$\dot{\bar{\mathbf{q}}} = \frac{1}{2}\begin{bmatrix} -\sin\frac{\theta}{2}\mathbf{e}^{\mathrm{T}} \\ \left[\sin\frac{\theta}{2}[\mathbf{e}\times] + \cos\frac{\theta}{2}[\mathbf{e}\mathbf{e}^{\mathrm{T}} - [\mathbf{e}\times]^2]\right] \end{bmatrix}\boldsymbol{\omega} . \tag{2.13}$$

We can further reduce Eq. (2.13) by utilizing the relationship

$$\mathbf{e}\mathbf{e}^{\mathrm{T}} - [\mathbf{e}\times]^2 = \mathbf{I}^{3\times 3} ,$$

and substituting the definition of the quaternion elements in Eq. (2.10) so that the time derivative of the quaternion reduces to

$$\dot{\bar{\mathbf{q}}} = \frac{1}{2}\begin{bmatrix} -\boldsymbol{\omega}^{\mathrm{T}}\mathbf{q} \\ q\boldsymbol{\omega} - \boldsymbol{\omega}\times\mathbf{q} \end{bmatrix} , \tag{2.14}$$

or

$$\dot{\bar{\mathbf{q}}} = \frac{1}{2}\begin{bmatrix} 0 \\ \boldsymbol{\omega} \end{bmatrix} \otimes \begin{bmatrix} q \\ \mathbf{q} \end{bmatrix} .$$

Alternatively, we may define a pure quaternion

$$\bar{\boldsymbol{\omega}} = \begin{bmatrix} 0 \\ \boldsymbol{\omega} \end{bmatrix},$$

so that we can write the quaternion dynamics equation in Eq. (2.14) as

$$\dot{\bar{\mathbf{q}}} = \frac{1}{2}\bar{\boldsymbol{\omega}} \otimes \bar{\mathbf{q}}\,. \tag{2.15}$$

2.4 Inertial Measurement Unit Modeling

An inertial measurement unit is typically comprised of an orthogonal triad of accelerometers to measure non-gravitational accelerations, as well as an orthogonal triad of gyroscopes to measure the rotation rate of the vehicle. In most contemporary space-based missions, the IMU is "strapped down" to the body of the vehicle so that it is necessary to consider its orientation both with respect to the vehicle, and the vehicle orientation with respect to inertial space in order to successfully interpret the measurements from the IMU. [11] The alternative to fixing the IMU to the vehicle is to suspend it within a control moment gyro (CMG) to attempt to fix the IMU in inertial space. However, there are issues with suspending the IMU (errors introduced by the time-varying orientation of the CMG, vibrations introduced by the CMG itself, etc.) that make it no longer the method of choice.

2.4.1 Accelerometer Model

The accelerometers measure non-gravitational linear acceleration in three orthogonal axes. The triad of accelerometers in the IMU package are

corrupted by misalignment and non-orthogonality errors. Each accelerometer is also subject to a random bias and scale factor errors, so that for every axis these error sources can be represented by the vectors $\mathbf{b}_a$ and $\mathbf{s}_a$, respectively. We can thus write the measured acceleration $\mathbf{a}_{ng,m}$ in terms of the actual non-gravitational acceleration $\mathbf{a}_{ng}$ as [5, 17]

$$\mathbf{a}_{ng,m} = (\mathbf{I}^{3\times3} + \mathbf{\Gamma}_a)(\mathbf{I}^{3\times3} + \mathbf{S}_a)(\mathbf{a}_{ng} + \mathbf{b}_a + \boldsymbol{\eta}_a)\,,$$

where $\mathbf{\Gamma}_a$ and $\mathbf{S}_a$ are the nonorthogonality/misalignment parameters and scale factor error in matrix form

$$\mathbf{\Gamma}_a = \begin{bmatrix} 0 & \gamma_{a,xz} & -\gamma_{a,xy} \\ -\gamma_{a,yz} & 0 & \gamma_{a,yx} \\ \gamma_{a,zy} & -\gamma_{a,zx} & 0 \end{bmatrix} \quad \text{and} \quad \mathbf{S}_a = \begin{bmatrix} s_{a,x} & 0 & 0 \\ 0 & s_{a,y} & 0 \\ 0 & 0 & s_{a,z} \end{bmatrix},$$

$\boldsymbol{\eta}_a$ is the accelerometer measurement noise modeled as a zero-mean Gaussian distributed white noise process with covariance

$$\mathrm{E}\left\{\boldsymbol{\eta}_a(t)\boldsymbol{\eta}_a^{\mathrm{T}}(\tau)\right\} = \mathbf{Q}_a\delta(t-\tau)\,,$$

and $\mathbf{b}_a$ is the random bias modeled as a zero-mean Gaussian distributed random constant with

$$\mathrm{E}\left\{\mathbf{b}_a\right\} = \mathbf{0}^{3\times1} \qquad \text{and} \qquad \mathrm{E}\left\{\mathbf{b}_a\mathbf{b}_a^{\mathrm{T}}\right\} = \mathbf{P}_{b_a}$$

We make the approximation
$(\mathbf{I}^{3\times3} + \mathbf{\Gamma}_a)(\mathbf{I}^{3\times3} + \mathbf{S}_a) \approx \mathbf{I}^{3\times3} + \mathbf{\Delta}_a$, where $\mathbf{\Delta}_a = \mathbf{\Gamma}_a + \mathbf{S}_a$ so that the measured non-gravitational acceleration is approximately

$$\mathbf{a}_{ng,m} = (\mathbf{I}^{3\times3} + \mathbf{\Delta}_a)(\mathbf{a}_{ng} + \mathbf{b}_a + \boldsymbol{\eta}_a)\,.$$

We invoke the Matrix Inversion Lemma so that (to first order in $\mathbf{\Delta}_a$) we have [13]

$$(\mathbf{I}^{3\times 3} + \mathbf{\Delta}_a)^{-1} \approx \mathbf{I}^{3\times 3} - \mathbf{\Delta}_a \,.$$

The non-gravitational acceleration is given by

$$\mathbf{a}_{ng} \approx (\mathbf{I}^{3\times 3} - \mathbf{\Delta}_a)\mathbf{a}_{ng,m} - \mathbf{b}_a - \boldsymbol{\eta}_a \,. \tag{2.16}$$

Noting that $\mathbf{\Delta}_a = \mathbf{\Gamma}_a + \mathbf{S}_a$, we have

$$\mathbf{a}_{ng} = \mathbf{a}_{ng,m} - \mathbf{N}(\mathbf{a}_{ng,m})\boldsymbol{\gamma}_a - \mathbf{D}(\mathbf{a}_{ng,m})\mathbf{s}_a - \mathbf{b}_a - \boldsymbol{\eta}_a \,, \tag{2.17}$$

where the matrices $\mathbf{N}(\mathbf{a}_{ng,m})$ and $\mathbf{D}(\mathbf{a}_{ng,m})$ are

$$\mathbf{N}(\mathbf{a}_{ng,m}) = \begin{bmatrix} -a_{ng,m,z} & a_{ng,m,y} & 0 & 0 & 0 & 0 \\ 0 & 0 & a_{ng,m,z} & -a_{ng,m,x} & 0 & 0 \\ 0 & 0 & 0 & 0 & -a_{ng,m,y} & a_{ng,m,x} \end{bmatrix}$$

$$\mathbf{D}(\mathbf{a}_{ng,m}) = \begin{bmatrix} a_{ng,m,x} & 0 & 0 \\ 0 & a_{ng,m,y} & 0 \\ 0 & 0 & a_{ng,m,z} \end{bmatrix},$$

and the nonorthogonality/misalignment parameter vector $\boldsymbol{\gamma}_a$ and scale factor error vector $\mathbf{s}_a$ both take the form

$$\boldsymbol{\gamma}_a = \begin{bmatrix} \gamma_{a,xy} \\ \gamma_{a,xz} \\ \gamma_{a,yx} \\ \gamma_{a,yz} \\ \gamma_{a,zx} \\ \gamma_{a,zy} \end{bmatrix} \quad \text{and} \quad \mathbf{s}_a = \begin{bmatrix} s_{a,x} \\ s_{a,y} \\ s_{a,z} \end{bmatrix},$$

where both vectors are modeled as zero-mean Gaussian distributed random constants with

$$\begin{aligned} \mathrm{E}\left\{\boldsymbol{\gamma}_a\right\} &= \mathbf{0}^{6\times 1} \\ \mathrm{E}\left\{\mathbf{s}_a\right\} &= \mathbf{0}^{3\times 1} \\ \mathrm{E}\left\{\boldsymbol{\gamma}_a \boldsymbol{\gamma}_a^{\mathrm{T}}\right\} &= \mathbf{P}_{\gamma_a} \\ \mathrm{E}\left\{\mathbf{s}_a \mathbf{s}_a^{\mathrm{T}}\right\} &= \mathbf{P}_{s_a} \end{aligned}$$

2.4.2 Gyroscope Model

The gyroscope model is very similar in form to the accelerometer model. The triad of gyroscopes is corrupted by random and systematic errors, including axes misalignment and non-orthogonality, bias and measurement noise. The measured rotation rate $\boldsymbol{\omega}_m$ in terms of the true rotation rate $\boldsymbol{\omega}$ and modeled error sources is [5, 17]

$$\boldsymbol{\omega}_m = (\mathbf{I}^{3\times 3} + \boldsymbol{\Gamma}_g)(\mathbf{I}^{3\times 3} + \mathbf{S}_g)(\boldsymbol{\omega} + \mathbf{b}_g + \boldsymbol{\eta}_g)\,, \tag{2.18}$$

where $\boldsymbol{\eta}_g$ is a zero-mean white noise process with covariance

$$\mathrm{E}\left\{\boldsymbol{\eta}_g(t)\boldsymbol{\eta}_g^{\mathrm{T}}(\tau)\right\} = \mathbf{Q}_g \delta(t-\tau)\,,$$

and $\mathbf{b}_g$ is the random bias modeled as a zero-mean Gaussian distributed random constant with

$$\mathrm{E}\left\{\mathbf{b}_g\right\} = \mathbf{0}^{3\times 1} \qquad \text{and} \qquad \mathrm{E}\left\{\mathbf{b}_g \mathbf{b}_g^{\mathrm{T}}\right\} = \mathbf{P}_{b_g}\,.$$

The misalignment/nonorthogonality matrix and scale factor error matrix take a similar form as their accelerometer counterparts as

$$\mathbf{\Gamma}_g = \begin{bmatrix} 0 & \gamma_{g,xz} & -\gamma_{g,xy} \\ -\gamma_{g,yz} & 0 & \gamma_{g,yx} \\ \gamma_{g,zy} & -\gamma_{g,zx} & 0 \end{bmatrix} \quad \text{and} \quad \mathbf{S}_g = \begin{bmatrix} s_{g,x} & 0 & 0 \\ 0 & s_{g,y} & 0 \\ 0 & 0 & s_{g,z} \end{bmatrix} .$$

We may follow a similar derivation to arrive at the actual rotation rate in terms of the measured value and modeled error terms as

$$\boldsymbol{\omega} = \boldsymbol{\omega}_m - \mathbf{N}(\boldsymbol{\omega}_m)\boldsymbol{\gamma}_g - \mathbf{D}(\boldsymbol{\omega}_m)\mathbf{s}_g - \mathbf{b}_g - \boldsymbol{\eta}_g \,, \tag{2.19}$$

where the matrices $\mathbf{N}(\boldsymbol{\omega}_m)$ and $\mathbf{D}(\boldsymbol{\omega}_m)$ take the form

$$\mathbf{N}(\boldsymbol{\omega}_m) = \begin{bmatrix} -\omega_{m,z} & \omega_{m,y} & 0 & 0 & 0 & 0 \\ 0 & 0 & \omega_{m,z} & -\omega_{m,x} & 0 & 0 \\ 0 & 0 & 0 & 0 & -\omega_{m,y} & \omega_{m,x} \end{bmatrix}$$

$$\mathbf{D}(\boldsymbol{\omega}_m) = \begin{bmatrix} \omega_{m,x} & 0 & 0 \\ 0 & \omega_{m,y} & 0 \\ 0 & 0 & \omega_{m,z} \end{bmatrix} ,$$

while the misalignment/nonorthogonality vector $\boldsymbol{\gamma}_g$ and scale factor error vector $\mathbf{s}_g$ take the form

$$\boldsymbol{\gamma}_g = \begin{bmatrix} \gamma_{g,xy} \\ \gamma_{g,xz} \\ \gamma_{g,yx} \\ \gamma_{g,yz} \\ \gamma_{g,zx} \\ \gamma_{g,zy} \end{bmatrix} \quad \text{and} \quad \mathbf{s}_g = \begin{bmatrix} s_{g,x} \\ s_{g,y} \\ s_{g,z} \end{bmatrix} . \tag{2.20}$$

The misalignment/nonorthogonality parameters and scale factor errors are modeled as zero-mean Gaussian distributed random constants with

$$\begin{aligned} \mathrm{E}\left\{\boldsymbol{\gamma}_g\right\} &= \mathbf{0}^{6\times 1} \\ \mathrm{E}\left\{\mathbf{s}_g\right\} &= \mathbf{0}^{3\times 1} \\ \mathrm{E}\left\{\boldsymbol{\gamma}_g\boldsymbol{\gamma}_g^{\mathrm{T}}\right\} &= \mathbf{P}_{\gamma_g} \\ \mathrm{E}\left\{\mathbf{s}_g\mathbf{s}_g^{\mathrm{T}}\right\} &= \mathbf{P}_{s_g}\,. \end{aligned}$$

2.5 Landing Site Dynamics

The position of the landing site is defined by its selenodetic altitude, latitude, and longitude. The nominal values for these parameters are assumed to be known. The landing site position in the inertial frame is found via

$$\mathbf{r}_{land}^{i} = \mathbf{T}_{f}^{i}\mathbf{r}_{land}^{f}\,, \tag{2.21}$$

where $\mathbf{T}_f^i$ is the transformation matrix that maps the planet-fixed frame to the inertial frame, and $\mathbf{r}_{land}^f$ is the position of the landing site in that planet-fixed frame. The planet may be modeled as an oblate spheroid so that the position of the landing site in the planet fixed frame is given by [3]

$$\mathbf{r}_{land}^{f} = \begin{bmatrix} (N+h)\cos\phi\cos\lambda \\ (N+h)\cos\phi\sin\lambda \\ (N(1-e^2)+h)\sin\lambda \end{bmatrix}\,, \tag{2.22}$$

where h is the selenodetic altitude above the oblate spheroid, ϕ is the selenodetic latitude, λ is the landing site longitude, and e is the first eccentricity. For the moon, the first eccentricity has the value $e = 0.0012$. N is the radius

of curvature and takes the form

$$N = \frac{R_e}{\sqrt{1 - e^2 \sin^2 \phi}}, \tag{2.23}$$

where R_e is the equatorial radius of the moon, with $R_e = 1738.1\,[\text{km}]$.

A typical issue with surface mapping of extraterrestrial bodies is that of map-tie error. Photographs and lidar range measurements of a planetary surface will return the features of that planet in relation to other features, but how the entire map is oriented upon the planet may be in error. Thus, the planet map may be well known in a surface-fixed frame. However, the misalignment of the planet surface map to the planet itself results in errors when rotating the location of a planet feature from a surface-fixed frame to the inertial frame. We may therefore add map-tie error angles ϕ_{map} and λ_{map} to the latitude and longitude of a surface feature to adjust the map correctly on the surface of the planet. The inclusion of the map-tie error angles leads to the planet-fixed landing site position and radius of curvature to be given as

$$\mathbf{r}^f_{land} = \begin{bmatrix} (N+h)\cos(\phi + \phi_{map})\cos(\lambda + \lambda_{map}) \\ (N+h)\cos(\phi + \phi_{map})\sin(\lambda + \lambda_{map}) \\ (N(1-e^2)+h)\sin(\lambda + \lambda_{map}) \end{bmatrix}$$

$$N = \frac{R_e}{\sqrt{1 - e^2 \sin^2 \phi + \phi_{map}}}.$$

2.6 System and Estimation Error Dynamics

This section describes the spacecraft and environment model dynamics and the associated error dynamics.

2.6.1 System Dynamics

The vehicle position and velocity in the inertial reference frame are

$$\dot{\mathbf{r}}^i_{imu} = \mathbf{v}^i_{imu} \tag{2.24}$$

$$\dot{\mathbf{v}}^i_{imu} = \mathbf{a}^i_g(\mathbf{r}^i_{cg}) + \mathbf{T}^i_b \mathbf{T}^b_c \mathbf{a}^c_{ng} \,. \tag{2.25}$$

The position of the vehicle center of gravity is located at

$$\mathbf{r}^i_{cg} = \mathbf{r}^i_{imu} + \mathbf{T}^i_b(\mathbf{r}^b_{cg/imu} + \Delta\mathbf{r}^b_{cg/imu}) \,, \tag{2.26}$$

where $\mathbf{T}^i_b \triangleq \mathbf{T}^i_b(\bar{\mathbf{q}}^i_b)$ is a function of the attitude quaternion and $\mathbf{T}^b_c$ is a known, fixed transformation matrix. The rotational dynamics of the vehicle (see Eq. (2.15)) are described via

$$\dot{\bar{\mathbf{q}}}^b_i = \frac{1}{2}\bar{\boldsymbol{\omega}}^b \otimes \bar{\mathbf{q}}^b_i \,,$$

where the quaternion represents the rotation of the body reference frame with respect to the inertial reference frame and $\bar{\boldsymbol{\omega}}^b$ is given by

$$\bar{\boldsymbol{\omega}}^b = \begin{bmatrix} 0 \\ \boldsymbol{\omega}^b \end{bmatrix} \,,$$

where $\boldsymbol{\omega}^b$ is the angular velocity of the vehicle as seen in the vehicle body frame. The transformation matrix $\mathbf{T}^i_b \in \Re^{3\times3}$ is related to the vehicle attitude quaternion by

$$\mathbf{T}^i_b = \mathbf{T}^{\mathrm{T}}(\bar{\mathbf{q}}^b_i) = \left[\left(q^{b^2}_i + \mathbf{q}^{b^{\mathrm{T}}}_i \mathbf{q}^b_i\right)\mathbf{I}^{3\times3} - 2q^b_i[\mathbf{q}^b_i\times] + 2[\mathbf{q}^b_i\times]^2\right]^{\mathrm{T}} \,. \tag{2.27}$$

The rest of the system is comprised of error sources and are collected by type as IMU errors, map tie errors, and sensor biases. All of these error sources are

modeled as zero-mean Gaussian distributed random constants. The variance of each error source is fixed as a system parameter. The IMU error sources are further divided as accelerometer and gyroscope error sources and their dynamics are given by

$$\dot{\mathbf{b}}_a = \mathbf{0}^{3\times1} + \mathbf{w}_{b_a}^{3\times1} \tag{2.28a}$$

$$\dot{\mathbf{b}}_g = \mathbf{0}^{3\times1} + \mathbf{w}_{b_g}^{3\times1} \tag{2.28b}$$

$$\dot{\mathbf{s}}_a = \mathbf{0}^{3\times1} + \mathbf{w}_{s_a}^{3\times1} \tag{2.28c}$$

$$\dot{\mathbf{s}}_g = \mathbf{0}^{3\times1} + \mathbf{w}_{s_g}^{3\times1} \tag{2.28d}$$

$$\dot{\boldsymbol{\gamma}}_a = \mathbf{0}^{6\times1} + \mathbf{w}_{\gamma_a}^{6\times1} \tag{2.28e}$$

$$\dot{\boldsymbol{\gamma}}_g = \mathbf{0}^{6\times1} + \mathbf{w}_{\gamma_g}^{6\times1}\,, \tag{2.28f}$$

where $\mathbf{w}_{b_a}$, $\mathbf{w}_{b_g}$, etc. are process noise added to the dynamics of the IMU corruption parameters. The process noise is added to the dynamics to account for the truth that the dynamics model is inherently imperfect, and the effects unaccounted for may be represented as noise. Process noise is an input to the navigation filter and is used to prevent over-confidence in an estimate by introducing a persistent excitement, driving the filter to continue to actively estimate these parameters. The deviation in the position of the CG with respect to the IMU is modeled similarly as

$$\Delta\dot{\mathbf{r}}_{cg/imu} = \mathbf{0}^{3\times1} + \mathbf{w}_{\Delta r}^{3\times1}\,, \tag{2.29}$$

as are the map tie errors

$$\dot{\phi}_{map} = 0 + \mathbf{w}_{\phi}^{3\times1} \tag{2.30a}$$

$$\dot{\lambda}_{map} = 0 + \mathbf{w}_{\lambda}^{3\times1}\,, \tag{2.30b}$$

and the sensor biases

$$\dot{b}_{alt} = 0 + w_{b_{alt}} \tag{2.31a}$$

$$\dot{\mathbf{b}}_{vel} = \mathbf{0}^{3\times1} + \mathbf{w}_{b_{vel}}^{3\times1} \tag{2.31b}$$

$$\dot{\mathbf{b}}_{sc} = \mathbf{0}^{3\times1} + \mathbf{w}_{b_{sc}}^{3\times1} \tag{2.31c}$$

$$\dot{\mathbf{b}}_{tc} = \mathbf{0}^{3\times1} + \mathbf{w}_{b_{tc}}^{3\times1}\,. \tag{2.31d}$$

Eq. (2.24) - Eq. (2.31) represent the true dynamics as modeled in the simulation and also the basis for the design of the EKF. If we concatenate the states from Eq. (2.24) - Eq. (2.31), we have the truth state vector

$$\mathbf{x} = \begin{bmatrix} \mathbf{r}_{imu}^{i} \\ \mathbf{v}_{imu}^{i} \\ \bar{\mathbf{q}}_{i}^{b} \\ \Delta\mathbf{r}_{cg/imu}^{b} \\ \mathbf{b}_{a}^{c} \\ \mathbf{s}_{a} \\ \boldsymbol{\gamma}_{a} \\ \mathbf{b}_{g}^{c} \\ \mathbf{s}_{g} \\ \boldsymbol{\gamma}_{g} \\ \phi_{map} \\ \lambda_{map} \\ b_{alt} \\ \mathbf{b}_{vel} \\ \mathbf{b}_{sc} \\ \mathbf{b}_{tc} \end{bmatrix} \in \Re^{48\times1}\,. \tag{2.32}$$

The estimated translational and rotational dynamics are

$$\dot{\hat{\mathbf{r}}}^i_{imu} = \hat{\mathbf{v}}^i_{imu} \tag{2.33}$$

$$\dot{\hat{\mathbf{v}}}^i_{imu} = \mathbf{a}^i_g(\hat{\mathbf{r}}^i_{cg}) + \hat{\mathbf{T}}^i_b \mathbf{T}^b_c \hat{\mathbf{a}}^c_{ng} \tag{2.34}$$

$$\dot{\hat{\mathbf{q}}}^b_i = \frac{1}{2}\hat{\boldsymbol{\omega}}^b \otimes \hat{\mathbf{q}}^b_i \,, \tag{2.35}$$

where the estimated position of the CG is

$$\hat{\mathbf{r}}^i_{cg} = \hat{\mathbf{r}}^i_{imu} + \hat{\mathbf{T}}^i_b \hat{\mathbf{r}}^b_{cg/imu} \,, \tag{2.36}$$

and the estimated position of the CG with respect to the IMU is

$$\hat{\mathbf{r}}^b_{cg/imu} = \mathbf{r}^b_{cg/imu} + \Delta\hat{\mathbf{r}}^b_{cg/imu} \,. \tag{2.37}$$

The estimated transformation matrix that rotates the vehicle body frame into the inertial frame is related to the estimated attitude quaternion via

$$\hat{\mathbf{T}}^i_b = \mathbf{T}^{\mathrm{T}}(\hat{\hat{\mathbf{q}}}^b_i) = \left[\left(\hat{q}^{b^2}_i + \hat{\mathbf{q}}^{b^{\mathrm{T}}}_i \hat{\mathbf{q}}^b_i\right)\mathbf{I}^{3\times 3} - 2\hat{q}^b_i[\hat{\mathbf{q}}^b_i\times] + 2[\hat{\mathbf{q}}^b_i\times]^2\right]^{\mathrm{T}} . \tag{2.38}$$

The estimated values for all the random constants which represent the error sources due to IMU error sources, CG location deviation, map tie error, and sensor bias errors follow zero dynamics. The IMU error sources are modeled

as constants via

$$\dot{\hat{\mathbf{b}}}_a = \mathbf{0}^{3\times 1} \tag{2.39a}$$

$$\dot{\hat{\mathbf{b}}}_g = \mathbf{0}^{3\times 1} \tag{2.39b}$$

$$\dot{\hat{\mathbf{s}}}_a = \mathbf{0}^{3\times 1} \tag{2.39c}$$

$$\dot{\hat{\mathbf{s}}}_g = \mathbf{0}^{3\times 1} \tag{2.39d}$$

$$\dot{\hat{\boldsymbol{\gamma}}}_a = \mathbf{0}^{6\times 1} \tag{2.39e}$$

$$\dot{\hat{\boldsymbol{\gamma}}}_g = \mathbf{0}^{6\times 1}\,. \tag{2.39f}$$

The estimated deviation in the CG position with respect to the IMU follows zero dynamics as

$$\Delta\dot{\hat{\mathbf{r}}}_{cg/imu} = \mathbf{0}^{3\times 1}\,, \tag{2.40}$$

while the estimated map tie errors are

$$\dot{\hat{\phi}}_{map} = 0 \tag{2.41a}$$

$$\dot{\hat{\lambda}}_{map} = 0\,, \tag{2.41b}$$

and the estimated sensor biases are

$$\dot{\hat{b}}_{alt} = 0 \tag{2.42a}$$

$$\dot{\hat{\mathbf{b}}}_{vel} = \mathbf{0}^{3\times 1} \tag{2.42b}$$

$$\dot{\hat{\mathbf{b}}}_{sc} = \mathbf{0}^{3\times 1} \tag{2.42c}$$

$$\dot{\hat{\mathbf{b}}}_{tc} = \mathbf{0}^{3\times 1}\,. \tag{2.42d}$$

The estimated state vector is thus

$$\hat{\mathbf{x}} = \begin{bmatrix} \hat{\mathbf{r}}^{i}_{imu} \\ \hat{\mathbf{v}}^{i}_{imu} \\ \hat{\bar{\mathbf{q}}}^{b}_{i} \\ \Delta\hat{\mathbf{r}}^{b}_{cg/imu} \\ \hat{\mathbf{b}}^{c}_{a} \\ \hat{\mathbf{s}}_{a} \\ \hat{\boldsymbol{\gamma}}_{a} \\ \hat{\mathbf{b}}^{c}_{g} \\ \hat{\mathbf{s}}_{g} \\ \hat{\boldsymbol{\gamma}}_{g} \\ \hat{\phi}_{map} \\ \hat{\lambda}_{map} \\ \hat{h}_{alt} \\ \hat{\mathbf{b}}_{vel} \\ \hat{\mathbf{b}}_{sc} \\ \hat{\mathbf{b}}_{tc} \end{bmatrix} \in \Re^{48\times 1} \tag{2.43}$$

2.6.2 Estimation Error Dynamics

The navigation system integrates the system dynamics to propagate the state estimate forward in time. In addition, the navigation system integrates the error dynamics equations describing the accuracy of the state estimate. The state estimate certainty is propagated forward as a state estimate error covariance matrix and the state estimate error dynamics equations are utilized to achieve this end. The following sections will derive the system error dynamics equations for integration and propagation of the state estimate error covariance.

2.6.2.1 Position and Velocity Error Dynamics

The position estimation error is found via differencing as

$$\delta\mathbf{r}^i_{imu} = \mathbf{r}^i_{imu} - \hat{\mathbf{r}}^i_{imu}\,.$$

We take the time derivative to yielding

$$\delta\dot{\mathbf{r}}^i_{imu} = \dot{\mathbf{r}}^i_{imu} - \dot{\hat{\mathbf{r}}}^i_{imu}\,,$$

or equivalently

$$\delta\dot{\mathbf{r}}^i_{imu} = \mathbf{v}^i_{imu} - \hat{\mathbf{v}}^i_{imu}\,. \tag{2.44}$$

The velocity error is found via differencing to be

$$\delta\mathbf{v}^i_{imu} = \mathbf{v}^i_{imu} - \hat{\mathbf{v}}^i_{imu}\,.$$

The time derivative of the velocity estimation error is

$$\delta\dot{\mathbf{v}}^i_{imu} = \dot{\mathbf{v}}^i_{imu} - \dot{\hat{\mathbf{v}}}^i_{imu}\,. \tag{2.45}$$

The definitions for the true and estimated acceleration as evaluated at the IMU (from Eq. (2.25) and Eq. (2.34), respectively) may be substituted into Eq. (2.45) to acquire

$$\delta\dot{\mathbf{v}}^i_{imu} = \mathbf{a}^i_g(\mathbf{r}^i_{cg}) - \mathbf{a}^i_g(\hat{\mathbf{r}}^i_{cg}) + \mathbf{T}^i_b\mathbf{T}^b_c\mathbf{a}^c_{ng} - \hat{\mathbf{T}}^i_b\mathbf{T}^b_c\hat{\mathbf{a}}^c_{ng}\,, \tag{2.46}$$

where $\mathbf{T}^i_b \triangleq \mathbf{T}^i_b(\bar{\mathbf{q}}^i_b)$ and $\hat{\mathbf{T}}^i_b \triangleq \hat{\mathbf{T}}^i_b(\hat{\bar{\mathbf{q}}}^i_b)$. We may expand the true gravitational acceleration in a first-order Taylor series about the estimated position of the CG and neglect the higher-order terms to obtain

$$\mathbf{a}^i_g(\mathbf{r}^i_{cg}) = \mathbf{a}^i_g(\hat{\mathbf{r}}^i_{cg}) + \mathbf{G}\delta\mathbf{r}^i_{cg}\,, \tag{2.47}$$

where the CG position deviation $\delta\mathbf{r}^i_{cg}$ is the difference between the true and estimated CG position and the first spatial derivative of the gravitational acceleration is the gravity gradient matrix where

$$\mathbf{G} = \left[\left. \frac{\partial \mathbf{a}^i_g}{\partial \mathbf{r}^i_{cg}} \right|_{\mathbf{r}^i_{cg}=\hat{\mathbf{r}}^i_{cg}} \right] .$$

The deviation in the position of the CG in inertial space is obtained from Eq. (2.26) and Eq. (2.36) as

$$\delta\mathbf{r}^i_{cg} = \mathbf{r}^i_{cg} - \hat{\mathbf{r}}^i_{cg}$$

or

$$\delta\mathbf{r}^i_{cg} = \delta\mathbf{r}^i_{imu} + (\mathbf{T}^i_b - \hat{\mathbf{T}}^i_b)\mathbf{r}^b_{cg/imu} + \mathbf{T}^i_b\Delta\mathbf{r}^b_{cg/imu} - \hat{\mathbf{T}}^i_b\Delta\hat{\mathbf{r}}^b_{cg/imu} \,. \tag{2.48}$$

The transformation matrix $\mathbf{T}^i_b$ may be approximated to first order in $\delta\boldsymbol{\alpha}$ in terms of the estimated $\hat{\mathbf{T}}^i_b$ as (see Appendix A for more information)

$$\mathbf{T}^i_b = \hat{\mathbf{T}}^i_b + \hat{\mathbf{T}}^i_b[\delta\boldsymbol{\alpha}] \,. \tag{2.49}$$

The deviation of the position of the CG in Eq. (2.48) may be written as

$$\delta\mathbf{r}^i_{cg} = \delta\mathbf{r}^i_{imu} - \hat{\mathbf{T}}^i_b \left[[\mathbf{r}^b_{cg/imu}\times]\delta\boldsymbol{\alpha} - [\Delta\mathbf{r}^b_{cg/imu}\times]\delta\boldsymbol{\alpha} + \delta\Delta\mathbf{r}^b_{cg/imu} \right] . \tag{2.50}$$

The true CG displacement in Eq. (2.50) may be formulated as an estimate plus an error term as

$$\Delta\mathbf{r}^b_{cg/imu} = \Delta\hat{\mathbf{r}}^b_{cg/imu} + \delta\Delta\mathbf{r}^b_{cg/imu} \,,$$

so that

$$\hat{\mathbf{T}}_b^i[\Delta\mathbf{r}_{cg/imu}^b\times]\delta\boldsymbol{\alpha} = \hat{\mathbf{T}}_b^i[(\Delta\hat{\mathbf{r}}_{cg/imu}^b + \delta\Delta\mathbf{r}_{cg/imu}^b)\times]\delta\boldsymbol{\alpha}\,.$$

We neglect higher-order terms yielding

$$\hat{\mathbf{T}}_b^i[\Delta\mathbf{r}_{cg/imu}^b\times]\delta\boldsymbol{\alpha} = \hat{\mathbf{T}}_b^i[\Delta\hat{\mathbf{r}}_{cg/imu}^b\times]\delta\boldsymbol{\alpha}\,. \tag{2.51}$$

Substituting Eq. (2.51) into Eq. (2.50) yields

$$\delta\mathbf{r}_{cg}^i = \delta\mathbf{r}_{imu}^i - \hat{\mathbf{T}}_b^i[\hat{\mathbf{r}}_{cg/imu}^b\times]\delta\boldsymbol{\alpha} + \hat{\mathbf{T}}_b^i\delta\Delta\mathbf{r}_{cg/imu}^b\,. \tag{2.52}$$

Substituting Eq. (2.52) into Eq. (2.47) leads to

$$\mathbf{a}_g^i(\mathbf{r}_{cg}^i) = \mathbf{a}_g^i(\hat{\mathbf{r}}_{cg}^i) + \mathbf{G}\delta\mathbf{r}_{imu}^i - \mathbf{G}\hat{\mathbf{T}}_b^i[\hat{\mathbf{r}}_{cg/imu}^b\times]\delta\boldsymbol{\alpha} + \mathbf{G}\hat{\mathbf{T}}_b^i\delta\Delta\mathbf{r}_{cg/imu}^b\,. \tag{2.53}$$

Substituting Eq. (2.53) into Eq. (2.46) yields

$$\delta\dot{\mathbf{v}}_{imu}^i = \mathbf{G}\delta\mathbf{r}_{imu}^i - \mathbf{G}\hat{\mathbf{T}}_b^i[\hat{\mathbf{r}}_{cg/imu}^b\times]\delta\boldsymbol{\alpha} + \mathbf{G}\hat{\mathbf{T}}_b^i\delta\Delta\mathbf{r}_{cg/imu}^b + \left(\mathbf{T}_b^i\mathbf{T}_c^b\mathbf{a}_{ng}^c - \hat{\mathbf{T}}_b^i\mathbf{T}_c^b\hat{\mathbf{a}}_{ng}^c\right) \tag{2.54}$$

In Eq. (2.54), we can approximate the last term on the right-hand side as

$$\begin{aligned}\mathbf{T}_b^i\mathbf{T}_c^b\mathbf{a}_{ng}^c - \hat{\mathbf{T}}_b^i\mathbf{T}_c^b\hat{\mathbf{a}}_{ng}^c &= \hat{\mathbf{T}}_b^i\mathbf{T}_c^b\mathbf{a}_{ng}^c + \hat{\mathbf{T}}_b^i[\delta\boldsymbol{\alpha}\times]\mathbf{T}_c^b\mathbf{a}_{ng}^c - \hat{\mathbf{T}}_b^i\mathbf{T}_c^b\hat{\mathbf{a}}_{ng}^c \\ &= \hat{\mathbf{T}}_b^i\mathbf{T}_c^b\delta\mathbf{a}_{ng}^c + \hat{\mathbf{T}}_b^i[\delta\boldsymbol{\alpha}\times]\mathbf{T}_c^b\mathbf{a}_{ng}^c\,,\end{aligned}$$

where $\delta\mathbf{a}_{ng}^c = \mathbf{a}_{ng}^c - \hat{\mathbf{a}}_{ng}^c$. Therefore, Eq. (2.54) reduces to

$$\begin{aligned}\delta\dot{\mathbf{v}}_{imu}^i = \mathbf{G}\delta\mathbf{r}_{imu}^i &- \mathbf{G}\hat{\mathbf{T}}_b^i[\hat{\mathbf{r}}_{cg/imu}^b\times]\delta\boldsymbol{\alpha} + \mathbf{G}\hat{\mathbf{T}}_b^i\delta\Delta\mathbf{r}_{cg/imu}^b \\ &+ \hat{\mathbf{T}}_b^i\mathbf{T}_c^b\delta\mathbf{a}_{ng}^c + \hat{\mathbf{T}}_b^i[\delta\boldsymbol{\alpha}\times]\mathbf{T}_c^b\mathbf{a}_{ng}^c\,.\end{aligned} \tag{2.55}$$

The last term in Eq. (2.55) contains the true non-gravitational acceleration, which may be written as the estimated acceleration plus the deviation so that

$$\hat{\mathbf{T}}_b^i[\delta\boldsymbol{\alpha}\times]\mathbf{T}_c^b\mathbf{a}_{ng}^c = \hat{\mathbf{T}}_b^i[\delta\boldsymbol{\alpha}\times]\mathbf{T}_c^b(\hat{\mathbf{a}}_{ng}^c + \delta\mathbf{a}_{ng}^c)\,,$$

and neglecting second-order terms yields

$$\hat{\mathbf{T}}_b^i[\delta\boldsymbol{\alpha}\times]\mathbf{T}_c^b\mathbf{a}_{ng}^c = \hat{\mathbf{T}}_b^i[\delta\boldsymbol{\alpha}\times]\mathbf{T}_c^b\hat{\mathbf{a}}_{ng}^c\,.$$

The velocity estimation error in Eq. (2.54) reduces to

$$\begin{aligned}\delta\dot{\mathbf{v}}_{imu}^i = \mathbf{G}\delta\mathbf{r}_{imu}^i - \mathbf{G}\hat{\mathbf{T}}_b^i[\hat{\mathbf{r}}_{cg/imu}^b\times]\delta\boldsymbol{\alpha} + \mathbf{G}\hat{\mathbf{T}}_b^i\delta\Delta\mathbf{r}_{cg/imu}^b \\ + \hat{\mathbf{T}}_b^i\mathbf{T}_c^b\delta\mathbf{a}_{ng}^c + \hat{\mathbf{T}}_b^i[\delta\boldsymbol{\alpha}\times]\mathbf{T}_c^b\hat{\mathbf{a}}_{ng}^c\,.\end{aligned}$$

Using Eq. (2.17) expressed in the IMU case reference frame, we have

$$\begin{aligned}\delta\mathbf{a}_{ng}^c &= \mathbf{a}_{ng}^c - \hat{\mathbf{a}}_{ng}^c \\ &= -\mathbf{N}(\mathbf{a}_{ng,m}^c)\delta\boldsymbol{\gamma}_a - \mathbf{D}(\mathbf{a}_{ng,m}^c)\delta\mathbf{s}_a - \delta\mathbf{b}_a^c - \boldsymbol{\eta}_a^c\,,\end{aligned}$$

where the individual error term deviations take the form

$$\begin{aligned}\delta\mathbf{b}_a^c &= \mathbf{b}_a^c - \hat{\mathbf{b}}_a^c \\ \delta\mathbf{s}_a &= \mathbf{s}_a - \hat{\mathbf{s}}_a \\ \delta\boldsymbol{\gamma}_a^c &= \boldsymbol{\gamma}_a^c - \hat{\boldsymbol{\gamma}}_a^c\,.\end{aligned}$$

Eq. (2.56) can thus be written as

$$\begin{aligned}\delta\dot{\mathbf{v}}_{imu}^i &= \mathbf{G}\delta\mathbf{r}_{imu}^i - \mathbf{G}\hat{\mathbf{T}}_b^i[\hat{\mathbf{r}}_{cg/imu}^b\times]\delta\boldsymbol{\alpha} + \mathbf{G}\hat{\mathbf{T}}_b^i\delta\Delta\mathbf{r}_{cg/imu}^b - \hat{\mathbf{T}}_b^i\mathbf{T}_c^b\mathbf{N}(\mathbf{a}_{ng,m}^c)\delta\boldsymbol{\gamma}_a \\ &\quad - \hat{\mathbf{T}}_b^i\mathbf{T}_c^b\mathbf{D}(\mathbf{a}_{ng,m}^c)\delta\mathbf{s}_a - \hat{\mathbf{T}}_b^i\mathbf{T}_c^b\delta\mathbf{b}_a^c - \hat{\mathbf{T}}_b^i\mathbf{T}_c^b\boldsymbol{\eta}_a^c + \hat{\mathbf{T}}_b^i[\delta\boldsymbol{\alpha}\times]\mathbf{T}_c^b\hat{\mathbf{a}}_{ng}^c \\ &= \mathbf{G}\delta\mathbf{r}_{imu}^i - \left(\mathbf{G}\hat{\mathbf{T}}_b^i[\hat{\mathbf{r}}_{cg/imu}^b\times] + \mathbf{G}\hat{\mathbf{T}}_b^i[\mathbf{T}_c^b\hat{\mathbf{a}}_{ng}^c\times]\right)\delta\boldsymbol{\alpha} + \mathbf{G}\hat{\mathbf{T}}_b^i\delta\Delta\mathbf{r}_{cg/imu}^b \\ &\quad - \hat{\mathbf{T}}_b^i\mathbf{T}_c^b\mathbf{N}(\mathbf{a}_{ng,m}^c)\delta\boldsymbol{\gamma}_a - \hat{\mathbf{T}}_b^i\mathbf{T}_c^b\mathbf{D}(\mathbf{a}_{ng,m}^c)\delta\mathbf{s}_a \\ &\quad - \hat{\mathbf{T}}_b^i\mathbf{T}_c^b\delta\mathbf{b}_a^c - \hat{\mathbf{T}}_b^i\mathbf{T}_c^b\boldsymbol{\eta}_a^c\,.\end{aligned} \tag{2.56}$$

Eq. (2.56) will be utilized in the integration of the state estimate error covariance.

2.6.2.2 Attitude Error Dynamics

The attitude estimation error employs the multiplicative error quaternion

$$\delta\bar{\mathbf{q}}_i^b = \bar{\mathbf{q}}_i^b \otimes \hat{\bar{\mathbf{q}}}_i^{b^{-1}} . \tag{2.57}$$

The time derivative of the error quaternion is

$$\delta\dot{\bar{\mathbf{q}}}_i^b = \dot{\bar{\mathbf{q}}}_i^b \otimes \hat{\bar{\mathbf{q}}}_i^{b^{-1}} + \bar{\mathbf{q}}_i^b \otimes \dot{\hat{\bar{\mathbf{q}}}}_i^{b^{-1}} .$$

Recall from Eq. (2.15) that the time derivative of the true attitude quaternion $\bar{\mathbf{q}}_i^b$ is

$$\dot{\bar{\mathbf{q}}}_i^b = \frac{1}{2}\bar{\boldsymbol{\omega}}^b \otimes \bar{\mathbf{q}}_i^b ,$$

which when substituted into the time-derivative of the attitude quaternion error yields

$$\delta\dot{\bar{\mathbf{q}}}_i^b = \frac{1}{2}\bar{\boldsymbol{\omega}}^b \otimes \bar{\mathbf{q}}_i^b \otimes \hat{\bar{\mathbf{q}}}_i^{b^{-1}} + \frac{1}{2}\bar{\mathbf{q}}_i^b \otimes \hat{\bar{\mathbf{q}}}_i^{b^{-1}} \otimes \hat{\bar{\boldsymbol{\omega}}}^{b^{-1}} \tag{2.58}$$

or, more compactly

$$\delta\dot{\bar{\mathbf{q}}}_i^b = \frac{1}{2}\bar{\boldsymbol{\omega}}^b \otimes \delta\bar{\mathbf{q}}_i^b + \frac{1}{2}\delta\bar{\mathbf{q}}_i^b \otimes \hat{\bar{\boldsymbol{\omega}}}^{b^{-1}} , \tag{2.59}$$

where $\bar{\boldsymbol{\omega}}^b$ is the angular velocity in pure quaternion form and $\hat{\bar{\boldsymbol{\omega}}}^b$ is the estimated angular velocity in pure quaternion form. Eq. (2.59) can be expanded and written as

$$\delta\dot{\bar{\mathbf{q}}}_i^b = \frac{1}{2}\begin{bmatrix} -\delta\boldsymbol{\omega}^{b^{\mathrm{T}}}\delta\mathbf{q}_i^b \\ \delta q_i^b\delta\boldsymbol{\omega}^b - 2\hat{\boldsymbol{\omega}}^b \times \delta\mathbf{q}_i^b - \delta\boldsymbol{\omega}^b \times \delta\mathbf{q}_i^b \end{bmatrix} ,$$

where $\delta\boldsymbol{\omega}^b$ is the angular velocity error defined as $\delta\boldsymbol{\omega}^b = \boldsymbol{\omega}^b - \hat{\boldsymbol{\omega}}^b$. We invoke the small-angle approximation and neglect higher-order terms to obtain

$$\delta\dot{\bar{\mathbf{q}}}_i^b = \begin{bmatrix} \delta\dot{q}_i^b \\ \delta\dot{\mathbf{q}}_i^b \end{bmatrix} = \begin{bmatrix} 0 \\ -\hat{\boldsymbol{\omega}}^b \times \delta\mathbf{q}_i^b + \frac{1}{2}\delta\boldsymbol{\omega}^b \end{bmatrix} . \tag{2.60}$$

Using Eq. (2.19) we find that

$$\begin{aligned} \delta\boldsymbol{\omega}^b &= \mathbf{T}_c^b(\boldsymbol{\omega}^c - \hat{\boldsymbol{\omega}}^c) \\ &= \mathbf{T}_c^b(-\mathbf{N}(\boldsymbol{\omega}_m)\delta\boldsymbol{\gamma}_g - \mathbf{D}(\boldsymbol{\omega}_m)\delta\mathbf{s}_g - \delta\mathbf{b}_g^c - \boldsymbol{\eta}_g^c) , \end{aligned} \tag{2.61}$$

where the individual deviations are found by subtracting the estimated value from the truth. Substituting Eq. (2.61) into Eq. (2.60) yields

$$\delta\dot{\mathbf{q}}_i^b = -[\mathbf{T}_c^b\hat{\boldsymbol{\omega}}^c\times]\delta\mathbf{q}_i^b - \frac{1}{2}\mathbf{T}_c^b(\mathbf{N}(\boldsymbol{\omega}_m)\delta\boldsymbol{\gamma}_g + \mathbf{D}(\boldsymbol{\omega}_m)\delta\mathbf{s}_g + \delta\mathbf{b}_g + \boldsymbol{\eta}_g^c) . \tag{2.62}$$

Consider the small angle approximation

$$\delta\mathbf{q}_i^b \approx \frac{1}{2}\delta\boldsymbol{\alpha} ,$$

where $\delta\boldsymbol{\alpha}$ are error angles that relate to roll, pitch, and yaw of the vehicle. Because this is a small angle approximation, the Euler sequence that produces this orientation may be taken in any order. We neglect the scalar portion of the error quaternion differential equation and only consider the vector portion which is now re-cast as a differential equation of the estimation error of the roll, pitch, and yaw angles as

$$\delta\dot{\boldsymbol{\alpha}} = -[\mathbf{T}_c^b\hat{\boldsymbol{\omega}}^c\times]\delta\boldsymbol{\alpha} - \mathbf{T}_c^b\mathbf{N}(\boldsymbol{\omega}_m)\delta\boldsymbol{\gamma}_g - \mathbf{T}_c^b\mathbf{D}(\boldsymbol{\omega}_m)\delta\mathbf{s}_g - \mathbf{T}_c^b\delta\mathbf{b}_g - \mathbf{T}_c^b\boldsymbol{\eta}_g^c \tag{2.63}$$

2.6.2.3 Systematic Error Dynamics

The systematic errors associated with the IMU errors and sensor biases are modeled as random constants. In the case of a generalized bias, the deviation may be written as

$$\delta\mathbf{b} = \mathbf{b} - \hat{\mathbf{b}}\,,$$

so that when the first derivative with respect to time is taken, the bias deviation dynamics becomes

$$\delta\dot{\mathbf{b}} = \dot{\mathbf{b}} - \dot{\hat{\mathbf{b}}}\,.$$

Recall that the IMU bias, scale factor uncertainty, and misalignment/ nonorthogonality parameters follow zero dynamics. The estimated dynamics of these parameters is thus also zero. Therefore, the dynamics of the IMU error sources may be written as

$$\delta\dot{\mathbf{b}}_a = \mathbf{0}^{3\times1} + \mathbf{w}_{b_a}^{3\times1} \tag{2.64a}$$

$$\delta\dot{\mathbf{b}}_g = \mathbf{0}^{3\times1} + \mathbf{w}_{b_g}^{3\times1} \tag{2.64b}$$

$$\delta\dot{\mathbf{s}}_a = \mathbf{0}^{3\times1} + \mathbf{w}_{s_a}^{3\times1} \tag{2.64c}$$

$$\delta\dot{\mathbf{s}}_g = \mathbf{0}^{3\times1} + \mathbf{w}_{s_g}^{3\times1} \tag{2.64d}$$

$$\delta\dot{\boldsymbol{\gamma}}_g = \mathbf{0}^{6\times1} + \mathbf{w}_{\gamma_a}^{6\times1} \tag{2.64e}$$

$$\delta\dot{\boldsymbol{\gamma}}_g = \mathbf{0}^{6\times1} + \mathbf{w}_{\gamma_g}^{6\times1}\,. \tag{2.64f}$$

where $\mathbf{w}_{b_a}$, $\mathbf{w}_{b_g}$, etc. represent the process noise introduced into the system to account for unknown dynamics and to assist the navigation filter in estimation.

The generalized dynamics of a system process bias may also be extended to the map-tie error dynamics. The map-tie estimation error differential equations may be written as

$$\delta\dot{\phi}_{map} = 0 + \mathbf{w}_{\phi}^{3\times1} \tag{2.65}$$

$$\delta\dot{\lambda}_{map} = 0 + \mathbf{w}_{\lambda}^{3\times1}\,. \tag{2.66}$$

Finally, the estimation error differential equations for the sensor biases will take the forms

$$\delta\dot{b}_{alt} = 0 + w_{b_a} \tag{2.67a}$$

$$\delta\dot{\mathbf{b}}_{vel} = \mathbf{0}^{3\times1} + \mathbf{w}_{b_{vel}}^{3\times1} \tag{2.67b}$$

$$\delta\dot{\mathbf{b}}_{sc} = \mathbf{0}^{3\times1} + \mathbf{w}_{b_{sc}}^{3\times1} \tag{2.67c}$$

$$\delta\dot{\mathbf{b}}_{tc} = \mathbf{0}^{3\times1} + \mathbf{w}_{b_{tc}}^{3\times1}\,. \tag{2.67d}$$

2.6.2.4 Error Dynamics Summary

It was found in Eq. (2.44) that the position estimation error differential equation is

$$\delta\dot{\mathbf{r}}_{imu}^{i} = \mathbf{v}_{imu}^{i} - \hat{\mathbf{v}}_{imu}^{i}\,,$$

and in Eq. (2.56) the velocity estimation error differential equation is

$$\begin{aligned}\delta\dot{\mathbf{v}}_{imu}^{i} = {} & \mathbf{G}\delta\mathbf{r}_{imu}^{i} - \left(\mathbf{G}\hat{\mathbf{T}}_{b}^{i}[\hat{\mathbf{r}}_{cg/imu}^{b}\times] + \mathbf{G}\hat{\mathbf{T}}_{b}^{i}[\mathbf{T}_{c}^{b}\hat{\mathbf{a}}_{ng}^{c}\times]\right)\delta\boldsymbol{\alpha} + \mathbf{G}\hat{\mathbf{T}}_{b}^{i}\delta\Delta\mathbf{r}_{cg/imu}^{b} \\ & - \hat{\mathbf{T}}_{b}^{i}\mathbf{T}_{c}^{b}\mathbf{N}(\mathbf{a}_{ng,m}^{c})\delta\boldsymbol{\gamma}_{a} - \hat{\mathbf{T}}_{b}^{i}\mathbf{T}_{c}^{b}\mathbf{D}(\mathbf{a}_{ng,m}^{c})\delta\mathbf{s}_{a} \\ & - \hat{\mathbf{T}}_{b}^{i}\mathbf{T}_{c}^{b}\delta\mathbf{b}_{a}^{c} - \hat{\mathbf{T}}_{b}^{i}\mathbf{T}_{c}^{b}\boldsymbol{\eta}_{a}^{c}\,.\end{aligned}$$

The attitude estimation error differential equation was found in Eq. (2.63) to be

$$\delta\dot{\boldsymbol{\alpha}} = -[\mathbf{T}_c^b\hat{\boldsymbol{\omega}}^c\times]\delta\boldsymbol{\alpha} - \mathbf{T}_c^b\mathbf{N}(\boldsymbol{\omega}_m)\delta\boldsymbol{\gamma}_g - \mathbf{T}_c^b\mathbf{D}(\boldsymbol{\omega}_m)\delta\mathbf{s}_g - \mathbf{T}_c^b\delta\mathbf{b}_g - \mathbf{T}_c^b\boldsymbol{\eta}_g^c\,.$$

The IMU error sources were found in Eq. (2.64) to obey

$$\begin{aligned}
\delta\dot{\mathbf{b}}_a &= \mathbf{0}^{3\times1} + \mathbf{w}_{b_a}^{3\times1} \\
\delta\dot{\mathbf{b}}_g &= \mathbf{0}^{3\times1} + \mathbf{w}_{b_g}^{3\times1} \\
\delta\dot{\mathbf{s}}_a &= \mathbf{0}^{3\times1} + \mathbf{w}_{s_a}^{3\times1} \\
\delta\dot{\mathbf{s}}_g &= \mathbf{0}^{3\times1} + \mathbf{w}_{s_g}^{3\times1} \\
\delta\dot{\boldsymbol{\gamma}}_g &= \mathbf{0}^{6\times1} + \mathbf{w}_{\gamma_a}^{6\times1} \\
\delta\dot{\boldsymbol{\gamma}}_g &= \mathbf{0}^{6\times1} + \mathbf{w}_{\gamma_g}^{6\times1}\,,
\end{aligned}$$

while the map-tie errors were found in Eq. (2.65) and Eq. (2.66) to be

$$\begin{aligned}
\delta\dot{\phi}_{map} &= 0 + \mathbf{w}_{\phi}^{3\times1} \\
\delta\dot{\lambda}_{map} &= 0 + \mathbf{w}_{\lambda}^{3\times1}\,,
\end{aligned}$$

and the sensor bias error differential equations were found in Eq. (2.67) to be

$$\begin{aligned}
\delta\dot{b}_{alt} &= 0 + w_{b_a} \\
\delta\dot{\mathbf{b}}_{vel} &= \mathbf{0}^{3\times1} + \mathbf{w}_{b_{vel}}^{3\times1} \\
\delta\dot{\mathbf{b}}_{sc} &= \mathbf{0}^{3\times1} + \mathbf{w}_{b_{sc}}^{3\times1} \\
\delta\dot{\mathbf{b}}_{tc} &= \mathbf{0}^{3\times1} + \mathbf{w}_{b_{tc}}^{3\times1}\,.
\end{aligned}$$

Chapter 3

Navigation Algorithm

This chapter describes the navigation algorithm. The sensor models are described, as well as the sensitivity of the sensor measurement to deviations in the spacecraft state. The navigation algorithm employs an extended Kalman filter (EKF) to propagate the spacecraft state estimate and state estimation error covariance forward in time with use of the IMU measurement values and acceleration/angular velocity error dynamics. The EKF also updates the state estimate and estimation error covariance from external measurements and estimated measurement residuals. The EKF is desribed in this chapter, as well as mathematical aids used in the simulation to add robustness to the EKF algorithm and its assumptions therein.

3.1 Measurement Models

3.1.1 Altimeter

The altimeter is a spherical altimeter which can be generalized as a nonlinear function of the altimeter position plus a bias and noise as

$$h_k = h(\mathbf{r}^i_{alt,k}) + b_{alt} + \eta_{alt,k}\,,$$

where the measurement is available at a discrete time t_k, denoted by h_k, and $\mathbf{r}^i_{alt,k}$ is the position of the altimeter as seen in the inertial frame, b_{alt} is the altimeter bias, modeled as a zero-mean Gaussian distributed random constant, and $\eta_{alt,k}$ is the altimeter measurement noise, modeled as a zero mean white noise sequence with variance R_{alt}. The estimated altimeter measurement value is

$$\hat{h}_k = h(\hat{\mathbf{r}}^i_{alt,k}) + \hat{b}_{alt,k}\,,$$

and the measurement deviation is

$$\begin{aligned}
\delta h_k &= h_k - \hat{h}_k \\
&= \left[h(\mathbf{r}^i_{alt,k}) - h(\hat{\mathbf{r}}^i_{alt,k})\right] + \delta b_{alt,k} + \eta_{alt,k} \\
&= \left[\left(\frac{\partial h(\mathbf{r}^i_{alt})}{\partial \mathbf{r}^i_{alt}}\right)_{\mathbf{r}^i_{alt,k}=\hat{\mathbf{r}}^i_{alt,k}}\right] \delta\mathbf{r}^i_{alt,k} + \delta b_{alt,k} + \eta_{alt,k} \\
&= h_{\mathbf{r},k}\delta\mathbf{r}^i_{alt,k} + \delta b_{alt,k} + \eta_{alt,k}\,, \qquad (3.1)
\end{aligned}$$

where $h_{\mathbf{r},k} = \left.\frac{\partial h(\mathbf{r}^i_{alt})}{\partial \mathbf{r}^i_{alt}}\right|_{\mathbf{r}^i_{alt,k}=\hat{\mathbf{r}}^i_{alt,k}}$ and $\delta\mathbf{r}^i_{alt} = \mathbf{r}^i_{alt} - \hat{\mathbf{r}}^i_{alt}$. The position of the altimeter in inertial space is

$$\mathbf{r}^i_{alt,k} = \mathbf{r}^i_{imu,k} + \mathbf{T}^i_b(\bar{\mathbf{q}}^i_{b,k})\mathbf{r}^b_{alt/imu}\,, \qquad (3.2)$$

where $\mathbf{r}^b_{alt/imu}$ is the position of the altimeter with respect to the IMU as seen in the vehicle body frame. The estimated position of the altimeter is

$$\hat{\mathbf{r}}^i_{alt,k} = \hat{\mathbf{r}}^i_{imu,k} + \hat{\mathbf{T}}^i_b(\hat{\bar{\mathbf{q}}}^i_{b,k})\mathbf{r}^b_{alt/imu}\,, \qquad (3.3)$$

The altimeter position deviation is thus

$$\delta\mathbf{r}^i_{alt,k} = \delta\mathbf{r}^i_{imu,k} + \left[\mathbf{T}^i_{b,k} - \hat{\mathbf{T}}^i_{b,k}\right]\mathbf{r}^b_{alt/imu}\,, \qquad (3.4)$$

where $\mathbf{T}^i_{b,k} = \mathbf{T}^i_b(\bar{\mathbf{q}}^i_{b,k})$ and $\hat{\mathbf{T}}^i_{b,k} = \hat{\mathbf{T}}^i_b(\hat{\bar{\mathbf{q}}}^i_{b,k})$. The transformation from the body reference frame to the inertial reference frame may be estimated to first order as

$$\mathbf{T}^i_{b,k} \approx \hat{\mathbf{T}}^i_{b,k} + \hat{\mathbf{T}}^i_{b,k}[\delta\boldsymbol{\alpha}_k\times]\,, \tag{3.5}$$

so that when Eq. (3.5) is substituted into Eq. (3.4), we will have

$$\begin{aligned}\delta\mathbf{r}^i_{alt,k} &= \delta\mathbf{r}^i_{imu,k} + \hat{\mathbf{T}}^i_{b,k}[\delta\boldsymbol{\alpha}_k\times]\mathbf{r}^b_{alt/imu} \\ &= \delta\mathbf{r}^i_{imu,k} - \hat{\mathbf{T}}^i_{b,k}[\mathbf{r}^b_{alt/imu}\times]\delta\boldsymbol{\alpha}_k\,. \end{aligned}\tag{3.6}$$

Substituting Eq. (3.6) into Eq. (3.1) will yield

$$\delta h_k = h_{\mathbf{r},k}\delta\mathbf{r}^i_{imu,k} - h_{\mathbf{r},k}\hat{\mathbf{T}}^i_{b,k}[\mathbf{r}^b_{alt/imu}\times]\delta\boldsymbol{\alpha}_k + \delta b_{alt,k} + \eta_{alt,k}\,. \tag{3.7}$$

The spherical altimeter function is

$$h_{sph,k} = \|\mathbf{r}^i_{alt,k}\| - r_{moon}\,. \tag{3.8}$$

The partial derivative of Eq. (3.8) is

$$\begin{aligned}\frac{\partial h_{sph}}{\partial\mathbf{r}^i_{alt}} &= \frac{\partial}{\partial\mathbf{r}^i_{alt}}\|\mathbf{r}^i_{alt}\| - r_{moon} \\ &= \frac{\partial}{\partial\mathbf{r}^i_{alt}}\sqrt{\mathbf{r}^{i^{\mathrm{T}}}_{alt}\mathbf{r}^i_{alt}} \\ &= \frac{\mathbf{r}^{i^{\mathrm{T}}}_{alt}}{r^i_{alt}}\,. \end{aligned}\tag{3.9}$$

Substituting Eq. (3.9) into Eq. (3.7) will yield the final form as

$$\delta h_k = \frac{\hat{\mathbf{r}}^{i^{\mathrm{T}}}_{alt,k}}{\hat{r}^i_{alt}}\delta\mathbf{r}^i_{imu,k} - \frac{\hat{\mathbf{r}}^{i^{\mathrm{T}}}_{alt,k}}{\hat{r}^i_{alt,k}}\hat{\mathbf{T}}^i_{b,k}[\mathbf{r}^b_{alt/imu}\times]\delta\boldsymbol{\alpha}_k + \delta b_{alt,k} + \eta_{alt,k}\,. \tag{3.10}$$

3.1.2 Velocimeter

A velocimeter gives a measurement of the relative velocity of the instrument with respect to the local spherical surface. This can be modeled as

$$\mathbf{v}^v_{rel,k} = \mathbf{T}^v_b \mathbf{T}^b_{i,k} \left[\mathbf{v}^i_{vel,k} - \boldsymbol{\omega}_L \times \mathbf{r}^i_{vel,k} \right] + \mathbf{b}^v_{vel,k} + \boldsymbol{\eta}_{vel,k} \,, \tag{3.11}$$

where $\boldsymbol{\omega}_L$ is the rotation rate of the Moon with respect to inertial space, $\mathbf{r}^i_{vel}$ and $\mathbf{v}^i_{vel}$ are the position/velocity of the velocimeter as seen in the inertial frame, respectively, $\mathbf{b}_{vel}$ is the velocimeter bias, and $\boldsymbol{\eta}_{vel}$ is the velocimeter measurement noise which is modeled as a Gaussian white noise sequence with

$$\mathrm{E}\left\{\boldsymbol{\eta}_{vel}\right\} = \mathbf{0}^{3\times 1} \qquad \text{and} \qquad \mathrm{E}\left\{\boldsymbol{\eta}_{vel}\boldsymbol{\eta}^{\mathrm{T}}_{vel}\right\} = \mathbf{R}^{3\times 3}_{vel}$$

The estimated value for the velocimeter measurement is

$$\hat{\mathbf{v}}^v_{rel,k} = \mathbf{T}^v_b \hat{\mathbf{T}}^b_{i,k} \left[\hat{\mathbf{v}}^i_{vel,k} - \boldsymbol{\omega}_L \times \hat{\mathbf{r}}^i_{vel,k} \right] + \hat{\mathbf{b}}^v_{vel,k} \,. \tag{3.12}$$

If the measurement deviation is defined as $\delta\mathbf{v}^v_{rel} = \mathbf{v}^v_{rel} - \hat{\mathbf{v}}^v_{rel}$, then substituting the true and estimated measurements from Eq. (3.11) and Eq. (3.12), respectively, yields

$$\begin{aligned} \delta\mathbf{v}^v_{rel,k} = {} & \mathbf{T}^v_b \mathbf{T}^b_{i,k} \left[\mathbf{v}^i_{vel,k} - \boldsymbol{\omega}_L \times \mathbf{r}^i_{vel,k} \right] + \mathbf{b}^v_{vel,k} + \boldsymbol{\eta}_{vel,k} \\ & - \mathbf{T}^v_b \hat{\mathbf{T}}^b_{i,k} \left[\hat{\mathbf{v}}^i_{vel,k} - \boldsymbol{\omega}_L \times \hat{\mathbf{r}}^i_{vel,k} \right] - \hat{\mathbf{b}}^v_{vel,k} \end{aligned} \tag{3.13}$$

The true inertial-to-body transformation matrix may be approximated to first order as

$$\mathbf{T}^b_i \approx \hat{\mathbf{T}}^b_i - [\delta\boldsymbol{\alpha}\times]\hat{\mathbf{T}}^b_i \,, \tag{3.14}$$

so that when Eq. (3.14) is substituted into Eq. (3.13) we obtain

$$\begin{aligned}\delta\mathbf{v}^v_{rel,k} = \mathbf{T}^v_b\hat{\mathbf{T}}^b_{i,k}\left[\delta\mathbf{v}^i_{vel,k} - \boldsymbol{\omega}_L \times \hat{\mathbf{r}}^i_{vel,k}\right] \\ - \mathbf{T}^v_b[\delta\boldsymbol{\alpha}_k\times]\hat{\mathbf{T}}^b_{i,k}\left[\mathbf{v}^i_{vel,k} - \boldsymbol{\omega}_L \times \mathbf{r}^i_{vel,k}\right] + \delta\mathbf{b}^v_{vel,k} + \boldsymbol{\eta}^v_{vel,k}\,,\end{aligned} \tag{3.15}$$

where the individual deviations are

$$\begin{aligned}\delta\mathbf{v}^i_{vel,k} &= \mathbf{v}^i_{vel,k} - \hat{\mathbf{v}}^i_{vel,k} \\ \delta\mathbf{r}^i_{vel,k} &= \mathbf{r}^i_{vel,k} - \hat{\mathbf{r}}^i_{vel,k} \\ \delta\mathbf{b}^v_{vel,k} &= \mathbf{b}^v_{vel,k} - \hat{\mathbf{b}}^v_{vel,k}\,.\end{aligned}$$

We may use these definitions to recast true values as their estimate and deviation. We begin with the second term in Eq. (3.15) so that

$$\mathbf{T}^v_b[\delta\boldsymbol{\alpha}_k\times]\hat{\mathbf{T}}^b_{i,k}\mathbf{v}^i_{vel,k} = \mathbf{T}^v_b[\delta\boldsymbol{\alpha}_k\times]\hat{\mathbf{T}}^b_{i,k}(\hat{\mathbf{v}}^i_{vel,k} + \delta\mathbf{v}^i_{vel,k})\,,$$

which approximated to first order reduces to

$$\mathbf{T}^v_b[\delta\boldsymbol{\alpha}_k\times]\hat{\mathbf{T}}^b_{i,k}(\hat{\mathbf{v}}^i_{vel,k} + \delta\mathbf{v}^i_{vel,k}) = \mathbf{T}^v_b[\delta\boldsymbol{\alpha}_k\times]\hat{\mathbf{T}}^b_{i,k}\hat{\mathbf{v}}^i_{vel,k}\,. \tag{3.16}$$

Similarly, examining the second half of the second term we can expand the true velocimeter position as

$$\mathbf{T}^v_b[\delta\boldsymbol{\alpha}_k\times]\hat{\mathbf{T}}^b_{i,k}(\boldsymbol{\omega}_L \times \mathbf{r}^i_{vel,k}) = \mathbf{T}^v_b[\delta\boldsymbol{\alpha}_k\times]\hat{\mathbf{T}}^b_{i,k}[\boldsymbol{\omega}_L \times (\hat{\mathbf{r}}^i_{vel,k} + \delta\mathbf{r}^i_{vel,k})]\,, \tag{3.17}$$

so that when we neglect second order terms we will acquire

$$\mathbf{T}^v_b[\delta\boldsymbol{\alpha}_k\times]\hat{\mathbf{T}}^b_{i,k}[\boldsymbol{\omega}_L \times (\hat{\mathbf{r}}^i_{vel,k} + \delta\mathbf{r}^i_{vel,k})] = \mathbf{T}^v_b[\delta\boldsymbol{\alpha}_k\times]\hat{\mathbf{T}}^b_{i,k}(\boldsymbol{\omega}_L \times \hat{\mathbf{r}}^i_{vel,k})\,. \tag{3.18}$$

Substituting Eq. (3.16) and Eq. (3.18) into Eq. (3.15) yields

$$\delta\mathbf{v}^v_{rel,k} = \mathbf{T}^v_b\hat{\mathbf{T}}^b_{i,k}\left[\delta\mathbf{v}^i_{vel,k} - \boldsymbol{\omega}_k \times \delta\mathbf{r}^i_{vel,k}\right] + \mathbf{T}^v_b\left[\hat{\mathbf{T}}^b_{i,k}[\hat{\mathbf{v}}^i_{vel,k} - \boldsymbol{\omega} \times \hat{\mathbf{r}}^i_{vel,k}]\times\right]\delta\boldsymbol{\alpha}_k + \delta\mathbf{b}^v_{vel,k} + \boldsymbol{\eta}^v_{vel,k}\,. \tag{3.19}$$

The true and estimated position of the velocimeter in inertial space are given by

$$\mathbf{r}^i_{vel,k} = \mathbf{r}^i_{imu,k} + \mathbf{T}^i_{b,k}\mathbf{r}^b_{vel/imu}$$
$$\hat{\mathbf{r}}^i_{vel,k} = \hat{\mathbf{r}}^i_{imu,k} + \hat{\mathbf{T}}^i_{b,k}\mathbf{r}^b_{vel/imu}\,,$$

respectively. The position of the velocimeter with respect to the IMU as seen in the body frame is constant in time and assumed to be perfectly known through preflight calibration. The deviation of the velocimeter position in inertial space is

$$\delta\mathbf{r}^i_{vel,k} = \delta\mathbf{r}^i_{imu,k} + \left(\mathbf{T}^i_{b,k} - \hat{\mathbf{T}}^i_{b,k}\right)\mathbf{r}^b_{vel/imu}\,.$$

The true body-to-inertial rotation matrix may be approximated to first order as

$$\mathbf{T}^i_{b,k} \approx \hat{\mathbf{T}}^i_{b,k} + \hat{\mathbf{T}}^i_{b,k}[\delta\boldsymbol{\alpha}_k\times]\,,$$

so that the velocimeter position deviation may be written as

$$\delta\mathbf{r}^i_{vel,k} = \delta\mathbf{r}^i_{imu,k} - \hat{\mathbf{T}}^i_{b,k}[\mathbf{r}^b_{vel/imu}\times]\delta\boldsymbol{\alpha}_k\,. \tag{3.20}$$

The true and estimated velocity of the velocimeter in the inertial frame are given by

$$\mathbf{v}^i_{vel,k} = \mathbf{v}^i_{imu,k} + \mathbf{T}^i_{b,k}[\boldsymbol{\omega}^b_k \times \mathbf{r}^b_{vel/imu}]$$
$$\hat{\mathbf{v}}^i_{vel,k} = \hat{\mathbf{v}}^i_{imu,k} + \hat{\mathbf{T}}^i_{b,k}[\hat{\boldsymbol{\omega}}^b_k \times \mathbf{r}^b_{vel/imu}]\,,$$

respectively. The deviation of the inertial velocity of the velocimeter is

$$\delta\mathbf{v}^i_{vel,k} = \delta\mathbf{v}^i_{imu,k} + \mathbf{T}^i_{b,k}[\boldsymbol{\omega}^b_k \times \mathbf{r}^b_{vel/imu}] - \hat{\mathbf{T}}^i_{b,k}[\hat{\boldsymbol{\omega}}^b_k \times \mathbf{r}^b_{vel/imu}]\,. \tag{3.21}$$

The true body-to-inertial rotation matrix may be approximated to first order so that

$$\begin{aligned}\delta\mathbf{v}^i_{vel,k} &= \delta\mathbf{v}^i_{imu,k} + \hat{\mathbf{T}}^i_{b,k}[\boldsymbol{\omega}^b_k \times \mathbf{r}^b_{vel/imu}] + \hat{\mathbf{T}}^i_{b,k}[\delta\boldsymbol{\alpha}_k\times][\boldsymbol{\omega}^b_k \times \mathbf{r}^b_{vel/imu}] \\ &\quad - \hat{\mathbf{T}}^i_{b,k}[\hat{\boldsymbol{\omega}}^b_k \times \mathbf{r}^b_{vel/imu}] \\ &= \delta\mathbf{v}^i_{imu,k} - \hat{\mathbf{T}}^i_{b,k}[\mathbf{r}^b_{vel/imu}\times]\delta\boldsymbol{\omega}^b_k - \hat{\mathbf{T}}^i_{b,k}\left[[\boldsymbol{\omega}^b_k \times \mathbf{r}^b_{vel/imu}]\times\right]\delta\boldsymbol{\alpha}_k\,.\end{aligned}$$

We may expand the true vehicle rotation rate in the body frame as its estimate plus the deviation so that the final term takes the form

$$\hat{\mathbf{T}}^i_{b,k}\left[[\boldsymbol{\omega}^b_k \times \mathbf{r}^b_{vel/imu}]\times\right]\delta\boldsymbol{\alpha}_k = \hat{\mathbf{T}}^i_{b,k}\left[[(\hat{\boldsymbol{\omega}}^b_k + \delta\boldsymbol{\omega}^b_k) \times \mathbf{r}^b_{vel/imu}]\times\right]\delta\boldsymbol{\alpha}_k\,,$$

Neglecting second-order terms yields

$$\hat{\mathbf{T}}^i_{b,k}\left[[(\hat{\boldsymbol{\omega}}^b - k + \delta\boldsymbol{\omega}^b_k) \times \mathbf{r}^b_{vel/imu}]\times\right]\delta\boldsymbol{\alpha}_k = \hat{\mathbf{T}}^i_{b,k}\left[[\hat{\boldsymbol{\omega}}^b_k \times \mathbf{r}^b_{vel/imu}]\times\right]\delta\boldsymbol{\alpha}_k\,,$$

The deviation of the inertial velocity of the velocimeter is thus

$$\delta\mathbf{v}^i_{vel,k} = \delta\mathbf{v}^i_{imu,k} - \hat{\mathbf{T}}^i_{b,k}[\mathbf{r}^b_{vel/imu}\times]\delta\boldsymbol{\omega}^b - \hat{\mathbf{T}}^i_{b,k}\left[(\hat{\boldsymbol{\omega}}^b \times \mathbf{r}^b_{vel/imu})\times\right]\delta\boldsymbol{\alpha}\,. \tag{3.22}$$

It has been shown in Eq. (2.61) that the vehicle rotation rate deviation takes the form

$$\delta\boldsymbol{\omega}^b = -\mathbf{T}^b_c\mathbf{N}(\boldsymbol{\omega}_m)\delta\boldsymbol{\gamma}_g - \mathbf{T}^b_c\mathbf{D}(\boldsymbol{\omega}_m)\delta\mathbf{s}_g - \mathbf{T}^b_c\delta\mathbf{b}^c_g - \mathbf{T}^b_c\boldsymbol{\eta}^c_g\,,$$

which when substituted into Eq. (3.22) yields

$$\begin{aligned}\delta\mathbf{v}^i_{vel,k} = {} & \delta\mathbf{v}^i_{imu,k} + \hat{\mathbf{T}}^i_{b,k}[\mathbf{r}^b_{vel/imu}\times]\mathbf{T}^b_c\mathbf{N}(\boldsymbol{\omega}_{m,k})\delta\boldsymbol{\gamma}_{g,k} \\ & + \hat{\mathbf{T}}^i_{b,k}[\mathbf{r}^b_{vel/imu}\times]\mathbf{T}^b_c\mathbf{D}(\boldsymbol{\omega}_{m,k})\delta\mathbf{s}_{g,k} + \hat{\mathbf{T}}^i_{b,k}[\mathbf{r}^b_{vel/imu}\times]\mathbf{T}^b_c\delta\mathbf{b}^c_{g,k} \\ & + \hat{\mathbf{T}}^i_{b,k}[\mathbf{r}^b_{vel/imu}\times]\mathbf{T}^b_c\boldsymbol{\eta}^c_{g,k} - \hat{\mathbf{T}}^i_{b,k}\left[(\hat{\boldsymbol{\omega}}^b_k \times \mathbf{r}^b_{vel/imu})\times\right]\delta\boldsymbol{\alpha}_k\,.\end{aligned} \tag{3.23}$$

Using $\delta\mathbf{r}^i_{vel}$ and $\delta\mathbf{v}^i_{vel}$, we will arrive at the final solution as

$$\begin{aligned}\delta\mathbf{v}^v_{rel,k} = {} & -\mathbf{T}^v_b\hat{\mathbf{T}}^b_{i,k}[\boldsymbol{\omega}_L\times]\delta\mathbf{r}^i_{imu,k} + \mathbf{T}^v_b\hat{\mathbf{T}}^b_{i,k}\delta\mathbf{v}^i_{imu,k} \\ & + \mathbf{T}^v_b\left[(\hat{\boldsymbol{\omega}}^b_k \times \mathbf{r}^b_{vel/imu})\times\right]\delta\boldsymbol{\alpha}_k + \mathbf{T}^v_b\hat{\mathbf{T}}^b_{i,k}[\boldsymbol{\omega}_L\times]\hat{\mathbf{T}}^i_{b,k}[\mathbf{r}^b_{vel/imu}\times]\delta\boldsymbol{\alpha}_k \\ & + \mathbf{T}^v_b\left[\hat{\mathbf{T}}^i_{b,k}(\hat{\mathbf{v}}^i_{vel,k} - \boldsymbol{\omega}_L \times \hat{\mathbf{r}}^i_{vel,k})\times\right]\delta\boldsymbol{\alpha}_k + \mathbf{T}^v_b[\mathbf{r}^b_{vel/imu}\times]\mathbf{T}^b_c\delta\mathbf{b}^c_{g,k} \\ & + \mathbf{T}^v_b[\mathbf{r}^b_{vel/imu}\times]\mathbf{T}^b_c\mathbf{D}(\boldsymbol{\omega}_{m,k})\delta\mathbf{s}_{g,k} + \mathbf{T}^v_b[\mathbf{r}^b_{vel/imu}\times]\mathbf{T}^b_c\mathbf{N}(\boldsymbol{\omega}_{m,k})\delta\boldsymbol{\gamma}_{g,k} \\ & + \delta\mathbf{b}^v_{vel,k} + \mathbf{T}^v_b[\mathbf{r}^b_{vel/imu}\times]\mathbf{T}^b_c\boldsymbol{\eta}^c_{g,k} + \boldsymbol{\eta}^v_{vel,k}\,.\end{aligned} \tag{3.24}$$

3.1.3 Quaternion Star Camera Model

The navigation algorithm employs a quaternion star camera as the primary attitude measurement. The sensor output is a quaternion that rotates the star camera reference frame into a stellar reference frame. The measurement is corrupted by bias and noise. The star camera measurement is modeled as

$$\bar{\mathbf{q}}^{sc}_{sr,k} = \bar{\mathbf{q}}_{b,\eta,k} \otimes \bar{\mathbf{q}}^{sc}_b \otimes \bar{\mathbf{q}}^b_{i,k} \otimes \bar{\mathbf{q}}^i_{sr}\,, \tag{3.25}$$

where $\bar{\mathbf{q}}_{b,\eta,k}$ is the error quaternion that introduces bias and error and $\bar{\mathbf{q}}^i_{sr}$ is the quaternion that rotates the inertial reference frame into the stellar reference frame. The stellar reference frame is assumed to be fixed at a constant

orientation with respect to the inertial reference frame, and is perfectly known. The error quaternion is

$$\bar{\mathbf{q}}_{b,\eta,k} = \begin{bmatrix} \cos\left(\frac{\theta_{sc,k}}{2}\right) \\ \sin\left(\frac{\theta_{sc,k}}{2}\right) \frac{\boldsymbol{\theta}_{sc,k}}{\theta_{sc,k}} \end{bmatrix}, \tag{3.26}$$

where

$$\boldsymbol{\theta}_{sc,k} = \mathbf{b}_{sc} + \boldsymbol{\eta}_{sc,k}\,. \tag{3.27}$$

In Eq. (3.27), $\mathbf{b}_{sc}$ is the star camera bias, and $\boldsymbol{\eta}_{sc,k}$ is the star camera measurement noise which is modeled as a Gaussian white noise process with

$$\mathrm{E}\left\{\boldsymbol{\eta}_{sc}\right\} = \mathbf{0}^{3\times 1} \qquad \text{and} \qquad \mathrm{E}\left\{\boldsymbol{\eta}_{sc}\boldsymbol{\eta}_{sc}^{\mathrm{T}}\right\} = \mathbf{R}_{sc}^{3\times 3}\,.$$

The estimated measurement is given by

$$\hat{\bar{\mathbf{q}}}_{sr,k}^{sc} = \hat{\bar{\mathbf{q}}}_{b,k} \otimes \bar{\mathbf{q}}_{b}^{sc} \otimes \hat{\bar{\mathbf{q}}}_{i,k}^{b} \otimes \bar{\mathbf{q}}_{sr}^{i}\,. \tag{3.28}$$

The measurement and the estimated measurement are quaternions and a multiplicative approach is used to find the difference

$$\delta\bar{\mathbf{q}}_{sr,k}^{sc} = \bar{\mathbf{q}}_{sr,k}^{sc} \otimes \hat{\bar{\mathbf{q}}}_{sr,k}^{sc^{-1}}\,. \tag{3.29}$$

The measurement deviation is given by

$$\delta\bar{\mathbf{q}}_{sr,k}^{sc} = \bar{\mathbf{q}}_{b,\eta,k} \otimes \bar{\mathbf{q}}_{b}^{sc} \otimes \bar{\mathbf{q}}_{i,k}^{b} \otimes \bar{\mathbf{q}}_{sr}^{i} \otimes \bar{\mathbf{q}}_{sr}^{i^{-1}} \otimes \hat{\bar{\mathbf{q}}}_{i,k}^{b^{-1}} \otimes \bar{\mathbf{q}}_{b}^{sc^{-1}} \otimes \hat{\bar{\mathbf{q}}}_{b,k}^{-1}\,. \tag{3.30}$$

The product $\bar{\mathbf{q}}_{sr}^{i} \otimes \bar{\mathbf{q}}_{sr}^{i^{-1}}$ results in the identity quaternion so that Eq. (3.30) reduces to

$$\delta\bar{\mathbf{q}}_{sr,k}^{sc} = \bar{\mathbf{q}}_{b,\eta,k} \otimes \bar{\mathbf{q}}_{b}^{sc} \otimes \bar{\mathbf{q}}_{i,k}^{b} \otimes \hat{\bar{\mathbf{q}}}_{i,k}^{b^{-1}} \otimes \bar{\mathbf{q}}_{b}^{sc^{-1}} \otimes \hat{\bar{\mathbf{q}}}_{b,k}^{-1}\,. \tag{3.31}$$

With the definition

$$\delta\bar{\mathbf{q}}_{i,k}^{b} = \bar{\mathbf{q}}_{i,k}^{b} \otimes \hat{\bar{\mathbf{q}}}_{i,k}^{b^{-1}}\,, \tag{3.32}$$

the terms $\bar{\mathbf{q}}_{b}^{sc} \otimes \bar{\mathbf{q}}_{i,k}^{b} \otimes \hat{\bar{\mathbf{q}}}_{i,k}^{b^{-1}} \otimes \bar{\mathbf{q}}_{b}^{sc^{-1}}$ reduce to

$$\bar{\mathbf{q}}_{b}^{sc} \otimes \bar{\mathbf{q}}_{i,k}^{b} \otimes \hat{\bar{\mathbf{q}}}_{i,k}^{b^{-1}} \otimes \bar{\mathbf{q}}_{b}^{sc^{-1}} = \bar{\mathbf{q}}_{b}^{sc} \otimes \delta\bar{\mathbf{q}}_{i,k}^{b} \otimes \bar{\mathbf{q}}_{b}^{sc^{-1}} \tag{3.33}$$

and

$$\bar{\mathbf{q}}_{b}^{sc} \otimes \delta\bar{\mathbf{q}}_{i,k}^{b} \otimes \bar{\mathbf{q}}_{b}^{sc^{-1}} = \begin{bmatrix} \delta q_{i,k}^{b} \\ \mathbf{T}_{b}^{sc}\delta\mathbf{q}_{i,k}^{b} \end{bmatrix}\,, \tag{3.34}$$

Eq. (3.34) is substituted into Eq. (3.31) leads to

$$\delta\bar{\mathbf{q}}_{sr,k}^{sc} = \bar{\mathbf{q}}_{b,\eta,k} \otimes \begin{bmatrix} \delta q_{i,k}^{b} \\ \mathbf{T}_{b}^{sc}\delta\mathbf{q}_{i,k}^{b} \end{bmatrix} \otimes \hat{\bar{\mathbf{q}}}_{b,k}^{-1}\,. \tag{3.35}$$

The bias-error quaternion from the measurement equation can be redefined in terms of its estimate and a deviation as

$$\bar{\mathbf{q}}_{b,\eta,k} = \delta\bar{\mathbf{q}}_{b,\eta,k} \otimes \hat{\bar{\mathbf{q}}}_{b,k} \tag{3.36}$$

Substituting Eq. (3.36) into Eq. (3.35) yields

$$\delta\bar{\mathbf{q}}_{sr,k}^{sc} = \delta\bar{\mathbf{q}}_{b,\eta,k} \otimes \hat{\bar{\mathbf{q}}}_{b,k} \otimes \begin{bmatrix} \delta q_{i,k}^{b} \\ \mathbf{T}_{b}^{sc}\delta\mathbf{q}_{i,k}^{b} \end{bmatrix} \otimes \hat{\bar{\mathbf{q}}}_{b,k}^{-1}\,. \tag{3.37}$$

Similar to the step taken to acquire Eq. (3.33), the last three terms of Eq. (3.37) can be collected as

$$\hat{\bar{\mathbf{q}}}_{b,k} \otimes \begin{bmatrix} \delta q_{i,k}^{b} \\ \mathbf{T}_{b}^{sc}\delta\mathbf{q}_{i,k}^{b} \end{bmatrix} \otimes \hat{\bar{\mathbf{q}}}_{b,k}^{-1} = \begin{bmatrix} \delta q_{i,k}^{b} \\ \hat{\mathbf{T}}_{b,k}\mathbf{T}_{b}^{sc}\delta\mathbf{q}_{i}^{b} \end{bmatrix}\,, \tag{3.38}$$

from which it follows that

$$\delta\bar{\mathbf{q}}_{sr,k}^{sc} = \delta\bar{\mathbf{q}}_{b,\eta,k} \otimes \begin{bmatrix} \hat{\mathbf{T}}_{b,k}\mathbf{T}_{b}^{sc}\delta\mathbf{q}_{i}^{b} \\ \delta q_{i,k}^{b} \end{bmatrix}\,. \tag{3.39}$$

Expanding the quaternion multiplication in Eq. (3.39) yields

$$\delta\bar{\mathbf{q}}^{sc}_{sr,k} = \begin{bmatrix} \delta q_{b,\eta,k} \\ \delta \mathbf{q}_{b,\eta,k} \end{bmatrix} \otimes \begin{bmatrix} \delta q^{b}_{i,k} \\ \hat{\mathbf{T}}_{b,k}\mathbf{T}^{sc}_{b}\delta\mathbf{q}^{b}_{i,k} \end{bmatrix} \tag{3.40}$$

$$= \begin{bmatrix} \delta q_{b,\eta,k}\delta q^{b}_{i,k} - \delta\mathbf{q}^{\mathrm{T}}_{b,\eta,k}\left[\hat{\mathbf{T}}_{b,k}\mathbf{T}^{sc}_{b}\delta\mathbf{q}^{b}_{i,k}\right] \\ \delta q^{b}_{i,k}\delta\mathbf{q}_{b,\eta,k} + \delta q_{b,\eta,k}\hat{\mathbf{T}}_{b,k}\mathbf{T}^{sc}_{b}\delta\mathbf{q}^{b}_{i,k} + \left[\hat{\mathbf{T}}_{b,k}\mathbf{T}^{sc}_{b}\delta\mathbf{q}^{b}_{i,k}\times\right]\delta\mathbf{q}_{b,\eta,k} \end{bmatrix}. \tag{3.41}$$

If we now assume small angles for both $\bar{\mathbf{q}}^{b}_{i}$ and $\bar{\mathbf{q}}_{b,\eta,k}$ and neglect second-order terms, Eq. (3.41) reduces to

$$\delta\bar{\mathbf{q}}^{sc}_{sr,k} = \begin{bmatrix} 1 \\ \delta\mathbf{q}_{b,\eta,k} + \hat{\mathbf{T}}_{b,k}\mathbf{T}^{sc}_{b}\delta\mathbf{q}^{b}_{i,k} \end{bmatrix}. \tag{3.42}$$

If we return to the definition of the corruption quaternion and the estimated corruption quaternion and recast their definitions under a small angle approximation, then they will take the form

$$\bar{\mathbf{q}}_{b,\eta,k} = \begin{bmatrix} 1 \\ \frac{1}{2}\boldsymbol{\theta}_{sc} \end{bmatrix},$$

and

$$\hat{\bar{\mathbf{q}}}_{b,k} = \begin{bmatrix} 1 \\ \frac{1}{2}\hat{\mathbf{b}}_{sc} \end{bmatrix},$$

respectively. Under this realization, the deviation of the true corruption quaternion and the estimated corruption quaternion will now be

$$\delta\bar{\mathbf{q}}_{b,\eta,k} = \bar{\mathbf{q}}_{b,\eta,k} \otimes \hat{\bar{\mathbf{q}}}^{-1}_{b,k}$$

and

$$\begin{bmatrix} 1 \\ \frac{1}{2}\boldsymbol{\theta}_{sc,k} \end{bmatrix} \otimes \begin{bmatrix} 1 \\ \frac{1}{2}\hat{\mathbf{b}}_{sc,k} \end{bmatrix} = \begin{bmatrix} 1 \\ \frac{1}{2}\boldsymbol{\theta}_{sc,k} - \frac{1}{2}\hat{\mathbf{b}}_{sc,k} \end{bmatrix}. \tag{3.43}$$

The true corruption $\boldsymbol{\theta}_{sc,k}$ includes both the star camera bias and noise so that the vector part of the corruption quaternion deviation is given by

$$\delta\mathbf{q}_{b,\eta,k} = \frac{1}{2}\delta\mathbf{b}_{sc} + \frac{1}{2}\boldsymbol{\eta}_{sc}\,, \tag{3.44}$$

where $\delta\mathbf{b}_{sc,k} = \mathbf{b}_{sc} - \hat{\mathbf{b}}_{sc,k}$. Under small angle approximations, the vector part of both the attitude quaternion deviation and the quaternion star camera measurement deviation can be realized as

$$\delta\mathbf{q}^{b}_{i,k} \approx \frac{1}{2}\delta\boldsymbol{\alpha}_k \qquad \text{and} \qquad \delta\mathbf{q}^{sc}_{sr,k} \approx \frac{1}{2}\boldsymbol{\psi}_k\,, \tag{3.45}$$

so that the quaternion star camera measurement deviation may be written as

$$\boldsymbol{\psi}_k = \hat{\mathbf{T}}_{b,k}\mathbf{T}^{sc}_{b}\delta\boldsymbol{\alpha}_k + \delta\mathbf{b}_{sc,k} + \boldsymbol{\eta}_{sc,k}\,. \tag{3.46}$$

3.1.4 Terrain Camera Model

A terrain camera tracks the position of a reference point on the surface (typically a landmark of interest or high visibility) to aid in precision navigation for landing. The measurement model utilized in this simulation is described as the position of the terrain camera with respect to a surface-fixed reference point, as seen in the surface-fixed frame. This can be written as

$$\mathbf{r}^{s}_{tc/ref,k} = \mathbf{T}^{s}_{f,k}\mathbf{T}^{f}_{i,k}\mathbf{r}^{i}_{imu,k} + \mathbf{T}^{s}_{f,k}\mathbf{T}^{f}_{i,k}\mathbf{T}^{i}_{b,k}\mathbf{r}^{b}_{tc/imu} - \mathbf{T}^{s}_{f,k}\mathbf{r}^{f}_{ref} + \mathbf{b}^{s}_{tc} + \boldsymbol{\eta}^{s}_{tc,k}\,, \tag{3.47}$$

where $\mathbf{r}^{b}_{tc/imu}$ is the position of the terrain camera with respect to the vehicle IMU as seen in the vehicle body frame, $\mathbf{r}^{f}_{ref}$ is the position of the reference point with respect to the center of the planet as seen in the planet-fixed frame, $\mathbf{b}^{s}_{tc}$

is the terrain camera measurement bias and $\boldsymbol{\eta}^s_{tc,k}$ is the terrain camera noise. The terrain camera bias is modeled as a zero-mean Gaussian distributed random constant, while the terrain camera measurement noise is modeled as a zero-mean white noise sequence. The transformation matrix $\mathbf{T}^s_{f,k}$ maps the planet-fixed frame to the surface-fixed frame. The transformation matrix $\mathbf{T}^f_{i,k}$ maps the inertial frame to the planet-fixed frame. The position of the surface reference point in planet-centered planet-fixed coordinates in terms of selenodetic parameters is given by [3, 19]

$$\mathbf{r}^f_{ref} = \begin{bmatrix} (N + h_{ref}) \cos\phi \cos\lambda \\ (N + h_{ref}) \cos\phi \sin\lambda \\ (N\,(1 - e^2) + h_{ref}) \sin\phi \end{bmatrix}, \tag{3.48}$$

where the latitude and longitude ϕ and θ are the sum of the reference point latitude and longitude plus map tie error as

$$\phi = \phi_{ref} + \phi_{map,k}$$

$$\lambda = \lambda_{ref} + \lambda_{map}\,.$$

In Eq. (3.48), h_{ref} is the selenodetic altitude of the surface reference point, e is the first eccentricity of the reference ellipsoid [19], and N is given by

$$N = \frac{R_e}{\sqrt{1 - e^2 \sin\phi^2}}\,, \tag{3.49}$$

where R_e is the equatorial radius. The subscript ref refers to the reference point, while the subscript map refers to the global map tie error value. Under this realization of the surface relative terrain camera, the estimated measurement value is given by

$$\hat{\mathbf{r}}^s_{tc/ref,k} = \hat{\mathbf{T}}^s_{f,k}\mathbf{T}^f_{i,k}\hat{\mathbf{r}}^i_{imu,k} + \hat{\mathbf{T}}^s_{f,k}\mathbf{T}^f_{i,k}\hat{\mathbf{T}}^i_{b,k}\mathbf{r}^b_{tc/imu} - \hat{\mathbf{T}}^s_{f,k}\hat{\mathbf{r}}^f_{ref,k} + \hat{\mathbf{b}}^s_{tc,k}\,, \tag{3.50}$$

where the estimated position of the reference point in the surface-fixed frame and estimated transformation from the planet-fixed to the surface-fixed frame utilize the estimated reference point coordinates as

$$\hat{\mathbf{r}}^f_{ref,k} = \mathbf{r}^f_{ref}(\hat{\phi}_k,\, \hat{\lambda}_k)$$
$$\hat{\mathbf{T}}^s_{f,k} = \mathbf{T}^s_{f,k}(\hat{\phi}_k,\, \hat{\lambda}_k)$$

and the estimated reference point coordinates are given by

$$\hat{\phi}_k = \phi_{ref} + \hat{\phi}_{map,k}$$
$$\hat{\lambda}_k = \lambda_{ref} + \hat{\lambda}_{map,k}\,.$$

We may now define the measurement deviation as the difference of the measurement value from the estimated measurement value, or

$$\delta\mathbf{r}^s_{tc/ref,k} = \mathbf{r}^s_{tc/ref,k} - \hat{\mathbf{r}}^s_{tc/ref,k}\,.$$

Introducing the definitions for the measurement value and estimated measurement value (from Eq. (3.47) and Eq. (3.50), respectively) yields

$$\begin{aligned}\delta\mathbf{r}^s_{tc/ref,k} = &\left[\mathbf{T}^s_{f,k}\mathbf{T}^f_{i,k}\mathbf{r}^i_{imu,k} - \hat{\mathbf{T}}^s_{f,k}\mathbf{T}^f_{i,k}\hat{\mathbf{r}}^i_{imu,k}\right] \\ &+ \left[\mathbf{T}^s_{f,k}\mathbf{T}^f_{i,k}\mathbf{T}^i_{b,k}\mathbf{r}^b_{tc/imu} - \hat{\mathbf{T}}^s_{f,k}\mathbf{T}^f_{i,k}\hat{\mathbf{T}}^i_{b,k}\mathbf{r}^b_{tc/imu}\right] - \left[\mathbf{T}^s_{f,k}\mathbf{r}^f_{ref} - \hat{\mathbf{T}}^s_{f,k}\hat{\mathbf{r}}^f_{ref,k}\right] \\ &+ \left[\mathbf{b}^s_{tc} - \hat{\mathbf{b}}^s_{tc,k}\right] + \boldsymbol{\eta}^s_{tc,k}\,.\end{aligned} \tag{3.51}$$

The position of the reference point may be expanded to first order about the estimated position of the reference point and the deviations in map tie error $\delta\phi_{map,k}$ and $\delta\lambda_{map,k}$ as

$$\mathbf{r}^f_{ref,k} = \hat{\mathbf{r}}^f_{ref,k} + \mathbf{r}^f_{ref,\phi,k}\delta\phi_{map,k} + \mathbf{r}^f_{ref,\lambda,k}\delta\lambda_{map,k}\,,$$

where

$$\mathbf{r}^f_{ref,\phi,k} = \begin{bmatrix} N_{\phi,k}\cos\hat{\phi}_k\cos\hat{\lambda}_k - (\hat{N}_k + h_{ref})\sin\hat{\phi}_k\cos\hat{\lambda}_k \\ N_{\phi,k}\cos\hat{\phi}_k\sin\hat{\lambda}_k - (\hat{N}_k + h_{ref})\sin\hat{\phi}_k\sin\hat{\lambda}_k \\ N_{\phi,k}(1-e^2)\sin\hat{\phi}_k + (\hat{N}_k(1-e^2) + h_{ref})\cos\hat{\phi}_k \end{bmatrix}$$

and

$$\mathbf{r}^f_{ref,\lambda,k} = \begin{bmatrix} -(\hat{N}_k + h_{ref})\cos\hat{\phi}_k\sin\hat{\lambda}_{tot} \\ (\hat{N}_k + h_{ref})\cos\hat{\phi}_k\cos\hat{\lambda}_{tot} \\ 0 \end{bmatrix} .$$

The values $\hat{N}_k$ and $N_{\phi,k}$ take the form

$$\hat{N}_k = \frac{R_e}{\sqrt{1 - e^2\sin^2\hat{\phi}_k}}$$
$$N_{\phi,k} = \frac{R_e e^2\sin\hat{\phi}_k\cos\hat{\phi}_k}{(1 - e^2\sin^2\hat{\phi}_k)^{3/2}} .$$

The transformation from the planet-fixed frame to the surface-fixed frame is expanded to first-order about the estimated transformation and the deviations in map tie error $\delta\phi_{map,k}$ and $\delta\lambda_{map,k}$ as

$$\mathbf{T}^s_{f,k} = \hat{\mathbf{T}}^s_{f,k} + \mathbf{T}^s_{f,\phi,k}\delta\phi_{map,k} + \mathbf{T}^s_{f,\lambda,k}\delta\lambda_{map,k} , \tag{3.52}$$

where the terms $\mathbf{T}^s_{f,\phi,k}$ and $\mathbf{T}^s_{f,\lambda,k}$ take the form

$$\mathbf{T}^s_{f,\phi,k} = \begin{bmatrix} 0 & 0 & 0 \\ -\cos\hat{\phi}_k\cos\hat{\lambda}_k & -\cos\hat{\phi}_k\sin\hat{\lambda}_k & -\sin\hat{\phi}_k \\ -\sin\hat{\phi}_k\cos\hat{\lambda}_k & -\sin\hat{\phi}_k\sin\hat{\lambda}_k & \cos\hat{\phi}_k \end{bmatrix}$$

and

$$\mathbf{T}^s_{f,\lambda,k} = \begin{bmatrix} -\cos\hat{\lambda}_k & -\sin\hat{\lambda}_k & 0 \\ \sin\hat{\phi}_k\sin\hat{\lambda}_k & -\sin\hat{\phi}_k\cos\hat{\lambda}_k & 0 \\ -\cos\hat{\phi}_k\sin\hat{\lambda}_k & \cos\hat{\phi}_k\cos\hat{\lambda}_k & 0 \end{bmatrix} .$$

The transformation from the vehicle body frame to the inertial frame may also be expanded about the estimated transformation to first order in $\delta\boldsymbol{\alpha}_k$ as

$$\mathbf{T}^i_{b,k} = \hat{\mathbf{T}}^i_{b,k} + \hat{\mathbf{T}}^i_{b,k}\left[\delta\boldsymbol{\alpha}_k\times\right] . \tag{3.53}$$

If we now substitute the definitions of $\mathbf{T}^s_{f,k}$ and $\mathbf{T}^i_{b,k}$ from Eq. (3.52) and Eq. (3.53), respectively, into the measurement deviation in Eq. (3.51), after rearranging terms and removing second-order terms we obtain

$$\begin{aligned}
\delta\mathbf{r}^s_{tc/ref,k} = {} & \hat{\mathbf{T}}^s_{f,k}\mathbf{T}^f_{i,k}\delta\mathbf{r}^i_{imu,k} + \mathbf{T}^s_{f,\phi,k}\left[\mathbf{T}^f_{i,k}\hat{\mathbf{r}}^i_{imu,k} + \mathbf{T}^f_{i,k}\hat{\mathbf{T}}^i_{b,k}\mathbf{r}^b_{tc/imu} - \hat{\mathbf{r}}^f_{ref,k}\right]\delta\phi_{map,k} \\
& + \mathbf{T}^s_{f,\lambda,k}\left[\mathbf{T}^f_{i,k}\hat{\mathbf{r}}^i_{imu,k} + \mathbf{T}^f_{i,k}\hat{\mathbf{T}}^i_{b,k}\mathbf{r}^b_{tc/imu} - \hat{\mathbf{r}}^f_{ref,k}\right]\delta\lambda_{map,k} \\
& + \hat{\mathbf{T}}^s_{f,k}\mathbf{T}^f_{i,k}\hat{\mathbf{T}}^i_{b,k}\left[\delta\boldsymbol{\alpha}_k\times\right]\mathbf{r}^b_{tc/imu} - \hat{\mathbf{T}}^s_{f,k}\delta\mathbf{r}^f_{ref,k} + \delta\mathbf{b}_{tc,k} + \boldsymbol{\eta}_{tc,k} ,
\end{aligned}$$

where

$$\begin{aligned}
\delta\mathbf{r}^i_{imu,k} &= \mathbf{r}^i_{imu,k} - \hat{\mathbf{r}}^i_{imu,k} \\
\delta\mathbf{r}^f_{ref,k} &= \mathbf{r}^f_{ref,k} - \hat{\mathbf{r}}^f_{ref,k}
\end{aligned}$$

and

$$\delta\mathbf{b}_{tc,k} = \mathbf{b}_{tc} - \hat{\mathbf{b}}_{tc,k}$$

If we expand the $\delta\mathbf{r}^f_{ref,k}$ term in Eq. (3.54) and utilize the first-order expansion of $\mathbf{r}^f_{ref,k}$ in $\delta\phi_{map,k}$ and $\delta\lambda_{map,k}$, we will have measurement deviation

$$\begin{aligned}
\delta\mathbf{r}^s_{tc/ref,k} = {} & \hat{\mathbf{T}}^s_{f,k}\mathbf{T}^f_{i,k}\delta\mathbf{r}^i_{imu,k} - \hat{\mathbf{T}}^s_{f,k}\mathbf{T}^f_{i,k}\hat{\mathbf{T}}^i_{b,k}\left[\mathbf{r}^b_{tc/imu}\times\right]\delta\boldsymbol{\alpha}_k \\
& + \left[\mathbf{T}^s_{f,\phi,k}\left[\mathbf{T}^f_{i,k}\hat{\mathbf{r}}^i_{imu,k} + \mathbf{T}^f_{i,k}\hat{\mathbf{T}}^i_{b,k}\mathbf{r}^b_{tc/imu} - \hat{\mathbf{r}}^f_{ref,k}\right] - \hat{\mathbf{T}}^s_{f,k}\mathbf{r}^f_{ref,\phi,k}\right]\delta\phi_{map,k} \\
& + \left[\mathbf{T}^s_{f,\lambda,k}\left[\mathbf{T}^f_{i,k}\hat{\mathbf{r}}^i_{imu,k} + \mathbf{T}^f_{i,k}\hat{\mathbf{T}}^i_{b,k}\mathbf{r}^b_{tc/imu} - \hat{\mathbf{r}}^f_{ref,k}\right] - \hat{\mathbf{T}}^s_{f,k}\mathbf{r}^f_{ref,\lambda,k}\right]\delta\lambda_{map,k} \\
& + \delta\mathbf{b}_{tc,k} + \boldsymbol{\eta}_{tc,k} .
\end{aligned} \tag{3.54}$$

3.2 Extended Kalman Filter

The continuous-discrete extended Kalman filter (EKF) is a direct extension of the optimal linear Kalman filter by utilizing non-linear functions for the system model and measurements. It has long been the de-facto industry standard and has been used in heritage missions, most notably the Apollo missions of the 1960's and 1970's and the U.S. Space Shuttle today. Dynamics and measurement models that govern space-based processes are inherently non-linear and are made usable for a linear update by use of a Taylor series expansion about the estimated state. The EKF has been heavily written and published and more information is available in Gelb [2], Maybeck [14], or Crassidis and Junkins [4].

The nonlinear dynamics model are given by

$$\dot{\mathbf{x}}(t) = \mathbf{f}(\mathbf{x}(t), t) + \mathbf{M}(t)\,\mathbf{w}(t) \qquad \text{for} \qquad t_{k-1} \leq t \leq t_k \tag{3.55}$$

where $\mathbf{x}(t)$ is the n-dimensional state of the system, $\mathbf{f}(\mathbf{x}(t), t)$ is the nonlinear system dynamics model, $\mathbf{M}(t)$ is a mapping matrix that maps the process noise (denoted as $\mathbf{w}(t)$) into the frame in which the estimation is taking place. The interval $t_{k-1} \leq t \leq t_k$ represents the time between external measurements. The process noise $\mathbf{w}(t)$ has random variable characteristics as

$$\mathrm{E}\{\mathbf{w}(t)\} = \mathbf{0} \qquad \text{and} \qquad \mathrm{E}\left\{\mathbf{w}(t)\mathbf{w}^{\mathrm{T}}(\tau)\right\} = \mathbf{Q}_{spec}\delta(t-\tau), \tag{3.56}$$

The process noise is assumed to be a zero-mean white noise process with a noise covariance of $\mathbf{Q}_{spec} \in \Re^{p\times p}$. $\mathbf{Q}_{spec}$ is an input to the EKF and can be

considered a primary avenue of tuning the filter. It accounts for uncertainties that are inevitably not captured in the nonlinear dynamics model.

The sensors used in the EKF design are also of nonlinear nature and are modeled as

$$\mathbf{y}_k = \mathbf{h}_k\left(\mathbf{x}_k\right) + \mathbf{v}_k\,. \tag{3.57}$$

where $\mathbf{x}_k = \mathbf{x}(t_k)$ and $\mathbf{y}_k = \mathbf{y}(t_k)$ are the state and measurement at time t_k, respectively. The nonlinear measurement model $\mathbf{h}_k(\mathbf{x}_k)$ is an m-dimensional vector that represents the measurement evaluated at the state $\mathbf{x}_k = \mathbf{x}\left(t_k\right)$. The measurement noise $\mathbf{v}_k$ has characteristics

$$\mathrm{E}\left\{\mathbf{v}_k\right\} = \mathbf{0} \qquad \text{and} \qquad \mathrm{E}\left\{\mathbf{v}_k\mathbf{v}_j^{\mathrm{T}}\right\} = \mathbf{R}_k\delta_{kj} \tag{3.58}$$

where k and j are different discrete measurement times. The measurement noise covariance $\mathbf{R}_k \in \Re^{m\times m}$ is an input to the EKF.

It is assumed that the system process noise and measurement noise are uncorrelated with respect to time, or

$$\mathrm{E}\left\{\mathbf{w}\left(t\right)\mathbf{v}_k^{\mathrm{T}}\right\} = \mathbf{0} \quad \forall \quad t, t_k. \tag{3.59}$$

The EKF operates by propagating the state estimate $\hat{\mathbf{x}}\left(t\right)$ and associated state estimate error covariance. The state estimate error is defined as

$$\mathbf{e}\left(t\right) = \mathbf{x}\left(t\right) - \hat{\mathbf{x}}\left(t\right)\,, \tag{3.60}$$

then we can realize the state estimate error characteristics as

$$\mathrm{E}\left\{\mathbf{e}(t)\right\} = \mathbf{0} \qquad \text{and} \qquad \mathrm{E}\left\{\mathbf{e}(t)\mathbf{e}^{\mathrm{T}}(t)\right\} = \mathbf{P}(t)\,. \tag{3.61}$$

The expected value of the state estimate error chosen as zero to create an unbiased filter. The state estimate error covariance $\mathbf{P}(t)$ is of great interest and will be shown to be pivotal in the EKF algorithm. The estimation error immediately before a measurement update at time t_k is

$$\mathbf{e}_k^- = \mathbf{x}_k - \hat{\mathbf{x}}_k^- \,, \tag{3.62}$$

and the estimation error immediately after a measurement update at time t_k is

$$\mathbf{e}_k^+ = \mathbf{x}_k - \hat{\mathbf{x}}_k^+ \,. \tag{3.63}$$

The superscripts $-$ and $+$ therefore represent the estimation error or state estimate immediately before or immediately after a measurement update, respectively.

3.2.1 Propagation

Recall that in the absence of external measurements, the EKF propagates the state estimate and the state estimate error covariance forward in time utilizing IMU measurements in the evolution of the state estimate and associated error covariance. The derivation of the EKF propagation begins with the general nonlinear system model

$$\dot{\mathbf{x}}(t) = \mathbf{f}(\mathbf{x}(t), t) + \mathbf{M}(t)\mathbf{w}(t) \qquad \text{for} \qquad t_{k-1} \leq t \leq t_k \,. \tag{3.64}$$

The estimate of the system is the expected value, or

$$\dot{\hat{\mathbf{x}}} = \mathrm{E}\left\{\mathbf{f}(\mathbf{x}(t), t)\right\} + \mathbf{M}(t)\mathrm{E}\left\{\mathbf{w}(t)\right\} \,. \tag{3.65}$$

The nonlinear system function $\mathbf{f}(\mathbf{x}(t), t)$ may be linearized about the current state estimate $\hat{\mathbf{x}}$ via a Taylor series expansion (and neglecting higher-order terms) so that

$$\dot{\hat{\mathbf{x}}} = \mathrm{E}\left\{\mathbf{f}(\hat{\mathbf{x}}(t), t) + \mathbf{F}(\hat{\mathbf{x}}(t), t)(\mathbf{x}(t) - \hat{\mathbf{x}}(t)\right\} + \mathbf{M}(t)\mathrm{E}\left\{\mathbf{w}(t)\right\}\,, \tag{3.66}$$

where $\mathbf{F}(\hat{\mathbf{x}}(t), t)$ is the state propagation matrix and is defined as

$$\mathbf{F}(\hat{\mathbf{x}}(t), t) = \left[\frac{\partial \mathbf{f}(\mathbf{x}(t), t)}{\partial \mathbf{x}(t)}\right]_{\mathbf{x}(t)=\hat{\mathbf{x}}(t)}.$$

Noting that only the deviation between the true and estimated state is a random variable (from the first term) then

$$\dot{\hat{\mathbf{x}}} = \mathbf{f}(\hat{\mathbf{x}}(t), t) + \mathbf{F}(\hat{\mathbf{x}}(t), t)\mathrm{E}\left\{(\mathbf{x}(t) - \hat{\mathbf{x}}(t))\right\} + \mathbf{M}(t)\mathrm{E}\left\{\mathbf{w}(t)\right\}\,. \tag{3.67}$$

If we apply the assumptions that the EKF is an unbiased estimator and the process noise is zero-mean, then

$$\mathrm{E}\left\{(\mathbf{x}(t) - \hat{\mathbf{x}}(t))\right\} = \mathbf{0} \qquad \text{and} \qquad \mathrm{E}\left\{\mathbf{w}(t)\right\} = \mathbf{0}\,,$$

adn the evolution of the estimated state reduces to

$$\dot{\hat{\mathbf{x}}}(t) = \mathbf{f}(\hat{\mathbf{x}}(t), t) \qquad \text{for} \qquad t_{k-1} \leq t \leq t_k\,. \tag{3.68}$$

Recall that the state estimation error is the difference of the true and estimated states, so that by introducing their definitions from Eq. (3.64) and Eq. (3.68) we have

$$\dot{\mathbf{e}}(t) = \dot{\mathbf{x}}(t) - \dot{\hat{\mathbf{x}}}(t) = \mathbf{f}(\mathbf{x}(t), t) + \mathbf{M}(t)\mathbf{w}(t) - \mathbf{f}(\hat{\mathbf{x}}(t), t)\,. \tag{3.69}$$

As was performed earlier, we may again take a first-order Taylor series expansion about the estimated state $\hat{\mathbf{x}}(t)$ (and neglect higher-order terms) to obtain

$$\dot{\mathbf{e}}(t) = \mathbf{F}(\hat{\mathbf{x}}(t), t)(\mathbf{x}(t) - \hat{\mathbf{x}}(t)) + \mathbf{M}(t)\mathbf{w}(t)\,, \tag{3.70}$$

over the interval $t_{k-1} \leq t \leq t_k$. The solution to Eq. (3.70) is [18]

$$\mathbf{e}(t) = \mathbf{\Phi}(t, t_{k-1})\mathbf{e}(t_{k-1}) + \int_{t_{k-1}}^{t} \mathbf{\Phi}(t, \tau)\mathbf{M}(\tau)\mathbf{w}(\tau)d\tau\,, \tag{3.71}$$

which is true for $t \geq t_{k-1}$. The state transition matrix which maps the state forward in time from t_{k-1} to t is designated by $\mathbf{\Phi}(t, t_{k-1})$. It follows the matrix differential equation

$$\dot{\mathbf{\Phi}}(t, t_{k-1}) = \mathbf{F}(\hat{\mathbf{x}}(t), t)\mathbf{\Phi}(t, t_{k-1})$$

with initial condition

$$\mathbf{\Phi}(t_{k-1}, t_{k-1}) = \mathbf{I}^{n\times n}\,.$$

Recall the definition of the state estimate error covariance as

$$\mathbf{P}(t) = \mathrm{E}\left\{\mathbf{e}(t)\mathbf{e}^{\mathrm{T}}(t)\right\}\,,$$

so that if the solution of the state estimation error of Eq. (3.72) is inserted, we will have the solution to the estimation error covariance as

$$\mathbf{P}(t) = \mathbf{\Phi}(t, t_{k-1})\mathbf{P}(t_{k-1})\mathbf{\Phi}^{\mathrm{T}}(t, t_{k-1}) + \int_{t_{k-1}}^{t} \mathbf{\Phi}(t, \tau)\mathbf{M}(\tau)\mathbf{Q}_{spec}(\tau)\mathbf{M}^{\mathrm{T}}(\tau)\mathbf{\Phi}^{\mathrm{T}}(t, \tau)d\tau\,. \tag{3.72}$$

The latter half of Eq. (3.72) within the integral may be redefined as matrix $\mathbf{Q}(t)$ as

$$\mathbf{Q}(t) = \int_{t_{k-1}}^{t} \mathbf{\Phi}(t, \tau)\mathbf{M}(\tau)\mathbf{Q}_{spec}(\tau)\mathbf{M}^{\mathrm{T}}(\tau)\mathbf{\Phi}^{\mathrm{T}}(t, \tau)d\tau\,. \tag{3.73}$$

Differentiating $\mathbf{Q}(t)$ with respect to time yields

$$\dot{\mathbf{Q}}(t) = \mathbf{F}(\hat{\mathbf{x}}(t), t)\mathbf{Q}(t) + \mathbf{Q}(t)\mathbf{F}^{\mathrm{T}}(\hat{\mathbf{x}}(t), t) + \mathbf{M}(t)\mathbf{Q}_{spec}(\tau)\mathbf{M}^{\mathrm{T}}(t)\,, \tag{3.74}$$

for $t_{k-1} \leq t \leq t_k$. The differential equation for $\mathbf{Q}(t)$ has the initial condition

$$\mathbf{Q}(t_{k-1}) = \mathbf{0}_{n\times n}\,. \tag{3.75}$$

The continuous-discrete EKF will propagate the state estimate and state estimate error covariance forward in time over $t_{k-1} \leq t \leq t_k$ until an update is made at time t_k (which is discussed in the next section). Upon update, the propagation re-initializes and propagates the state forward again. To propagate the state forward through the time interval between measurements, the state estimate is numerically integrated via

$$\dot{\hat{\mathbf{x}}}(t) = \mathbf{f}(\hat{\mathbf{x}}(t), t)\,, \tag{3.76}$$

with initial condition $\hat{\mathbf{x}}(t_{k-1})$. To propagate the state estimate error covariance through $t_{k-1} \leq t \leq t_k$, the differential equations

$$\dot{\mathbf{\Phi}}(t, t_{k-1}) = \mathbf{F}(\hat{\mathbf{x}}(t), t)\mathbf{\Phi}(t, t_{k-1}) \tag{3.77}$$

$$\dot{\mathbf{Q}}(t) = \mathbf{F}(\hat{\mathbf{x}}(t), t)\mathbf{Q}(t) + \mathbf{Q}(t)\mathbf{F}^{\mathrm{T}}(\hat{\mathbf{x}}(t), t) + \mathbf{M}(t)\mathbf{Q}_{spec}(\tau)\mathbf{M}^{\mathrm{T}}(t) \tag{3.78}$$

are numerically integrated through the time interval with initial conditions

$$\mathbf{\Phi}(t_{k-1}, t_{k-1}) = \mathbf{I}_{n\times n} \tag{3.79}$$

$$\mathbf{Q}(t_{k-1}) = \mathbf{0}_{n\times n}\,. \tag{3.80}$$

Upon obtaining $\mathbf{\Phi}(t_k, t_{k-1})$ and $\mathbf{Q}(t_k)$, the state estimate error covariance is mapped forward by

$$\mathbf{P}(t_k) = \mathbf{\Phi}(t_k, t_{k-1})\mathbf{P}(t_{k-1})\mathbf{\Phi}^{\mathrm{T}}(t_k, t_{k-1}) + \mathbf{Q}(t_k)\,. \tag{3.81}$$

The time interval for state estimate and error covariance propagation can be defined by a number of events. For this simulation those events include a new IMU measurement or the introduction of an external measurement. It is typical that the IMU delivers measurements at a higher rate than most external sensors, so the propagation routine is invoked for each IMU measurement for time intervals inversely proportional to the IMU measurement delivery rate. At any time a measurement is made available, the update algorithm is invoked.

3.2.2 Update

At the measurement time denoted by t_k, an external measurement is made available to the navigation algorithm. The difference between the actual and estimated measurement, combined with the measurement sensitivity evaluated at the estimated measurement value are utilized to update the state estimate and associated state estimate error covariance. The update is assumed to be instantaneous. The time before the update is labeled t_k^-, and the time after the update is labeled t_k^+. The nonlinear representation for the actual measurement takes the form

$$\mathbf{y}_k = \mathbf{h}_k(\mathbf{x}_k) + \mathbf{v}_k\,. \tag{3.82}$$

The estimated measurement is found by taking the expected value of the actual measurement as

$$\hat{\mathbf{y}}_k = \mathrm{E}\left\{\mathbf{y}_k\right\} = \mathrm{E}\left\{\mathbf{h}_k(\mathbf{x}_k)\right\} + \mathrm{E}\left\{\mathbf{v}_k\right\} . \tag{3.83}$$

In a similar manner to the propagation derivation, we now take a first-order Taylor series (neglecting higher-order terms) about the *a priori* state estimate $\hat{\mathbf{x}}_k^-$ so that

$$\hat{\mathbf{y}}_k = \mathrm{E}\left\{\mathbf{h}_k(\hat{\mathbf{x}}_k^-) + \mathbf{H}_k(\hat{\mathbf{x}}_k^-)(\mathbf{x}_k - \hat{\mathbf{x}}_k)\right\} + \mathrm{E}\left\{\mathbf{v}_k\right\} , \tag{3.84}$$

where $\mathbf{H}_k(\hat{\mathbf{x}}_k^-)$ is the measurement sensitivity matrix given by

$$\mathbf{H}_k(\hat{\mathbf{x}}_k^-) = \left[\frac{\partial \mathbf{h}_k(\mathbf{x}_k)}{\partial \mathbf{x}_k}\right]_{\mathbf{x}_k = \hat{\mathbf{x}}_k^-} . \tag{3.85}$$

Eq. (3.84) has random variables only in the quantity $(\mathbf{x}_k - \hat{\mathbf{x}}_k)$ and $\mathbf{v}_k$ and can be rewritten as

$$\hat{\mathbf{y}}_k = \mathbf{h}_k(\hat{\mathbf{x}}_k^-) + \mathbf{H}_k(\hat{\mathbf{x}}_k^-)\mathrm{E}\left\{(\mathbf{x}_k - \hat{\mathbf{x}}_k)\right\} + \mathrm{E}\left\{\mathbf{v}_k\right\} . \tag{3.86}$$

Recall that we have defined the EKF as an unbiased estimator so that
$\mathrm{E}\left\{(\mathbf{x}_k - \hat{\mathbf{x}}_k)\right\} = \mathbf{0}$, and that the measurement noise is assumed to be zero-mean so that
$\mathrm{E}\left\{\mathbf{v}_k\right\} = \mathbf{0}$. Thus, Eq. (3.86) reduces to

$$\hat{\mathbf{y}}_k = \mathbf{h}_k(\hat{\mathbf{x}}_k^-) . \tag{3.87}$$

The Kalman gain matrix is defined as

$$\mathbf{K}_k = \mathbf{P}_k^- \mathbf{H}_k^{\mathrm{T}}(\hat{\mathbf{x}}_k^-)\mathbf{W}_k^{-1} , \tag{3.88}$$

where $\mathbf{W}_k$ is the residual covariance matrix and is defined by

$$\mathbf{W}_k = \mathbf{H}_k(\hat{\mathbf{x}}_k^-)\mathbf{P}_k^-\mathbf{H}_k^{\mathrm{T}}(\hat{\mathbf{x}}_k^-) + \mathbf{R}_k \,, \tag{3.89}$$

where $\mathbf{R}_k$ is the measurement noise covariance. If we define the measurement residual as

$$\mathbf{r}_k = \mathbf{y}_k - \hat{\mathbf{y}}_k \,, \tag{3.90}$$

then the state estimate and state estimate error covariance may be updated with the Joseph formula as

$$\hat{\mathbf{x}}_k^+ = \hat{\mathbf{x}}_k^- + \mathbf{K}_k\mathbf{r}_k \tag{3.91}$$

$$\mathbf{P}_k^+ = \left[\mathbf{I}_{n\times n} - \mathbf{K}_k\mathbf{H}_k(\hat{\mathbf{x}}_k^-)\right]\mathbf{P}_k^-\left[\mathbf{I}_{n\times n} - \mathbf{K}_k\mathbf{H}_k(\hat{\mathbf{x}}_k^-)\right]^{\mathrm{T}} + \mathbf{K}_k\mathbf{R}_k\mathbf{K}_k^{\mathrm{T}} \,. \tag{3.92}$$

The updated state estimate and state estimate error covariance are called the *a posteriori* values, and are denoted with a superscript "+".

3.2.2.1 Multiplicative Attitude Update

In the propagation derivation of the attitude error, a multiplicative approach was considered which resulted in the attitude error being represented by $\delta\boldsymbol{\alpha} \in \Re^{3\times 1}$, This requires a small angle approximation, and reduces the size of the state estimate error covariance for propagation by one element while removing the unity norm constraint required of pure rotation quaternions. The state is then propagated utilizing small-angle approximations and associated quaternion of rotation is reconstructed. For the update, the elements of $\hat{\mathbf{x}}_k^+$ corresponding to the attitude are actually elements of the small-angle update

$\delta\boldsymbol{\alpha}_k^+$ so that the quaternion update is reconstructed as

$$\hat{\bar{\mathbf{q}}}_k^+ = \begin{bmatrix} 1 \\ \frac{1}{2}\delta\boldsymbol{\alpha}_k^+ \end{bmatrix} \otimes \hat{\bar{\mathbf{q}}}_k^- \,, \tag{3.93}$$

where $\hat{\bar{\mathbf{q}}}_k^-$ is the estimated attitude quaternion before the update. The updated attitude quaternion $\hat{\bar{\mathbf{q}}}_k^+$ holds the unity norm constraint only to first-order, so a normalization is required after the update to ensure that $\hat{\bar{\mathbf{q}}}_k^{+\mathrm{T}} \hat{\bar{\mathbf{q}}}_k^+ = 1$.

3.2.2.2 Kalman Gain

Recall that the expression for the Kalman gain $\mathbf{K}_k$ involved the inverse of the residual covariance matrix $\mathbf{W}_k$. The Kalman gain matrix can be rewritten as

$$\mathbf{K}_k \mathbf{W}_k = \mathbf{P}_k^- \mathbf{H}_k^{\mathrm{T}}(\hat{\mathbf{x}}_k^-) \,. \tag{3.94}$$

The issue here is that the inversion of a matrix with square dimension of 3 or greater becomes computationally intensive. Vector measurements (which are provided by the star camera, velocimeter, and terrain camera) are dimension of at least 3, and it is possible that multiple measurements are being processed simultaneously, thereby further impacting the computational burden. It is desirable then to attempt to avoid this calculation. Fortunately, we can use the fact that the residual covariance matrix is symmetric positive definite and may be represented as a lower triangular matrix and its transpose via a Cholesky decomposition as

$$\mathbf{W}_k = \mathbf{L}_k \mathbf{L}_k^{\mathrm{T}} \,, \tag{3.95}$$

so that the Kalman gain expression is

$$\mathbf{K}_k\mathbf{L}_k\mathbf{L}_k^{\mathrm{T}} = \mathbf{P}_k^-\mathbf{H}_k^{\mathrm{T}}(\hat{\mathbf{x}}_k^-)\,. \tag{3.96}$$

The matrix $\mathbf{K}_k\mathbf{L}_k$ can be found with forward substitution, and subsequently $\mathbf{K}_k$ may be found with backward substitution. This method will mitigate excessive computational burden of inverting a large residual covariance matrix.

3.2.3 Propagation Structure

Recall that the state estimate and estimation error covariance are propagated through the time interval $t \in [t_{k-1}, t_k]$ by first numerically integrating the equations

$$\begin{aligned}
\dot{\hat{\mathbf{x}}}(t) &= \mathbf{f}(\hat{\mathbf{x}}(t), t) \\
\dot{\mathbf{\Phi}}(t, t_{k-1}) &= \mathbf{F}(\hat{\mathbf{x}}(t), t)\mathbf{\Phi}(t, t_{k-1}) \\
\dot{\mathbf{Q}}(t) &= \mathbf{F}(\hat{\mathbf{x}}(t), t)\mathbf{Q}(t) + \mathbf{Q}(t)\mathbf{F}^{\mathrm{T}}(\hat{\mathbf{x}}(t), t) + \mathbf{M}(t)\mathbf{Q}_{spec}(\tau)\mathbf{M}^{\mathrm{T}}(t)
\end{aligned}$$

through the time interval with the initial conditions

$$\begin{aligned}
\hat{\mathbf{x}}(t_{k-1}) &= \hat{\mathbf{x}}_{k-1}^+ \\
\mathbf{\Phi}(t_{k-1}, t_{k-1}) &= \mathbf{I}_{n\times n} \\
\mathbf{Q}(t_{k-1}) &= \mathbf{0}_{n\times n}\,,
\end{aligned}$$

where $\hat{\mathbf{x}}_{k-1}^+$ is the *a posteriori* state estimate from the previous update. In the case where $t_{k-1} = t_0$, then $\hat{\mathbf{x}}_0^+ = \hat{\mathbf{x}}_0$. The resulting solutions will then be substituted into

$$\mathbf{P}(t_k) = \mathbf{\Phi}(t_k, t_{k-1})\mathbf{P}(t_{k-1})\mathbf{\Phi}^{\mathrm{T}}(t_k, t_{k-1}) + \mathbf{Q}(t_k)\,,$$

to obtain the state estimate and estimate error covariance at the interval end time t_k. In the case where $t_{k-1} = t_0$, then $\mathbf{P}(t_{k-1}) = \mathbf{P}_0$. We will define the propagated state estimate as

$$\hat{x} = \begin{pmatrix} \hat{\mathbf{r}}^i_{imu} \\ \hat{\mathbf{v}}^i_{imu} \\ \hat{\mathbf{q}}^b_i \\ \hat{\mathbf{r}}^b_{cg/imu,dev} \\ \hat{\mathbf{p}}_a \\ \hat{\mathbf{p}}_g \\ \hat{\mathbf{p}}_m \\ \hat{\mathbf{p}}_s \end{pmatrix}, \tag{3.97}$$

where the latter four vectors (labeled with $\mathbf{p}$) are parameter vectors for the accelerometer, gyroscope, map tie error, and sensors. They all take the forms

$$\mathbf{p}_a = \begin{bmatrix} \mathbf{b}_a \\ \mathbf{s}_a \\ \boldsymbol{\gamma}_a \end{bmatrix} \in \Re^{12\times 1}, \ \mathbf{p}_g = \begin{bmatrix} \mathbf{b}_g \\ \mathbf{s}_g \\ \boldsymbol{\gamma}_g \end{bmatrix} \in \Re^{12\times 1}, \ \mathbf{p}_m = \begin{bmatrix} \phi_{map,k} \\ \lambda_{map,k} \end{bmatrix} \in \Re^{2\times 1}, \text{ and } \mathbf{p}_s = \begin{bmatrix} b_{alt} \\ \mathbf{b}_{vel} \\ \mathbf{b}_{sc} \\ \mathbf{b}_{tc} \end{bmatrix} \in \Re^{10\times 1}. \tag{3.98}$$

It is understood that each bias term is situated in their respective sensor or IMU case frame. Note that the four element quaternion is present in the propagated state vector. This is different in the update stage where the update is given in $\delta\boldsymbol{\alpha}$ and must be translated into a quaternion to produce an *a posteriori* attitude quaternion estimate that is summarily propagated. The propagated state vector thus has 49 states in its full-order structure.

Recall that the state transition matrix is acquired by integrating the state propagation matrix $\mathbf{F}(\hat{\mathbf{x}}(t), t)$. Only the first three vectors (position, velocity, attitude quaternion) of the total state vector have nonzero dynamics.

The state propagation matrix can be partitioned as

$$\mathbf{F}(\hat{\mathbf{x}}(t), t) = \begin{bmatrix} \mathbf{F}_{dyn}^{9\times 9} & \mathbf{F}_{par}^{9\times 39} \\ \mathbf{0}^{39\times 9} & \mathbf{0}^{39\times 39} \end{bmatrix}, \tag{3.99}$$

where the submatrices $\mathbf{F}_{dyn}^{9\times 9}$ and $\mathbf{F}_{par}^{9\times 39}$ are the dynamics and parameter partitions, and can be further partitioned as

$$\mathbf{F}_{dyn} = \begin{bmatrix} \mathbf{0}^{3\times 3} & \mathbf{F}_{dyn,12} & \mathbf{0}^{3\times 3} \\ \mathbf{F}_{dyn,21} & \mathbf{0}^{3\times 3} & \mathbf{F}_{dyn,23} \\ \mathbf{0}^{3\times 3} & \mathbf{0}^{3\times 3} & \mathbf{F}_{dyn,33} \end{bmatrix}$$

$$\mathbf{F}_{par} = \begin{bmatrix} \mathbf{0}^{3\times 3} & \mathbf{0}^{3\times 12} & \mathbf{0}^{3\times 12} & \mathbf{0}^{3\times 2} & \mathbf{0}^{3\times 10} \\ \mathbf{F}_{par,21} & \mathbf{F}_{par,22} & \mathbf{0}^{3\times 12} & \mathbf{0}^{3\times 2} & \mathbf{0}^{3\times 10} \\ \mathbf{0}^{3\times 3} & \mathbf{0}^{3\times 12} & \mathbf{F}_{par,33} & \mathbf{0}^{3\times 2} & \mathbf{0}^{3\times 10} \end{bmatrix}.$$

The state propagation matrix is thus partitioned so that the differential equations that dictate the evolution of the estimation errors for position, velocity, and attitude are aligned with their respective elements within the state vector. That is to say, the first three row-groups of the state propagation matrix are dedicated to the error dynamics differential equations in terms of each error group. Therefore, each non-zero submatrix is a term associated with the differential equations of Eq. (2.48) and Eq. (2.63), and placed in the matrix in a position to align themselves both with the appropriate state vector element row, and error source term column. Each non-zero submatrix in the dynamics

and parameter submatrices of the state propagation matrix thus take the form

$$\begin{aligned}
\mathbf{F}_{dyn,12} &= \mathbf{I}^{3\times 3} \\
\mathbf{F}_{dyn,21} &= \mathbf{G}(\hat{\mathbf{r}}^i_{cg}) \\
\mathbf{F}_{dyn,23} &= -\left[\hat{\mathbf{T}}^i_b[\mathbf{T}^b_c\hat{\mathbf{a}}^c_{ng}\times] + \mathbf{G}(\hat{\mathbf{r}}^i_{cg})\hat{\mathbf{T}}^i_b[\hat{\mathbf{r}}^b_{cg/imu}\times]\right] \\
\mathbf{F}_{dyn,33} &= -[\mathbf{T}^b_c\hat{\boldsymbol{\omega}}^c\times]
\end{aligned}$$

and

$$\begin{aligned}
\mathbf{F}_{par,21} &= \mathbf{G}(\hat{\mathbf{r}}^i_{cg})\hat{\mathbf{T}}^i_b \\
\mathbf{F}_{par,22} &= -\hat{\mathbf{T}}^i_b\mathbf{T}^b_c\left[\mathbf{I}^{3\times 3}|\mathbf{D}(\mathbf{a}^c_{ng,m})|\mathbf{N}(\mathbf{a}^c_{ng,m})\right] \\
\mathbf{F}_{par,33} &= -\mathbf{T}^b_c\left[\mathbf{I}^{3\times 3}|\mathbf{D}(\boldsymbol{\omega}^c_m)|\mathbf{N}(\boldsymbol{\omega}^c_m)\right] \ .
\end{aligned}$$

With the nonlinear function $\mathbf{f}(\hat{\mathbf{x}}(t),t)$ and state propagation matrix $\mathbf{F}(\hat{\mathbf{x}}(t),t)$ at our disposal, it is necessary to obtain an initial estimate and initial estimate error covariance. The initial estimate and associated error covariance are typically created by allocating a standard deviation of certainty for each state-group and placing those values in the diagonal of $\mathbf{P}_0$. The initial covariance is then sampled to create an initial state estimate.

3.2.4 Update/Measurement Processing

To successfully update the state estimate and estimate error covariance, the measurement residual and measurement sensitivity evaluated at the *a priori* state estimate are required. The measurement residual and sensitivity

characteristics vary from sensor to sensor and will be discussed sequentially. If two or more measurements are processed simultaneously, then their residuals and sensitivity matrices are concatenated and processed in a single expression. If we have two measurement residuals

$$\mathbf{r}_{1,k} \qquad \text{and} \qquad \mathbf{r}_{2,k}\,,$$

and their associated sensitivity matrices as

$$\mathbf{H}_{1,k}(\hat{\mathbf{x}}_k^-) \qquad \text{and} \qquad \mathbf{H}_{2,k}(\hat{\mathbf{x}}_k^-)\,,$$

then we would concatenate the residuals and sensitivity matrices for simultaneous processing as

$$\mathbf{r}_k = \begin{bmatrix} \mathbf{r}_{1,k} \\ \mathbf{r}_{2,k} \end{bmatrix} \qquad \text{and} \qquad \mathbf{H}_k = \begin{bmatrix} \mathbf{H}_{1,k} \\ \mathbf{H}_{2,k} \end{bmatrix}\,. \tag{3.100}$$

Each measurement type has (likely) a unique residual and a unique measurement sensitivity matrix structure. However each measurement sensitivity matrix structure can be generalized and partitioned as

$$\mathbf{H}_k = \begin{bmatrix} \mathbf{H}_r^{m\times 3} & \mathbf{H}_v^{m\times 3} & \mathbf{H}_{\delta\alpha}^{m\times 3} & \mathbf{H}_{\Delta r_{cg/imu}}^{m\times 3} & \mathbf{H}_{p_a}^{m\times 12} & \mathbf{H}_{p_g}^{m\times 12} & \mathbf{H}_{p_m}^{m\times 2} & \mathbf{H}_{p_s}^{m\times 10} \end{bmatrix}\,. \tag{3.101}$$

The sensitivity matrix is therefore constructed to align with the elements of the propagated state estimate vector. Recall that the parameter vectors for the accelerometer, gyroscope, maptie, and sensors are

$$\mathbf{p}_a = \begin{bmatrix} \mathbf{b}_a \\ \mathbf{s}_a \\ \boldsymbol{\gamma}_a \end{bmatrix}\,, \quad \mathbf{p}_g = \begin{bmatrix} \mathbf{b}_g \\ \mathbf{s}_g \\ \boldsymbol{\gamma}_g \end{bmatrix}\,, \quad \mathbf{p}_m = \begin{bmatrix} \phi_{map,k} \\ \lambda_{map} \end{bmatrix}\,, \quad \text{and} \quad \mathbf{p}_s = \begin{bmatrix} b_{alt} \\ \mathbf{b}_{vel} \\ \mathbf{b}_{sc} \\ \mathbf{b}_{tc} \end{bmatrix}\,.$$

3.2.4.1 Altimeter

The estimated spherical altimeter measurement value at time t_k is

$$\hat{h}_k = \left[\hat{r}^{i,-}_{alt,k} - r_{moon}\right] + \hat{b}^{-}_{alt,k}\,, \tag{3.102}$$

where the *a priori* magnitude of the altimeter position is

$$\hat{r}^{i,-}_{alt,k} = \|\hat{\mathbf{r}}^{i,-}_{alt,k} + \hat{\mathbf{T}}^{i,-}_{b,k}\mathbf{r}^{b}_{alt/imu}\|\,. \tag{3.103}$$

If the actual measurement at time t_k is denoted h_k, then the deviation will yield Eq. (3.10) as

$$\delta h_k = \frac{\hat{\mathbf{r}}^{i^{\mathrm{T}}}_{alt,k}}{\hat{r}^{i}_{alt}}\delta\mathbf{r}^{i}_{imu,k} - \frac{\hat{\mathbf{r}}^{i^{\mathrm{T}}}_{alt,k}}{\hat{r}^{i}_{alt,k}}\hat{\mathbf{T}}^{i}_{b,k}[\mathbf{r}^{b}_{alt/imu}\times]\delta\boldsymbol{\alpha}_k + \delta b_{alt,k} + \eta_{alt,k}\,.$$

Thus, the sensitivity matrix section contributed by an altimeter reading will take the form

$$\mathbf{H}_{alt} = \begin{bmatrix}\mathbf{H}^{1\times3}_{r,alt} & \mathbf{0}^{1\times3} & \mathbf{H}^{1\times3}_{\delta\boldsymbol{\alpha},alt} & \mathbf{0}^{1\times3} & \mathbf{0}^{1\times12} & \mathbf{0}^{1\times12} & \mathbf{0}^{1\times2} & \mathbf{H}^{1\times10}_{b_{alt}}\end{bmatrix}\,,$$

where the populated columns are written as

$$\mathbf{H}_{r,alt} = \frac{\hat{\mathbf{r}}^{i^{\mathrm{T}}}_{alt,k}}{\hat{r}^{i}_{alt}} \tag{3.104}$$

$$\mathbf{H}_{\delta\boldsymbol{\alpha},alt} = -\frac{\hat{\mathbf{r}}^{i^{\mathrm{T}}}_{alt,k}}{\hat{r}^{i}_{alt,k}}\hat{\mathbf{T}}^{i}_{b,k}[\mathbf{r}^{b}_{alt/imu}\times] \tag{3.105}$$

$$\mathbf{H}_{b_{alt}} = \begin{bmatrix}1 & \mathbf{0}^{1\times9}\end{bmatrix}^{\mathrm{T}}\,. \tag{3.106}$$

3.2.4.2 Velocimeter

Recall from Eq. (3.12) that the estimated spherical surface relative velocity measurement value is

$$\hat{\mathbf{v}}^{v}_{rel,k} = \mathbf{T}^{v}_{b}\hat{\mathbf{T}}^{b}_{i,k}\left[\hat{\mathbf{v}}^{i}_{vel,k} - \boldsymbol{\omega}_L \times \hat{\mathbf{r}}^{i}_{vel,k}\right] + \hat{\mathbf{b}}^{v}_{vel,k}\,. \tag{3.107}$$

and that the measurement deviation takes the form

$$\begin{aligned}\delta\mathbf{v}^v_{rel,k} = &-\mathbf{T}^v_b\hat{\mathbf{T}}^b_{i,k}[\boldsymbol{\omega}_L\times]\delta\mathbf{r}^i_{imu,k} + \mathbf{T}^v_b\hat{\mathbf{T}}^b_{i,k}\delta\mathbf{v}^i_{imu,k} \\ &+ \mathbf{T}^v_b\left[(\hat{\boldsymbol{\omega}}^b_k\times\mathbf{r}^b_{vel/imu})\times\right]\delta\boldsymbol{\alpha}_k + \mathbf{T}^v_b\hat{\mathbf{T}}^b_{i,k}[\boldsymbol{\omega}_L\times]\hat{\mathbf{T}}^i_{b,k}[\mathbf{r}^b_{vel/imu}\times]\delta\boldsymbol{\alpha}_k \\ &+ \mathbf{T}^v_b\left[\hat{\mathbf{T}}^i_{b,k}(\hat{\mathbf{v}}^i_{vel,k} - \boldsymbol{\omega}_L\times\hat{\mathbf{r}}^i_{vel,k})\times\right]\delta\boldsymbol{\alpha}_k + \mathbf{T}^v_b[\mathbf{r}^b_{vel/imu}\times]\mathbf{T}^b_c\delta\mathbf{b}^c_{g,k} \\ &+ \mathbf{T}^v_b[\mathbf{r}^b_{vel/imu}\times]\mathbf{T}^b_c\mathbf{D}(\boldsymbol{\omega}_{m,k})\delta\mathbf{s}_{g,k} + \mathbf{T}^v_b[\mathbf{r}^b_{vel/imu}\times]\mathbf{T}^b_c\mathbf{N}(\boldsymbol{\omega}_{m,k})\delta\boldsymbol{\gamma}_{g,k} \\ &+ \delta\mathbf{b}^v_{vel,k} + \mathbf{T}^v_b[\mathbf{r}^b_{vel/imu}\times]\mathbf{T}^b_c\boldsymbol{\eta}^c_{g,k} + \boldsymbol{\eta}^v_{vel,k}\,.\end{aligned}$$

The measurement sensitivity matrix component contributed by a velocimeter measurement reading will thus take the form

$$\mathbf{H}_{vel} = \begin{bmatrix}\mathbf{H}^{3\times3}_{r,vel} & \mathbf{H}^{3\times3}_{v,vel} & \mathbf{H}^{3\times3}_{\delta\boldsymbol{\alpha},vel} & \mathbf{0}^{3\times3} & \mathbf{0}^{3\times12} & \mathbf{H}^{3\times12}_{p_g,vel} & \mathbf{0}^{3\times2} & \mathbf{H}^{3\times10}_{p_s,vel}\end{bmatrix} \quad (3.108)$$

where the individual components take the forms

$$\mathbf{H}_{r,vel} = -\mathbf{T}^v_b\hat{\mathbf{T}}^b_{i,k}[\boldsymbol{\omega}_L\times] \quad (3.109)$$

$$\mathbf{H}_{v,vel} = \mathbf{T}^v_b\hat{\mathbf{T}}^b_{i,k} \quad (3.110)$$

$$\begin{aligned}\mathbf{H}_{\delta\boldsymbol{\alpha},vel} = &\,\mathbf{T}^v_b\left[(\hat{\boldsymbol{\omega}}^b_k\times\mathbf{r}^b_{vel/imu})\times\right] + \mathbf{T}^v_b\hat{\mathbf{T}}^b_{i,k}[\boldsymbol{\omega}_L\times]\hat{\mathbf{T}}^i_{b,k}[\mathbf{r}^b_{vel/imu}\times] \\ &+ \mathbf{T}^v_b\left[\hat{\mathbf{T}}^i_{b,k}(\hat{\mathbf{v}}^i_{vel,k} - \boldsymbol{\omega}_L\times\hat{\mathbf{r}}^i_{vel,k})\times\right]\end{aligned} \quad (3.111)$$

$$\mathbf{H}_{p_g,vel} = \left[\mathbf{T}^v_b[\mathbf{r}^b_{vel/imu}\times]\mathbf{T}^b_c\middle|\mathbf{T}^v_b[\mathbf{r}^b_{vel/imu}\times]\mathbf{T}^b_c\mathbf{D}(\boldsymbol{\omega}_{m,k})\middle|\mathbf{T}^v_b[\mathbf{r}^b_{vel/imu}\times]\mathbf{T}^b_c\mathbf{N}(\boldsymbol{\omega}_{m,k})\right] \quad (3.112)$$

$$\mathbf{H}_{p_s,vel} = \begin{bmatrix}\mathbf{0}^{3\times1} & \mathbf{I}^{3\times3} & \mathbf{0}^{3\times6}\end{bmatrix} \quad (3.113)$$

3.2.4.3 Star Camera

The estimated value of the quaternion star camera measurement was shown in Eq. (3.28) to be

$$\hat{\bar{\mathbf{q}}}^{sc}_{sr,k} = \hat{\bar{\mathbf{q}}}_{b,k}\otimes\bar{\mathbf{q}}^{sc}_b\otimes\hat{\bar{\mathbf{q}}}^b_{i,k}\otimes\bar{\mathbf{q}}^i_{sr}\,.$$

so that the measurement deviation in error angles $\delta\boldsymbol{\alpha}$ takes the form

$$\boldsymbol{\psi}_k = \hat{\mathbf{T}}_{b,k}\mathbf{T}_b^{sc}\delta\boldsymbol{\alpha}_k + \delta\mathbf{b}_{sc,k} + \boldsymbol{\eta}_{sc,k}\,.$$

The sensitivity matrix component contributed by a star camera measurement is thus

$$\mathbf{H}_s c = \begin{bmatrix}\mathbf{0}^{3\times3} & \mathbf{0}^{3\times3} & \mathbf{H}_{\delta\alpha,sc}^{3\times3} & \mathbf{0}^{3\times3} & \mathbf{0}^{3\times12} & \mathbf{0}^{3\times12} & \mathbf{0}^{3\times2} & \mathbf{H}_{p_s,sc}^{3\times10}\end{bmatrix}\,,$$

where the individual components take the form

$$\begin{aligned}\mathbf{H}_{\delta\alpha,sc} &= \hat{\mathbf{T}}_{b,k}\mathbf{T}_b^{sc}\\ \mathbf{H}_{p_s,sc} &= \begin{bmatrix}\mathbf{0}^{3\times4} & \mathbf{I}^{3\times3} & \mathbf{0}^{3\times3}\end{bmatrix}\,.\end{aligned} \tag{3.114}$$

3.2.4.4 Terrain Camera

The estimated surface relative terrain camera measurement was found in Eq. (3.50) to be

$$\hat{\mathbf{r}}_{tc/ref,k}^s = \hat{\mathbf{T}}_{f,k}^s\mathbf{T}_{i,k}^f\hat{\mathbf{r}}_{imu,k}^i + \hat{\mathbf{T}}_{f,k}^s\mathbf{T}_{i,k}^f\hat{\mathbf{T}}_{b,k}^i\mathbf{r}_{tc/imu}^b - \hat{\mathbf{T}}_{f,k}^s\hat{\mathbf{r}}_{ref,k}^f + \hat{\mathbf{b}}_{tc,k}^s\,,$$

which leads to the terrain camera measurement deviation to be of the form

$$\begin{aligned}\delta\mathbf{r}_{tc/ref,k}^s = {}& \hat{\mathbf{T}}_{f,k}^s\mathbf{T}_{i,k}^f\delta\mathbf{r}_{imu,k}^i - \hat{\mathbf{T}}_{f,k}^s\mathbf{T}_{i,k}^f\hat{\mathbf{T}}_{b,k}^i\left[\mathbf{r}_{tc/imu}^b\times\right]\delta\boldsymbol{\alpha}\\ &+ \left[\mathbf{T}_{f,\phi,k}^s\left[\mathbf{T}_{i,k}^f\hat{\mathbf{r}}_{imu,k}^i + \mathbf{T}_{i,k}^f\hat{\mathbf{T}}_{b,k}^i\mathbf{r}_{tc/imu}^b - \hat{\mathbf{r}}_{ref,k}^f\right] - \hat{\mathbf{T}}_{f,k}^s\mathbf{r}_{ref,\phi,k}^f\right]\delta\phi_{map,k}\\ &+ \left[\mathbf{T}_{f,\lambda,k}^s\left[\mathbf{T}_{i,k}^f\hat{\mathbf{r}}_{imu,k}^i + \mathbf{T}_{i,k}^f\hat{\mathbf{T}}_{b,k}^i\mathbf{r}_{tc/imu}^b - \hat{\mathbf{r}}_{ref,k}^f\right] - \hat{\mathbf{T}}_{f,k}^s\mathbf{r}_{ref,\lambda,k}^f\right]\delta\lambda_{map,k}\\ &+ \delta\mathbf{b}_{tc,k} + \boldsymbol{\eta}_{tc,k}\,.\end{aligned}$$

The measurement sensitivity matrix component contributed by a terrain camera measurement is thus

$$\mathbf{H}_{tc} = \begin{bmatrix} \mathbf{H}_{r,tc}^{3\times3} & \mathbf{0}^{3\times3} & \mathbf{H}_{\delta\alpha,tc}^{3\times3} & \mathbf{0}^{3\times3} & \mathbf{0}^{3\times12} & \mathbf{0}^{3\times12} & \mathbf{H}_{p_m,tc}^{3\times2} & \mathbf{H}_{p_s,tc}^{3\times10} \end{bmatrix} ,$$

where the individual components take the form

$$\mathbf{H}_{r,tc} = \hat{\mathbf{T}}_{f,k}^{s}\mathbf{T}_{i,k}^{f} \tag{3.115}$$

$$\mathbf{H}_{\delta\alpha,tc} = -\hat{\mathbf{T}}_{f,k}^{s}\mathbf{T}_{i,k}^{f}\hat{\mathbf{T}}_{b,k}^{i}\left[\mathbf{r}_{tc/imu}^{b}\times\right] \tag{3.116}$$

$$\mathbf{H}_{p_m,tc} = \begin{bmatrix} \begin{bmatrix} \mathbf{T}_{f,\phi,k}^{s}\left[\mathbf{T}_{i,k}^{f}\hat{\mathbf{r}}_{imu,k}^{i} + \mathbf{T}_{i,k}^{f}\hat{\mathbf{T}}_{b,k}^{i}\mathbf{r}_{tc/imu}^{b} - \hat{\mathbf{r}}_{ref,k}^{f}\right] - \hat{\mathbf{T}}_{f,k}^{s}\mathbf{r}_{ref,\phi,k}^{f} \\ \mathbf{T}_{f,\lambda,k}^{s}\left[\mathbf{T}_{i,k}^{f}\hat{\mathbf{r}}_{imu,k}^{i} + \mathbf{T}_{i,k}^{f}\hat{\mathbf{T}}_{b,k}^{i}\mathbf{r}_{tc/imu}^{b} - \hat{\mathbf{r}}_{ref,k}^{f}\right] - \hat{\mathbf{T}}_{f,k}^{s}\mathbf{r}_{ref,\lambda,k}^{f} \end{bmatrix} \end{bmatrix}^{\mathrm{T}} \tag{3.117}$$

$$\mathbf{H}_{p_s,tc} = \begin{bmatrix} \mathbf{0}^{3\times7} & \mathbf{I}^{3\times3} \end{bmatrix} . \tag{3.118}$$

3.2.5 Robust Filtering

3.2.5.1 Thresholding

The IMU measurement of non-gravitational acceleration is corrupted by bias, scale factor and non-orthogonality, as well as measurement noise. In some space-borne applications, it may be acceptable to assume that the only non-gravitational force acting upon the vehicle is engine thrust. Additionally it may be acceptable to assume that the only torque acting upon the vehicle is due to maneuvering thrust. If neither input to the system are active, then the navigation filter will be integrating IMU measurements comprised of error sources only, thereby risking an increase in state estimation error. Thresholding prevents the navigation filter from integrating erroneous IMU

measurements by analyzing the covariance of the non-gravitational acceleration and making a decision based on scaling factors of whether to include the IMU measurement or not. [6]

The true non-gravitational acceleration in terms of the measured acceleration and error sources was found in Eq. (2.17) to be

$$\mathbf{a}_{ng} = \mathbf{a}_{ng,m} - \mathbf{b}_a - \mathbf{D}(\mathbf{a}_{ng,m})\mathbf{s}_a - \mathbf{N}(\mathbf{a}_{ng,m})\boldsymbol{\gamma}_a - \boldsymbol{\eta}_a \,,$$

and the associated estimated non-gravitational acceleration is

$$\hat{\mathbf{a}}_{ng} = \mathbf{a}_{ng,m} - \hat{\mathbf{b}}_a - \mathbf{D}(\mathbf{a}_{ng,m})\hat{\mathbf{s}}_a - \mathbf{N}(\mathbf{a}_{ng,m})\hat{\boldsymbol{\gamma}}_a \,.$$

The deviation (or error) in the non-gravitational acceleration is found by subtracting the estimated acceleration from the true acceleration yielding

$$\delta\mathbf{a}_{ng} = -\delta\mathbf{b}_a - \mathbf{D}(\mathbf{a}_{ng,m})\delta\mathbf{s}_a - \mathbf{N}(\mathbf{a}_{ng,m})\delta\boldsymbol{\gamma}_a - \boldsymbol{\eta}_a \,, \tag{3.119}$$

where

$$\delta\mathbf{b}_a = \mathbf{b}_a - \hat{\mathbf{b}}_a$$

$$\delta\mathbf{s}_a = \mathbf{s}_a - \hat{\mathbf{s}}_a$$

$$\delta\boldsymbol{\gamma}_a = \boldsymbol{\gamma}_a - \hat{\boldsymbol{\gamma}}_a \,.$$

The non-gravitational acceleration error covariance is defined as

$$\mathbf{P}_a = \mathrm{E}\left\{\delta\mathbf{a}_{ng}\delta\mathbf{a}_{ng}^{\mathrm{T}}\right\} \,.$$

We can assume that each error term is uncorrelated with other error terms so that when the definition of the acceleration deviation from Eq. (3.119) is

expanded in Eq. (3.120), we have

$$\mathbf{P}_a = \mathbf{P}_{b_a} + \mathbf{D}(\mathbf{a}_{ng,m})\mathbf{P}_{s_a}\mathbf{D}^{\mathrm{T}}(\mathbf{a}_{ng,m}) + \mathbf{N}(\mathbf{a}_{ng,m})\mathbf{P}_{\gamma_a}\mathbf{N}^{\mathrm{T}}(\mathbf{a}_{ng,m}) + \mathrm{E}\left\{\boldsymbol{\eta}_a\boldsymbol{\eta}_a^{\mathrm{T}}\right\} . \tag{3.120}$$

In Eq. (3.120), the covariances of the accelerometer bias, scale factor, non-orthogonality and misalignment errors are given by

$$\begin{aligned}\mathbf{P}_{b_a} &= \mathrm{E}\left\{\delta\mathbf{b}_a\delta\mathbf{b}_a^{\mathrm{T}}\right\} \\ \mathbf{P}_{s_a} &= \mathrm{E}\left\{\delta\mathbf{s}_a\delta\mathbf{s}_a^{\mathrm{T}}\right\} \\ \mathbf{P}_{\gamma_a} &= \mathrm{E}\left\{\delta\boldsymbol{\gamma}_a\delta\boldsymbol{\gamma}_a^{\mathrm{T}}\right\} .\end{aligned}$$

Due to the fact that the accelerometer measurement noise covariance is defined by the spectral density of the measurement noise, and that the accelerometer noise is a small component of the total accelerometer error, it is reasonable to exclude its impact on the accelerometer error covariance. This will reduce the accelerometer error covariance to

$$\mathbf{P}_a = \mathbf{P}_{b_a} + \mathbf{D}(\mathbf{a}_{ng,m})\mathbf{P}_{s_a}\mathbf{D}^{\mathrm{T}}(\mathbf{a}_{ng,m}) + \mathbf{N}(\mathbf{a}_{ng,m})\mathbf{P}_{\gamma_a}\mathbf{N}^{\mathrm{T}}(\mathbf{a}_{ng,m}) . \tag{3.121}$$

We can let the accelerometer bias, scale factor, and misalignment/non-orthogonality covariances be represented as

$$\begin{aligned}\mathbf{P}_{b_a} &= \sigma_{b_a}^2\mathbf{I}_{3\times3} \\ \mathbf{P}_{s_a} &= \sigma_{s_a}^2\mathbf{I}_{3\times3} \\ \mathbf{P}_{\gamma_a} &= \sigma_{\gamma_a}^2\mathbf{I}_{6\times6} ,\end{aligned}$$

where $\sigma_{b_a}^2$ is the standard deviation of the accelerometer bias, $\sigma_{s_a}^2$ is the standard deviation of the accelerometer scale factor, and $\sigma_{\gamma_a}^2$ is the misalignment/non-orthogonality standard deviation. The accelerometer error covariance will thus become

$$\mathbf{P}_a = \sigma_{b_a}^2 \mathbf{I}_{3\times 3} + \sigma_{s_a}^2 \mathbf{D}(\mathbf{a}_{ng,m})\mathbf{D}^{\mathrm{T}}(\mathbf{a}_{ng,m}) + \sigma_{\gamma_a}^2 \mathbf{N}(\mathbf{a}_{ng,m})\mathbf{N}^{\mathrm{T}}(\mathbf{a}_{ng,m})\,. \tag{3.122}$$

If the accelerometer error covariance takes the form

$$\mathbf{P}_a = \begin{bmatrix} \sigma_{a,x}^2 & 0 & 0 \\ 0 & \sigma_{a,y}^2 & 0 \\ 0 & 0 & \sigma_{a,z}^2 \end{bmatrix}\,, \tag{3.123}$$

then the matrix multiplications in Eq. (3.122) lead to

$$\sigma_{a,x}^2 = \sigma_{b_a}^2 + \sigma_{s_a}^2 (a_{ng,m,x})^2 + \sigma_{\gamma_a}^2 \left[(a_{ng,m,y})^2 + (a_{ng,m,z})^2\right] \tag{3.124}$$

$$\sigma_{a,y}^2 = \sigma_{b_a}^2 + \sigma_{s_a}^2 (a_{ng,m,y})^2 + \sigma_{\gamma_a}^2 \left[(a_{ng,m,x})^2 + (a_{ng,m,z})^2\right] \tag{3.125}$$

$$\sigma_{a,z}^2 = \sigma_{b_a}^2 + \sigma_{s_a}^2 (a_{ng,m,z})^2 + \sigma_{\gamma_a}^2 \left[(a_{ng,m,x})^2 + (a_{ng,m,y})^2\right]\,. \tag{3.126}$$

This derivation also applies to the analysis of the gyroscope measurement error covariance. Recall that the true rotation is the gyroscope measurement of rotation minus the error sources as

$$\boldsymbol{\omega} = \boldsymbol{\omega}_m - \mathbf{b}_g - \mathbf{D}(\boldsymbol{\omega}_m)\mathbf{s}_g\mathbf{N}(\boldsymbol{\omega}_m)\boldsymbol{\gamma}_g - \boldsymbol{\eta}_g\,, \tag{3.127}$$

so that the estimated rotation rate will take the form

$$\hat{\boldsymbol{\omega}} = \boldsymbol{\omega}_m - \hat{\mathbf{b}}_g - \mathbf{D}(\boldsymbol{\omega}_m)\hat{\mathbf{s}}_g\mathbf{N}(\boldsymbol{\omega}_m)\hat{\boldsymbol{\gamma}}_g\,. \tag{3.128}$$

The rotation rate error is $\delta\boldsymbol{\omega} = \boldsymbol{\omega} - \hat{\boldsymbol{\omega}}$ and the rotation rate error covariance can again take a diagonal form given by

$$\mathbf{P}_{\omega} = \mathrm{E}\left\{\delta\boldsymbol{\omega}\delta\boldsymbol{\omega}^{\mathrm{T}}\right\} = \begin{bmatrix} \sigma_{\omega,x}^2 & 0 & 0 \\ 0 & \sigma_{\omega,y}^2 & 0 \\ 0 & 0 & \sigma_{\omega,z}^2 \end{bmatrix} . \tag{3.129}$$

If we follow through in a similar manner to the accelerometer analysis we will arrive at the gyroscope measurement error covariance for each axis as

$$\sigma_{\omega,x}^2 = \sigma_{b_g}^2 + \sigma_{s_g}^2(\omega_{m,x})^2 + \sigma_{\gamma_g}^2\left[\omega_{m,y}^2 + \omega_{m,z}^2\right] \tag{3.130}$$

$$\sigma_{\omega,x}^2 = \sigma_{b_g}^2 + \sigma_{s_g}^2(\omega_{m,x})^2 + \sigma_{\gamma_g}^2\left[\omega_{m,y}^2 + \omega_{m,z}^2\right] \tag{3.131}$$

$$\sigma_{\omega,x}^2 = \sigma_{b_g}^2 + \sigma_{s_g}^2(\omega_{m,x})^2 + \sigma_{\gamma_g}^2\left[\omega_{m,y}^2 + \omega_{m,z}^2\right] . \tag{3.132}$$

With the error covariance for the acceleration and rotation rate errors available, we can implement a decision based upon a comparison of the estimated acceleration or rotation rate and a scaled multiple of the acceleration/rotation rate error covariance as

$$\|\hat{a}_{ng,i}\| < n_a\sigma_{a,i} , \tag{3.133}$$

where the subscript i refers to the i^{th} axis and n_a is a scaling factor for a tolerance band to activate thresholding. If the norm of the estimated acceleration in the i^{th} axis is less than a scaled multiple (such as a 1-σ or 2-σ confidence interval) of the non-gravitational acceleration error covariance, then thresholding is activated. The estimated non-gravitational acceleration will be set to zero, and the measured non-gravitational acceleration will be set to zero for the propagation. Likewise, if the estimated rotation rate satisfies

$$\|\hat{\omega}_i\| < n_g\sigma_{\omega_i} , \tag{3.134}$$

where n_g is the scaling of the confidence interval to activate thresholding on the gyroscope measurement. If thresholding is activated, then we set the measured rotation rate and estimated rotation rate to zero for the propagation.

3.2.5.2 Underweighting

Underweighting is a navigational aid that prevents filter divergence during a time when both the state estimate error covariance is large and an accurate measurement is made, possibly violating linearity assumptions in the update. It acts by "reducing" the impact of the measurement on the state estimation and estimation error covariance update. [7]

The Kalman gain is

$$\mathbf{K}_k = \mathbf{P}_k^- \mathbf{H}_k^{\mathrm{T}} \left(\hat{\mathbf{x}}_k^-\right) \left[\mathbf{H}_k \left(\hat{\mathbf{x}}_k^-\right) \mathbf{P}_k^- \mathbf{H}_k^{\mathrm{T}} \left(\hat{\mathbf{x}}_k^-\right) + \mathbf{R}_k\right]^{-1} . \tag{3.135}$$

If we introduce a symmetric positive definite underweighting factor U_k by adding it to the residual covariance term, we will have

$$\mathbf{K}_k = \mathbf{P}_k^- \mathbf{H}_k^{\mathrm{T}} \left[\mathbf{H}_k \mathbf{P}_k^- \mathbf{H}_k^{\mathrm{T}} + \mathbf{R}_k + \mathbf{U}_k\right]^{-1} . \tag{3.136}$$

This will increase the norm of the "denominator" of the gain, thus reducing the overall norm of the applied gain. If we substitute this modified Kalman gain into the covariance update equation of Eq. (3.91) we obtain

$$\mathbf{P}_k^+ = \mathbf{P}_k^- - \mathbf{P}_k^- \mathbf{H}_k^{\mathrm{T}} \left[\mathbf{H}_k \mathbf{P}_k^- \mathbf{H}_k^{\mathrm{T}} + \mathbf{R}_k + \mathbf{U}_k\right]^{-1} \mathbf{H}_k \mathbf{P}_k^- . \tag{3.137}$$

The measurement covariance due to the state estimation error can be found

by pre- and post-multiplying Eq. (3.137) by $\mathbf{H}_k$ and $\mathbf{H}_k^{\mathrm{T}}$, respectively, yielding

$$\mathbf{H}_k\mathbf{P}_k^{+}\mathbf{H}_k^{\mathrm{T}} = \mathbf{H}_k\mathbf{P}_k^{-}\mathbf{H}_k^{\mathrm{T}} - \mathbf{H}_k\mathbf{P}_k^{-}\mathbf{H}_k^{\mathrm{T}}\left[\mathbf{H}_k\mathbf{P}_k^{-}\mathbf{H}_k^{\mathrm{T}} + \mathbf{R}_k + \mathbf{U}_k\right]^{-1}\mathbf{H}_k\mathbf{P}_k^{-}\mathbf{H}_k^{\mathrm{T}}\,. \tag{3.138}$$

Now, we can define the difference in the *a priori* measurement covariance and the *a posteriori* measurement covariance due to the state estimation error as

$$\Delta(\mathbf{H}_k\mathbf{P}_k\mathbf{H}_k^{\mathrm{T}}) \triangleq \mathbf{H}_k\mathbf{P}_k^{-}\mathbf{H}_k^{\mathrm{T}} - \mathbf{H}_k\mathbf{P}_k^{+}\mathbf{H}_k^{\mathrm{T}}\,, \tag{3.139}$$

so that Eq. (3.137) can be reorganized and written as

$$\Delta(\mathbf{H}_k\mathbf{P}_k\mathbf{H}_k^{\mathrm{T}})\left[\mathbf{H}_k\mathbf{P}_k^{-}\mathbf{H}_k^{\mathrm{T}}\right]^{-1} = \mathbf{H}_k\mathbf{P}_k^{-}\mathbf{H}_k^{\mathrm{T}}\left[\mathbf{H}_k\mathbf{P}_k^{-}\mathbf{H}_k^{\mathrm{T}} + \mathbf{R}_k + \mathbf{U}_k\right]^{-1}\,. \tag{3.140}$$

Equation 3.137 is an expression for the "percentage" decrease in measurement covariance due to the state estimation error covariance. By rearranging terms and taking the matrix norm of both sides, we will utilize a matrix version of the Cauchy-Schwarz inequality to show that

$$\|\mathbf{H}_k\mathbf{P}_k^{-}\mathbf{H}_k^{\mathrm{T}}\| \leq \|\Delta(\mathbf{H}_k\mathbf{P}_k\mathbf{H}_k^{\mathrm{T}})\left[\mathbf{H}_k\mathbf{P}_k^{-}\mathbf{H}_k^{\mathrm{T}}\right]^{-1}\|\left[\|\mathbf{H}_k\mathbf{P}_k^{-}\mathbf{H}_k^{\mathrm{T}}\| + \|\mathbf{R}_k\| + \|\mathbf{U}_k\|\right]\,. \tag{3.141}$$

We can now move the $\left[\|\mathbf{H}_k\mathbf{P}_k^{-}\mathbf{H}_k^{\mathrm{T}}\| + \|\mathbf{R}_k\| + \|\mathbf{U}_k\|\right]$ term to the left of the inequality sign to get

$$\frac{\|\mathbf{H}_k\mathbf{P}_k^{-}\mathbf{H}_k^{\mathrm{T}}\|}{\|\mathbf{H}_k\mathbf{P}_k^{-}\mathbf{H}_k^{\mathrm{T}}\| + \|\mathbf{R}_k\| + \|\mathbf{U}_k\|} \leq \|\Delta(\mathbf{H}_k\mathbf{P}_k\mathbf{H}_k^{\mathrm{T}})\left[\mathbf{H}_k\mathbf{P}_k^{-}\mathbf{H}_k^{\mathrm{T}}\right]^{-1}\|\,. \tag{3.142}$$

Now we can let the percentage decrease in $\mathbf{H}_k\mathbf{P}_k^{-}\mathbf{H}_k^{\mathrm{T}}$ be represented by parameter p such that $0 < p \leq 1$, so we will have

$$\|\Delta(\mathbf{H}_k\mathbf{P}_k\mathbf{H}_k^{\mathrm{T}})\left[\mathbf{H}_k\mathbf{P}_k^{-}\mathbf{H}_k^{\mathrm{T}}\right]^{-1}\| = p\,, \tag{3.143}$$

and thus

$$\frac{\|\mathbf{H}_k\mathbf{P}_k^-\mathbf{H}_k^{\mathrm{T}}\|}{\|\mathbf{H}_k\mathbf{P}_k^-\mathbf{H}_k^{\mathrm{T}}\| + \|\mathbf{R}_k\| + \|\mathbf{U}_k\|} \leq p\,. \tag{3.144}$$

We can solve Eq. (3.144) for $\|\mathbf{H}_k\mathbf{P}_k^-\mathbf{H}_k^{\mathrm{T}}\|$ and find that

$$\|\mathbf{H}_k\mathbf{P}_k^-\mathbf{H}_k^{\mathrm{T}}\| \leq \frac{p}{1-p}\|\mathbf{R}_k\| + \frac{p}{1-p}\|\mathbf{U}_k\|\,. \tag{3.145}$$

or we can solve for the underweighting factor norm $\|\mathbf{U}_k\|$ to obtain

$$\|\mathbf{U}_k\| \geq \frac{1-p}{p}\|\mathbf{H}_k\mathbf{P}_k^-\mathbf{H}_k^{\mathrm{T}}\| - \|\mathbf{R}_k\|\,. \tag{3.146}$$

Eq. (3.146) only gives an inequality condition on the norm of the underweighting factor, but it leads to the natural selection of the underweighting factor as the minimum allowable value

$$\mathbf{U}_k = \frac{1-p}{p}\mathbf{H}_k\mathbf{P}_k^-\mathbf{H}_k^{\mathrm{T}}\,. \tag{3.147}$$

If we substitute the underweighting factor found in Eq. (3.147) into the modified Kalman gain update of Eq. (3.136) we obtain

$$\mathbf{K}_k = \mathbf{P}_k^-\mathbf{H}_k^{\mathrm{T}}\left[\frac{1}{p}\mathbf{H}_k\mathbf{P}_k^-\mathbf{H}_k^{\mathrm{T}} + \mathbf{R}_k\right]^{-1}\,. \tag{3.148}$$

With the underweighted Kalman gain at our disposal, it is desirable to determine the conditions which require underweighting. We can devise a condition as the "opposite" of Eq. (3.145) with a zero underweighting factor, so that the condition

$$\|\mathbf{H}_k\mathbf{P}_k^-\mathbf{H}_k^{\mathrm{T}}\| \geq \frac{p}{1-p}\|\mathbf{R}_k\|\,. \tag{3.149}$$

must be satisfied to implement underweighting for a chosen p. Recall that $0 < p \leq 1$. If $p = 1$ then there will be no underweighting. Conversely if $p \to 0$,

then the underweighting will be to the extreme where the measurement will impart almost no update on the state estimate or estimation error covariance.

We can generalize this derivation by considering a case where multiple measurements are being processed simultaneously, and each measurement may have a different underweighting factor. In this case, the total measurement will take the form

$$\mathbf{y}_k = \begin{bmatrix} \mathbf{y}_{1,k} \\ \mathbf{y}_{2,k} \end{bmatrix} .$$

The measurement sensitivity matrix and the measurement noise covariance can be segmented as

$$\mathbf{H}_k = \begin{bmatrix} \mathbf{H}_{1,k} \\ \mathbf{H}_{2,k} \end{bmatrix} \qquad \text{and} \qquad \mathbf{R}_k = \begin{bmatrix} \mathbf{R}_{1,k} & \mathbf{0} \\ \mathbf{0} & \mathbf{R}_{2,k} \end{bmatrix} . \tag{3.150}$$

The underweighting conditions for each measurement that must be satisfied to apply underweighting are thus

$$\|\mathbf{H}_{1,k}\mathbf{P}_k^-\mathbf{H}_{1,k}^{\mathrm{T}}\| \geq \frac{p_1}{1-p_1}\|\mathbf{R}_{1,k}\| , \tag{3.151a}$$

$$\|\mathbf{H}_{2,k}\mathbf{P}_k^-\mathbf{H}_{2,k}^{\mathrm{T}}\| \geq \frac{p_2}{1-p_2}\|\mathbf{R}_{2,k}\| . \tag{3.151b}$$

If both conditions are met, then the underweighting scaling matrix $\mathbf{S}_k$ can be constructed as

$$\mathbf{S}_k = \begin{bmatrix} \sqrt{k_1}\mathbf{I} & \mathbf{0} \\ \mathbf{0} & \sqrt{k_2}\mathbf{I} \end{bmatrix} , \tag{3.152}$$

where

$$k_1 = \frac{1}{p_1} \qquad \text{and} \qquad k_2 = \frac{1}{p_2} . \tag{3.153}$$

The underweighted Kalman gain is computed as

$$\mathbf{K}_k = \mathbf{P}_k^-\mathbf{H}_k^{\mathrm{T}}\left[\mathbf{S}_k\mathbf{H}_k\mathbf{P}_k^-\mathbf{H}_k^{\mathrm{T}}\mathbf{S}_k^{\mathrm{T}} + \mathbf{R}_k\right]^{-1} . \tag{3.154}$$

Chapter 4

Model Reduction to Sub-Optimal Filter

The navigation algorithm described in the previous chapters is a full-order system in the sense that all states are updated in the filter. This approach is the most comprehensive and is assumed to have the best performance. However, this comprehensive approach may be computationally intractable and a solution that is of comparable performance at a fraction of the computational burden may be available. To address this issue, an error budget is created to catalog the impact of the various error sources on the filter performance. A sensitivity analysis is performed using the error budget to determine how off-nominal values of particular state parameters affect the system performance. System performance can be measured by the state estimation error at a particular epoch or averaged over time depending upon the application. If it is found that off-nominal values of a particular system parameter do not significantly affect the system performance and if the error source does not contribute significantly to the estimation error, then it may be advantageous to remove that state from the filter. Conversely, it may be found that off-nominal values of a particular error source could lead to significant degredation in the navigation performance. It may be possible to find bounds on the off-nominal values of that error source to achieve a given estimation accuracy. In the former

case, the parameters may be removed from the system, and thus the system will need to be re-calibrated to account for the different scenario. In the end a reduced-order EKF may be obtained that closely matches the estimation performance of the full-order system, but at a fraction of the computational burden.

4.1 Error Budget and Sensitivity Analysis

A sensitivity analysis has been performed on the full-order navigational filter described in the previous chapters. Details of the sensitivity analysis can be found in a paper by DeMars and Bishop [8]. The sensitivity analysis provides sensitivity curves that display the impact on a state estimation error covariance from off-nominal values of various error sources. A sensitivity analysis uses an error budget. An error budget is a catalog of the impact of particular error sources upon the state estimate error covariance. It is created in two steps; first, a nominal simulation is executed and the time-history of the Kalman gain is saved. Second, subsequent simulations are executed, suppressing all error source groups but one and utilizing the nominal Kalman gain time-history. The error budget is then created by organizing the state estimate error covariance at an important epoch from each activated error source simulation. The result is a table of state estimate error covariance "contributions" from each error source. Below is an example error budget table illustrating the end result. The nominal root-sum-square of the individual contributions

Table 4.1: Example Error Budget

	State Group # 1	State Group # 2
Error Group # 1	a_1	b_1
Error Group # 2	a_2	b_2
Error Group # 3	a_3	b_3
Root Sum Square	a_{nom}	b_{nom}

is calculated as

$$a_{nom} = \sqrt{a_1^2 + a_2^2 + a_3^2}\,.$$

This value should be almost equal to the nominal filter covariance from the initial nominal run. The reader can imagine that in Table 4.1, State Group 1 could be the position (r_x^i, r_y^i, r_z^i), and the error groups contributing to the estimation covariance could be the initial error covariance for position, velocity, and attitude. Thus, a_1 would represent the position estimation error covariance at a particular epoch from activation of the initial position estimation error covariance (and suppression of all other error sources).

A sensitivity analysis is used to quantify the impact on the state estimation error covariance due to off-nominal values of each error group. The result of a sensitivity analysis are sensitivity curves which illustrate how the system reacts to increasing the contribution of a particular error group. A sensitivity curve can be found by re-calculating the root-sum-square estimation error covariance with a diminished and an augmented contribution from a particular error source. For example, to find the sensitivity curve for error group 2's impact upon state group 1, the off-nominal contributions are found

via

$$a_{off,1} = \sqrt{\alpha_1 a_1^2 + a_2^2 + a_3^2} \qquad \text{and} \qquad a_{off,2} = \sqrt{\alpha_2 a_1^2 + a_2^2 + a_3^2}\,,$$

where α_1 and α_2 are coefficients that either augment or diminish the value of the error group's contribution. For this example they may take the values of $\frac{1}{2}$ and 2, respectively. With the three root-sum-square values for estimation error covariance (diminished, nominal, augmented), a curve-fit may be placed through these values and their respective coefficients. The sensitivity curve that would result from this hypothetical analysis could take the form of Fig. 4.1.

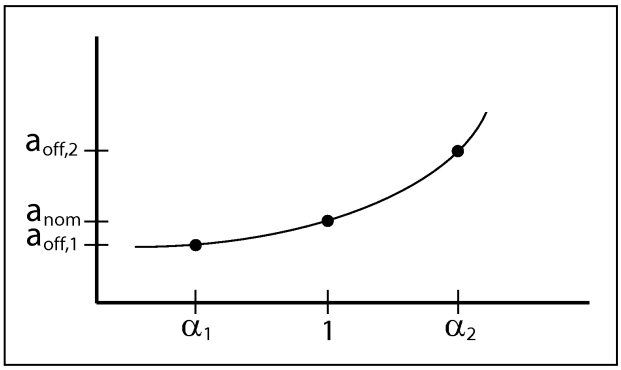

Figure 4.1: Hypothetical sensitivity curve from above calculations

Note that the curve has positive slope; that is to say that as the contribution from Error Group 1 increases, the root-sum-square error covariance increases. This means that the system is sensitive to off-nominal values of errors in Error Group 1. The level of sensitivity is reflected in the slope of the curve. If a system is completely insensitive to a particular error group

contribution, then the sensitivity curve will have near-zero slope. It may be possible then to remove the system consideration of these error sources without appreciably impacting the performance of the system. A new, sub-optimal estimator may then be designed that can largely capture the performance of the full-order system at a fraction of the computational burden and run-time.

For the sensitivity analysis performed on this system, the error budget was broken into 20 error source groups, and the epoch at which the state estimation error covariance is saved is at the time $t = 3900\,[\mathrm{s}]$, which is a short time before touchdown. The error source groups are listed below.

Initial Error Covariance

1. position uncertainty
2. velocity uncertainty
3. attitude uncertainty
4. uncertainty in the deviation from the nominal position of the C.G. with respect to the IMU
5. map tie uncertainty
6. accelerometer bias uncertainty
7. accelerometer scale-factor and nonorthogonality uncertainty
8. gyro bias uncertainty
9. gyro scale-factor and nonorthogonality uncertainty
10. altimeter bias uncertainty
11. velocimeter bias uncertainty
12. star camera bias uncertainty
13. terrain camera bias uncertainty

Process Noise

14. accelerometer random noise and bias noise
15. gyro random noise and bias noise
16. map tie random noise

Measurement Noise

17. altimeter noise
18. velocimeter noise
19. star camera noise
20. terrain camera noise

The state groups investigated are the physical state estimates of position, velocity, attitude, and map-tie error.

4.1.1 Scenario Investigated

The navigation system is simulated along a true path that models a descent-to-landing scenario. The path brings the vehicle from behind the north pole at an altitude of 100km to a landing site near the south pole. A depiction of the ground track, and a time profile of the altitude through the scenario are both shown in Fig. 4.2. The beginning of the path is shown as a green circle, and the landing site is shown with a red circle. The navigation system accepts measurements from the altimeter at 5 Hz, from the star camera at 1 Hz, from the terrain camera at 0.5 Hz, and from the velocimeter at 5 Hz. Between measurements, the navigation system propagates the state estimate and error covariance with IMU measurements at 100 Hz. Fig. 4.3 shows the time-windows in which each instrument is active.

The initial state estimate is obtained by sampling the initial state estimate error covariance. The standard deviation for the position and velocity are defined in the *uvw* reference frame. The *uvw* transformation rotates the position and velocity into, colloquially speaking, the "up", "along-track", and "cross-track" directions. The values for position and velocity are rotated into the *uvw* frame via a transformation matrix, defined as

$$\mathbf{T}_i^{uvw} = \begin{pmatrix} \hat{u}^{\mathrm{T}} \\ \hat{v}^{\mathrm{T}} \\ \hat{w}^{\mathrm{T}} \end{pmatrix} ,$$

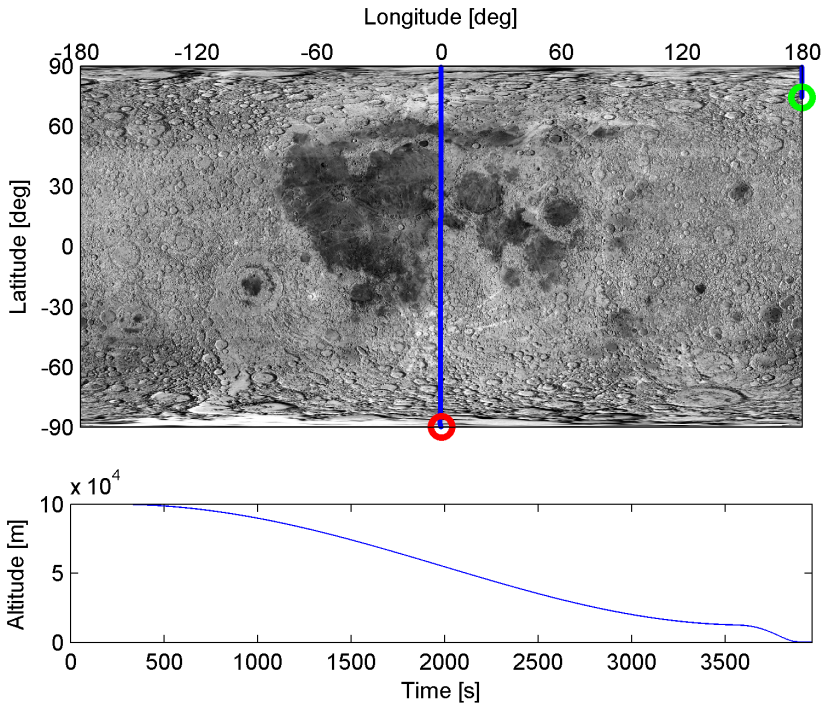

Figure 4.2: The true trajectory ground track and altitude profile

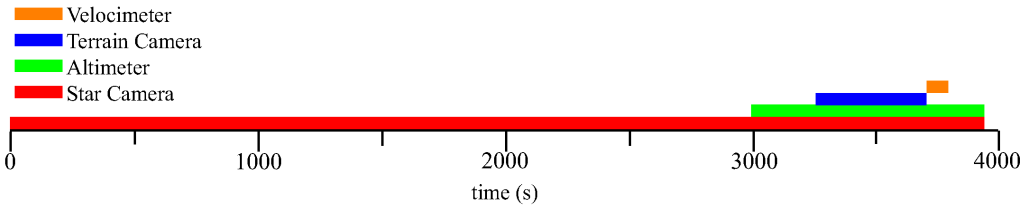

Figure 4.3: Active windows of external sensors

where $\hat{u}$, $\hat{v}$, and $\hat{w}$ are orthogonal unit vectors that establish the uvw

frame. Each unit vector is defined as

$$\hat{u} = \frac{-\mathbf{r}^i}{\|\mathbf{r}^i\|}$$
$$\hat{v} = \hat{u} \times \frac{-\mathbf{v}^i}{\|\mathbf{v}^i\|}$$
$$\hat{w} = \hat{u} \times \hat{v}\,.$$

This is to create a dispersion field of initial state estimates that is more realistic in nature, with the greatest uncertainty in position being in the "up" direction, and the greatest uncertainty in velocity being in the off-track direction. In Table 4.2 the standard deviations assigned to each parameter are shown.

The full-order navigation system error budget is created, and the reconstruction of the complete error budget is shown in Fig. 4.4. The nominal filter covariance is shown in red, and the reconstructed error covariance is shown in black. The reconstructed error covariance agrees with the filter covariance. It is desirable then that the reduced-order system exhibit a nominal filter covariance and sampled error variance time-history that closely matches those depicted in Fig. 4.4.

4.1.2 Sensitivity curves

This section shows the sensitivity curves of interest. First, sensitivity curves that display a high sensitivity to an error source are presented. The sensitivity curves for the error sources that do not contribute to the performance of the system are then displayed. By comparison it will be shown that deletion of these error sources from consideration of the filter will not signifi-

Table 4.2: Random error standard deviations

Physical State		
	r_u	1500 [m]
position	r_v	200 [m]
	r_w	50 [m]
	v_u	0.047 [m] [s]$^{-1}$
velocity	v_v	0.2 [m] [s]$^{-1}$
	v_w	1.5 [m] [s]$^{-1}$
attitude	$\delta\boldsymbol{\alpha}$	2.5×10^{-4} [rad]
Accelerometer Errors		
bias	$\mathbf{b}_a$	0.1 [mg]
scale-factor	$\mathbf{s}_a$	175 [ppm]
mis/non	$\boldsymbol{\gamma}_a$	5.0 [arcsec]
Gyro Errors		
bias	$\mathbf{b}_g$	0.05 [deg] [hr]$^{-1}$
scale-factor	$\mathbf{s}_g$	5.0 [ppm]
mis/non	$\boldsymbol{\gamma}_g$	5.0 [arcsec]
Sensor Bias		
Altimeter	b_{alt}	0.5 [m]
Velocimeter	$\mathbf{b}_{vel}$	0.0 [m] [s]$^{-1}$
Star Camera	$\mathbf{b}_{sc}$	20.0 [arcsec]
Terrain Camera	$\mathbf{b}_{tc}$	5.0 [m]
Map Tie Angle		
Latitude	ϕ_{map}	11.87 [arcsec]
Longitude	λ_{map}	11.87 [arcsec]

cantly affect the performance of the system. First, the system was found to be sensitive to off-nominal values of the initial error covariance for position and velocity. Below are sensitivity curves for off-nominal values of initial error covariance for map-tie angle. The four state groups investigated are the physical state groups of position, velocity, attitude, and map-tie error.

These sensitivity curves are presented to show the effects of off-nominal

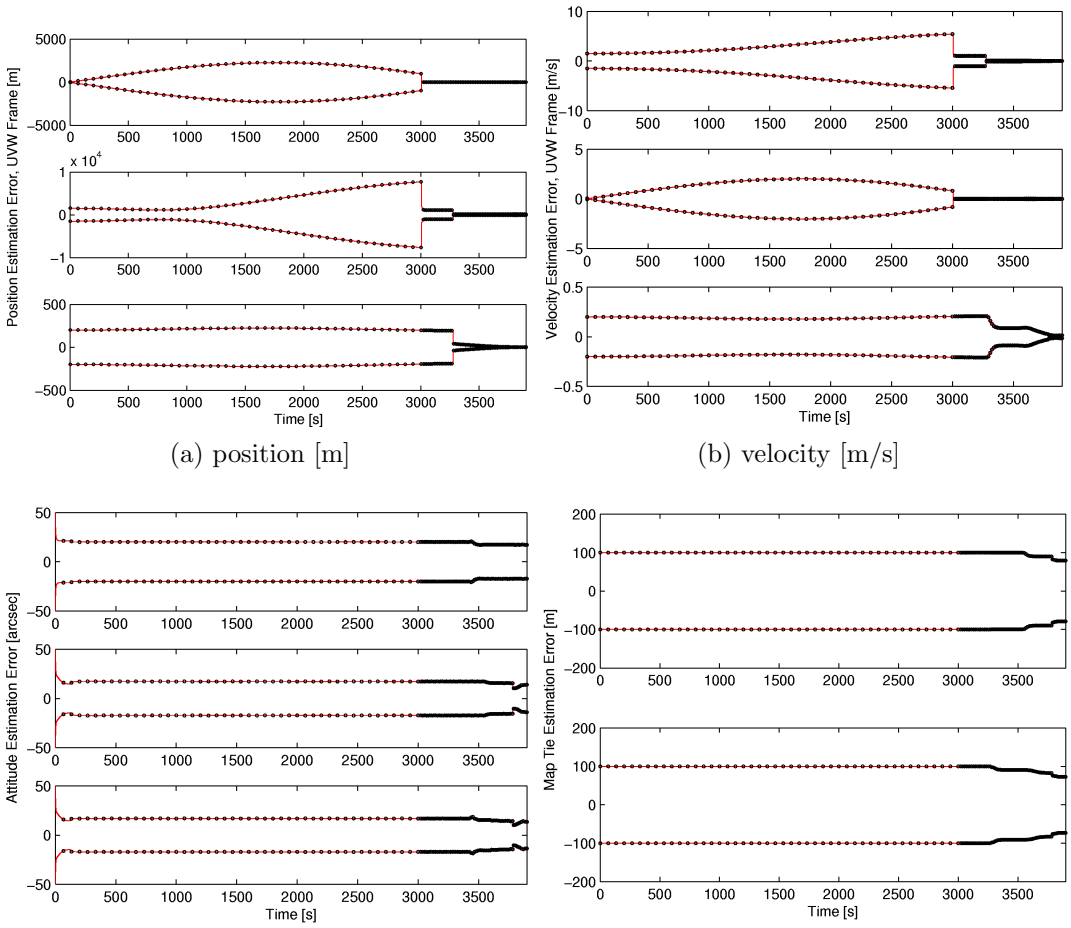

(a) position [m]

(b) velocity [m/s]

(c) attitude [arcsec]

(d) map-tie [m]

Figure 4.4: Error budget reconstruction of estimation error covariances for physical states

values for map-tie angle uncertainty. As the positive slopes show, the system is indeed sensitive to the initial covariance for map-tie angle uncertainty. Fig. 4.5a shows the increasing uncertainty in position at 3900 [s] due to increased initial uncertainty in map-tie error. Note the zero-slope in the first channel (u-direction) of position. There is no sensitivity in this direction due to

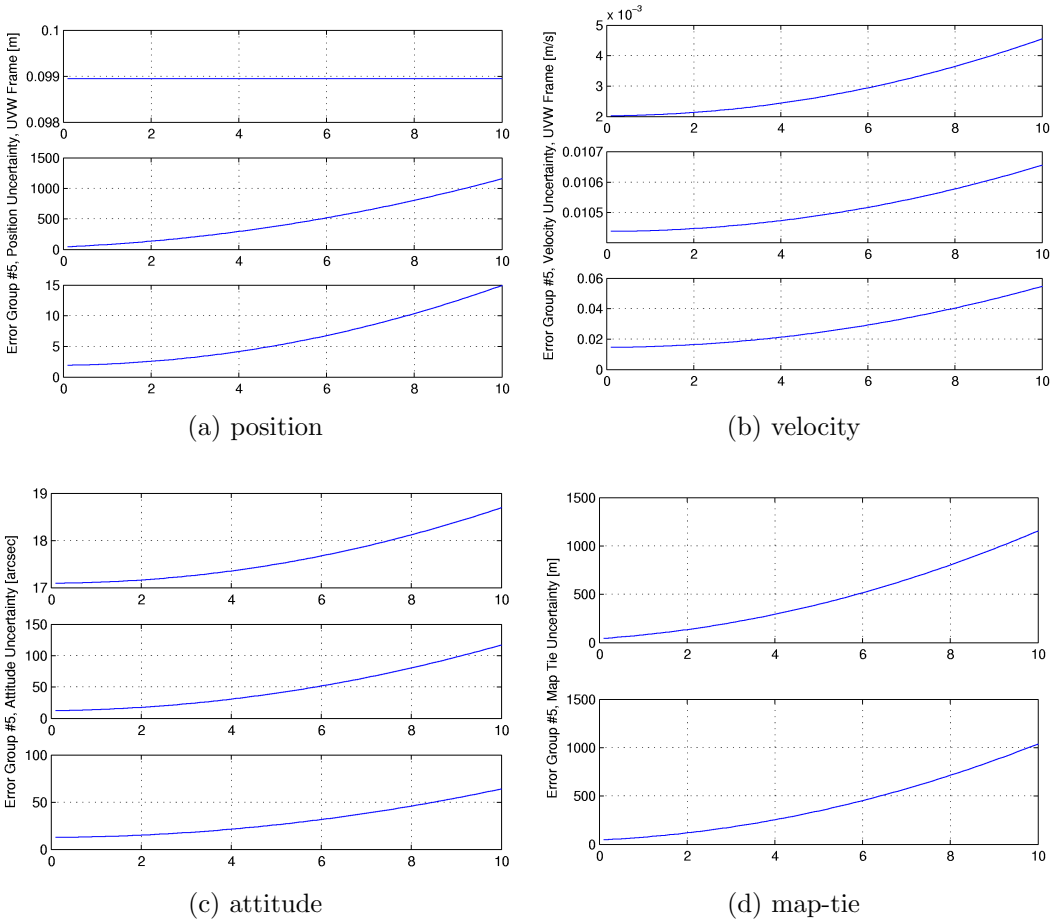

(a) position (b) velocity

(c) attitude (d) map-tie

Figure 4.5: Sensitivity curves from off-nominal initial map-tie angle uncertainty

the altimeter measurements which return a magnitude value in this direction; that is to say the system is not "fooled" by increased uncertainty in map-tie angle because the position in the u-direction is highly observable. However, the second channel (the v-direction) shows position uncertainty growing from near zero at the nominal map-tie uncertainty to over 1000 [m] at inflated map-

tie angle uncertainty. This evidences the high sensitivity of the system to map-tie angle uncertainty.

While there are positive slopes in Fig. 4.5b, the scale shows very little increase in velocity uncertainty due to inflated map-tie angle uncertainty. Fig. 4.5c, particularly the second channel (the pitch direction) shows that attitude uncertainty is sensitive to off-nominal values for initial map-tie angle uncertainty. Lastly and most obviously, the uncertainty at 3900 [s] in map-tie angle increases as the initial value for map-tie angle uncertainty increases.

To contrast these results which depict an error source that drives a significant portion of system performance, it has been found that uncertainty in the center-of-gravity displacement, as well as accelerometer and gyroscope scale factor and nonorthogonality uncertainty do not contribute significantly to the performance of the system. Below are sensitivity curves which depict the effect of off-nominal values for center-of-gravity displacement uncertainty on position and velocity. Both Fig. 4.6a and Fig. 4.6b show essentially zero slopes as the uncertainty of the displacement of the center of gravity increases. This is due to the fact that the displacement of the center of gravity is unobservable in the system, either directly or indirectly. Recall the external measurement sensitivities from Chapter 3 for each sensor. There is no direct sensitivity terms which involve the deviation of the center of gravity displacement. As these sensitivity curves evidence, there is also no indirect sensitivity of the external measurements to the center of gravity displacement. The center of gravity displacement is however estimated within the full-order system, and

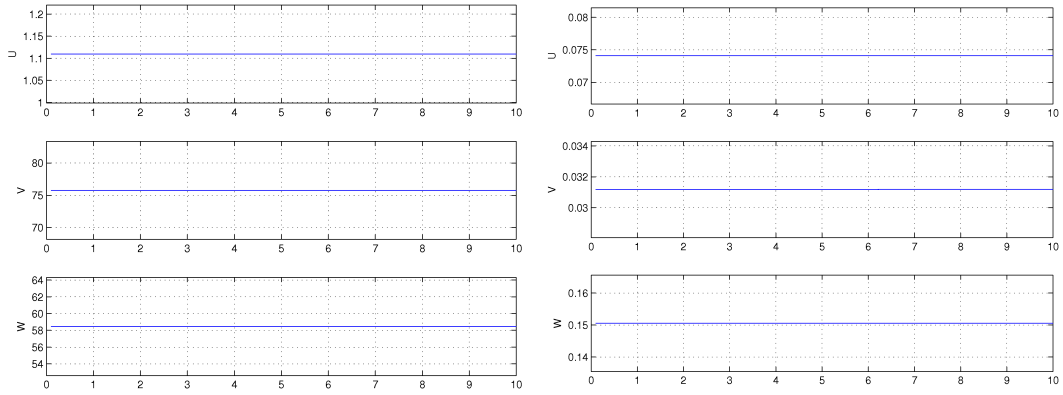

(a) position (b) velocity

Figure 4.6: Sensitivity curves from off-nominal initial center of gravity displacement uncertainty

occupies a three-element position vector. From this sensitivity analysis result, it may be prudent to remove the active estimation of the center of gravity displacement from the system.

Likewise, it has also been found that the uncertainty in the accelerometer scale factor and misalignment/nonorthogonality does not significantly affect system performance. Below are a pair of sensitivity curve plots which depict the uncertainty in position and velocity due to off-nominal values for initial uncertainty of accelerometer scale factor and misalignment/nonorthogonality. Whereas Fig. 4.7b shows a positive slope, the scale shows only a very slight increase in velocity uncertainty when the accelerometer scale factor and misalignment/nonorthogonality uncertainty is increased ten-fold. The scale of increased uncertainty is on the order of $0.01\,[\mathrm{m}]\,[\mathrm{s}]^{-1}$. There is no sensitivity of the position uncertainty to off-nominal values for accelerometer scale

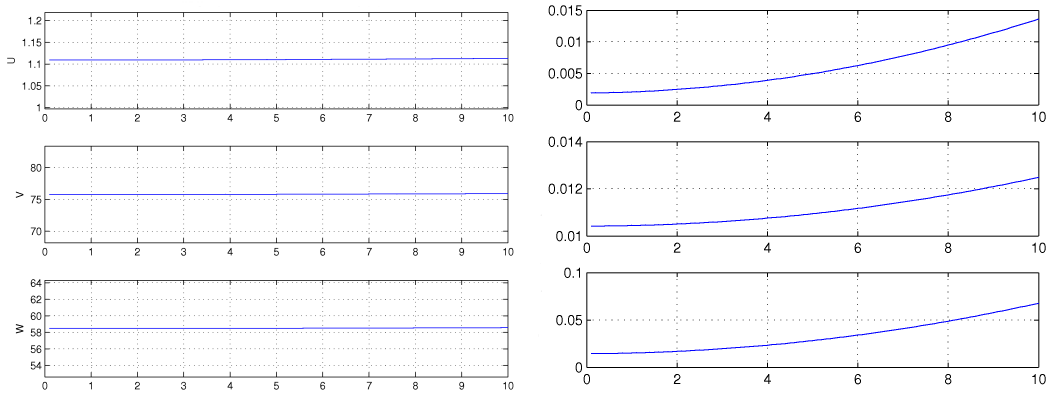

(a) position (b) velocity

Figure 4.7: Sensitivity curves from off-nominal initial accelerometer scale factor and misalignment/nonorthogonality uncertainty

factor and misalignment/nonorthogonality uncertainty. This result may be interpreted that the estimation of these parameters may be removed from the system. The accelerometer scale factor and misalignment/nonorthogonality parameters inhabit nine elements of the estimated state vector, and it may be prudent to remove their active estimation from the system with no appreciable impact to estimation performance while reducing computational burden.

Similarly, the system is largely insensitive to increased values of uncertainty in gyroscope scale factor and misalignment/ nonorthogonality parameters. Below are three sets of sensitivity curves which depict the uncertainty in position, velocity, and attitude from off-nominal values of initial uncertainty of gyroscope scale factor and misalignment/nonorthogonality parameters. Fig. 4.8b and Fig. 4.8c show a slight increase in velocity and attitude error, respectively, as the initial uncertainty in gyroscope scale factor

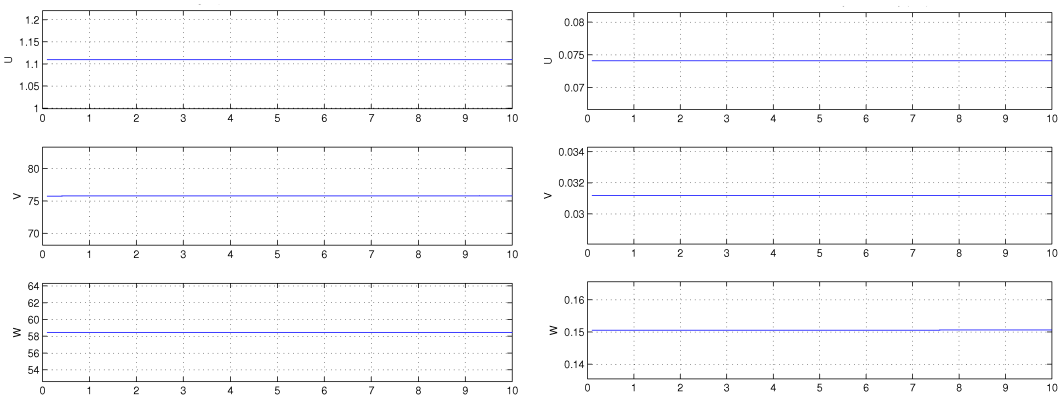

(a) position

(b) velocity

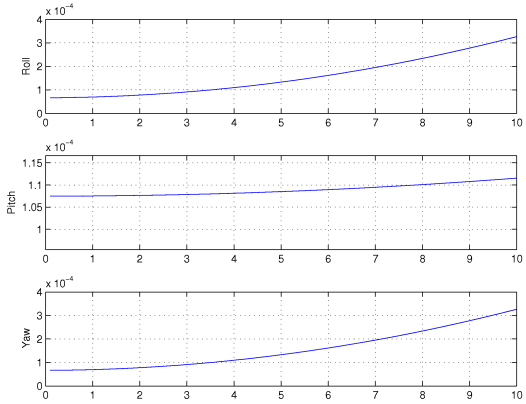

(c) attitude

Figure 4.8: Sensitivity curves from off-nominal initial gyroscope scale factor and misalignment/nonorthogonality uncertainty

and misalignment/nonorthogonality is increased ten-fold. However, the total increase in velocity and attitude uncertainty is on the order of 0.1 [m] $[s]^{-1}$, and 10 [arcsec], respectively. The gyroscope scale factor and misalignment/nonorthogonality parameters collectively occupy nine elements of the estimated state vector. The results of the sensitivity analysis suggest that it may be prudent to re-

move active estimation of these states to reduce the computational burden without significantly disturbing the estimation performance of the system.

The next section will describe the reduced model system which has removed active estimation of the center of gravity displacement, accelerometer scale factor and misalignment/nonorthogonality parameters, and gyroscope scale factor and misalignment/nonorthogonality parameters. That reduced model is analyzed and re-tuned for its best performance capability, and the reduced model estimation performance and computational time is then compared to that of the full-order system.

4.2 Reduced Model

The states which estimate the scale factor and nonorthogonality of the accelerometer and gyroscope were removed from the system. Additionally, the state that estimates the deviation of the position of the center of gravity with respect to the IMU has been removed. In all, this results in the removal of 21 state elements, reducing the length of the state vector from 49 state elements

to 28 state elements. The reduced state vector thus takes the form

$$\mathbf{x}(t) = \begin{bmatrix} \mathbf{r}_{imu}^{i} \\ \mathbf{v}_{imu}^{i} \\ \bar{\mathbf{q}}_{b}^{i} \\ \mathbf{b}_{acc} \\ \mathbf{b}_{gyro} \\ \phi_{map} \\ \theta_{map} \\ b_{alt} \\ \mathbf{b}_{vel} \\ \mathbf{b}_{sca} \\ \mathbf{b}_{tc} \end{bmatrix} \in \Re^{28\times 1} \tag{4.1}$$

The environment model of the vehicle IMU is still corrupted by scale factor and nonorthogonality, and the position of the center of gravity with respect to the IMU is still corrupted by a random deviation; the difference is that those error sources are no longer being actively estimated by the system. By not estimating their values, the system will behave differently unless proper tuning is utilized to re-capture the performance of the full-order system.

4.2.1 Dynamics

4.2.1.1 IMU modeling

The IMU is modeled as being corrupted by scale factor uncertainty and misalignment/nonorthogonality errors. The true acceleration as a function of the measured acceleration minus the error sources thus takes the form

$$\mathbf{a}_{ng} = \mathbf{a}_{ng,m} - \mathbf{N}(\mathbf{a}_{ng,m})\boldsymbol{\gamma}_a - \mathbf{D}(\mathbf{a}_{ng,m})\mathbf{s}_a - \mathbf{b}_a - \boldsymbol{\eta}_a \,.$$

However, the scale factor uncertainty and the misalignment/nonorthogonality parameters are not actively estimated. Rather, we assume their estimate to

be zero for all time and exclude their states from the state estimate vector. The estimated acceleration from an acceleration measurement can be written as

$$\hat{\mathbf{a}}_{ng} = \mathbf{a}_{ng,m} - \hat{\mathbf{b}}_a \,.$$

Similarly, the true angular velocity as a function of the measured value minus the error sources and the estimated angular velocity both take the form

$$\begin{aligned} \boldsymbol{\omega} &= \boldsymbol{\omega}_m - \mathbf{N}(\boldsymbol{\omega}_m)\boldsymbol{\gamma}_g - \mathbf{D}(\boldsymbol{\omega}_m)\mathbf{s}_g - \mathbf{b}_g - \boldsymbol{\eta}_g \\ \hat{\boldsymbol{\omega}} &= \boldsymbol{\omega}_m - \hat{\mathbf{b}_g} \,, \end{aligned}$$

respectively.

4.2.2 Thresholding

Since the estimated model for the accelerometer and gyroscope have now changed under the new reduced order system, it is now necessary to re-evaluate the thresholding process to mitigate the integration of IMU measurements comprised solely of error sources. For the accelerometer model, the deviation in non-gravitational acceleration will now take the form

$$\begin{aligned} \delta\mathbf{a}_{ng} &= \mathbf{a}_{ng} - \hat{\mathbf{a}}_{ng} \\ &= -\delta\mathbf{b}_a - \mathbf{N}(\mathbf{a}_{ng,m})\boldsymbol{\gamma}_a - \mathbf{D}(\mathbf{a}_{ng,m})\mathbf{s}_a - \mathbf{b}_a - \boldsymbol{\eta}_a \\ &= -\delta\mathbf{b}_a - \boldsymbol{\zeta}_a \,, \end{aligned}$$

where the augmented noise term $\boldsymbol{\zeta}_a$ takes the form

$$\boldsymbol{\zeta}_a = \mathbf{N}(\mathbf{a}_{ng,m})\boldsymbol{\gamma}_a + \mathbf{D}(\mathbf{a}_{ng,m})\mathbf{s}_a + \boldsymbol{\eta}_a \,.$$

Now, the acceleration covariance is defined as $\mathbf{P}_a = \mathrm{E}\left\{(\delta\mathbf{a}_n g)(\delta\mathbf{a}_n g)^{\mathrm{T}}\right\}$ and when written out, takes the form

$$\mathbf{P}_a = \mathbf{P}_{b_a} + \mathrm{E}\left\{(\boldsymbol{\zeta}_a)(\boldsymbol{\zeta}_a)^{\mathrm{T}}\right\} ,$$

where $\mathbf{P}_{b_a}$ takes the same form as in Eq. (3.121). Per the sensitivity analysis results, we may assume that the $\boldsymbol{\zeta}_a$ term is a small component of accelerometer error and may be neglected, so that the non-gravitational acceleration covariance may take the simple form

$$\mathbf{P}_a = \sigma_{b_a}^2 \mathbf{I}^{3\times 3} .$$

Recall that we defined $\mathbf{P}_a$ as a diagonal of variances as

$$\mathbf{P}_a = \begin{bmatrix} \sigma_{a,x}^2 & 0 & 0 \\ 0 & \sigma_{a,y}^2 & 0 \\ 0 & 0 & \sigma_{a,z}^2 \end{bmatrix} ,$$

where each term is

$$\begin{aligned} \sigma_{a,x}^2 &= \sigma_{b_a}^2 \\ \sigma_{a,y}^2 &= \sigma_{b_a}^2 \\ \sigma_{a,z}^2 &= \sigma_{b_a}^2 . \end{aligned}$$

Similarly, the angular velocity covariance may take a diagonal form, and each term of that diagonal may be written as

$$\begin{aligned} \sigma_{\omega,x}^2 &= \sigma_{b_a}^2 \\ \sigma_{\omega,y}^2 &= \sigma_{b_a}^2 \\ \sigma_{\omega,z}^2 &= \sigma_{b_a}^2 . \end{aligned}$$

The thresholding method is still implemented in the same manner. A tolerance band is created for each axis, so that if the inequality

$$\|\hat{a}_{ng,i}\| < n_a \sigma_{a,i}$$

holds true for a tolerance coefficient n_a per axis, then the estimated non-gravitational acceleration and the measured acceleration is set to zero. Likewise, if the inequality

$$\|\hat{\omega}_i\| < n_a \sigma_{\omega,i}$$

is true for a tolerance coefficient n_a for each axis, then the estimated angular velocity and measured angular velocity are set to zero.

4.3 Monte Carlo Analysis

The reduced-order system was tested for estimation performance using a monte carlo simulation. A monte carlo simulation is a numerical simulation that explores the different possibilities for simulation scenarios by assigning new values to each random variable for subsequent simulation runs. For the purpose of this analysis, the reduced system was simulated fifty times, each time with new values for each parameter and with a different sequence of random values for random noise parameters. Table 4.3 shows the different types of parameters that are re-assigned for each subsequent simulation.

The initial estimate in position, velocity, and attitude are randomly assigned within a Gaussian distributed field about the true initial position, velocity, and attitude. This will allow the analysis to explore the possible

Table 4.3: Parameters randomly assigned per simulation in monte carlo analysis

parameter	variable
intial estimate	$\hat{\mathbf{r}}$
	$\hat{\mathbf{v}}$
	$\hat{\bar{\mathbf{q}}}$
constants	$\mathbf{b}_{acc}$
	$\mathbf{b}_{gyro}$
	$\mathbf{b}_{alt}$
	$\mathbf{b}_{vel}$
	$\mathbf{b}_{sca}$
	$\mathbf{b}_{tc}$
noise	$\boldsymbol{\eta}_{acc}$
	$\boldsymbol{\eta}_{gyro}$
	$\boldsymbol{\eta}_{alt}$
	$\boldsymbol{\eta}_{sca}$
	$\boldsymbol{\eta}_{tc}$

outcomes that derive from different initial state estimates. It can test if the system is able to "recover" from a poor initial state estimate and provide an acceptable state estimation error. The random constants are system parameters such as IMU corruption sources and sensor biases. This will allow the monte carlo simulation to test how the system is able to handle varying qualities of measurements. Finally, the IMU and sensor noise random sequence is different for each simulation. Due to the acceptably large number of parameters that are altered between subsequent individual simulations, fifty simulations are enough to capture the statistical characteristics of the system as a whole. A higher number of simulations for the monte carlo analysis will not provide a significant change in the analysis results.

The simulation was run fifty times with new values for each and every parameter listed in Table 4.3 and the state estimation error and estimation error covariance were saved for the analysis. At every time step, the state estimate error variance is found across every simulation for each state estimate element. This will create a time-history of the sampled state estimate variance, which can be compared to the nominal navigation system estimate error covariance. A "tuned" navigation filter will have an estimation error covariance time-history that closely matches an error sample variance time-history. This means that the filter covariance closely models the uncertainties present in the system. The resulting monte carlo simulation plots are available in Fig. 4.9 for position, velocity, attitude, and map-tie angle error. The remaining plots for system biases and other error sources may be found in Appendix B.

The navigation filter error covariance time-history is shown in red, while the sampled estimation error variance from the monte carlo analysis is shown in black dots. The position and velocity plots are oriented into the *uvw* frame for a more readily-interpreted plot. The altimeter is active in the "up" direction, which is evidenced by the reduction of position estimation error and error covariance in the first channel at the altimeter activation time. Secondarily to the first channel, the position error in the second channel or along-track direction is reduced at altimeter activation. The reductions in velocity error and error covariance are mirrored in the first two channels at altimeter activation. The estimation error and error covariance are further reduced in every channel of position and velocity when the terrain camera is activated. The

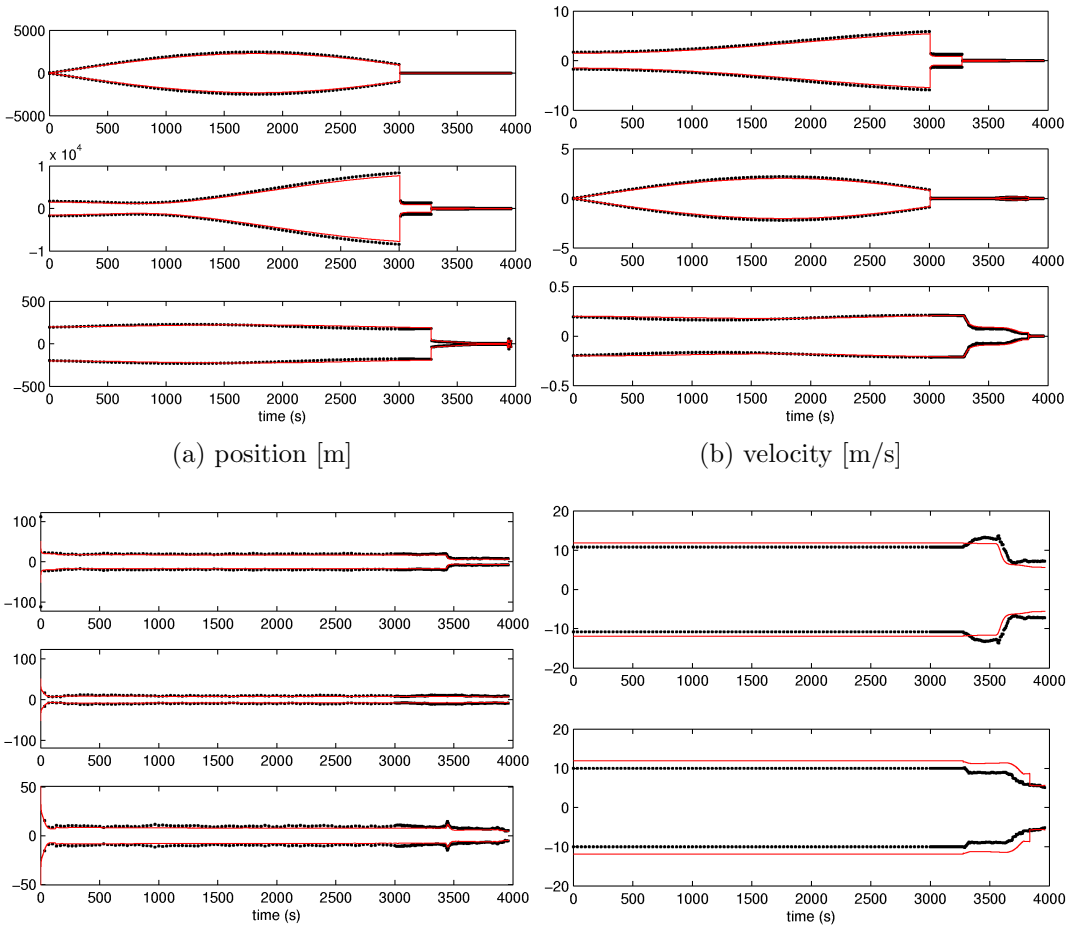

(a) position [m]

(b) velocity [m/s]

(c) attitude [arcsec]

(d) map-tie [arcsec]

Figure 4.9: Error variance and navigation filter covariance from reduced-order monte carlo analysis

attitude estimation error and covariance are reduced from their initial values as the star camera is active throughout the entire simulation and are further reduced when the terrain camera becomes active.

An important estimation performance indicator in this simulation is

the end-time uncertainty of position, velocity, attitude, and map-tie angle. This will dictate the precision of the knowledge of the physical state of the spacecraft with respect to the landing site, and can be the difference between a successful or failed landing. Recall that the position and velocity monte carlo plots are oriented in the *uvw* frame. Near the end-time of the simulation the vehicle enters a terminal descent which is a nearly vertical trajectory with respect to the center of the Moon. This creates a poorly-defined *uvw* frame, as evidenced by the small sudden increase in estimation error covariance and sample variance immediately before the end-time. This is a mathematical issue and not the result of actual increased uncertainty. Therefore the end-time position and velocity uncertainty may be assumed to be at least the value of the uncertainty preceding the dissolution of the *uvw* frame.

Under this assumption, the $1-\sigma$ position uncertainty as defined by the estimation error variance at the end-time is 0.50 [m], 37.9 [m], and 6.02 [m] in the u, v, and w directions, respectively. Again, there is a dissolution of the *uvw* frame at the terminal descent as the lander is moving in a purely vertical direction. Therefore the uncertainty is taken immediately before this dissolution.

The terminal velocity $1-\sigma$ uncertainty is $0.000844\,[\mathrm{m}]\,[\mathrm{s}]^{-1}$, $0.003017\,[\mathrm{m}]\,[\mathrm{s}]^{-1}$, and $0.00259\,[\mathrm{m}]\,[\mathrm{s}]^{-1}$ in the u, v, and w directions, respectively. The use of the surface-relative velocimeter aids in precision knowledge of the vehicle velocity. The vehicle attitude $1-\sigma$ uncertainty at the landing time is 7.974 [arcsec], 9.225 [arcsec], and 5.378 [arcsec] in the roll, pitch, and yaw directions, respec-

tively.

The shape of the filter covariance time-history of the reduced-order filter in Fig. 4.9 closely agrees with the nominal filter covariance time-history of the full-order filter depicted in the error budget reconstruction in Fig. 4.4. This means the reduced-order filter is providing comparable estimation accuracy and is successfully modeling the uncertainty dynamics.

4.3.1 Computational Comparison

The reduced-order system and the full-order system were profiled during their respective monte carlo simulations. This provides a workable average for the computer run-time for each individual run. While the computer run-time is obviously dependent upon the power of the machine in which the simulation takes place, it is acceptable to assume that the percentage decrease in computer run-time would be similar across all machines.

After several monte carlo simulations of the full-order system on a mid-range PC laptop, fifty individual runs would clock in at approximately 18000 [sec]. Alternatively, monte carlo simulations of the reduced-order system would clock in at approximately 5500 [sec] for fifty individual simulations. This amounts to a substantial 67.56% decrease in computer run-time.

The dramatic reduction in computational burden is attributed to the smaller scale of matrix calculations performed in the propagation stage of the navigation algorithm. Recall that the estimation error covariance is propa-

gated forward in time via Eq. (3.81) as

$$\mathbf{P}(t_k) = \mathbf{\Phi}(t_k, t_{k-1})\mathbf{P}(t_{k-1})\mathbf{\Phi}^{\mathrm{T}}(t_k, t_{k-1}) + \mathbf{Q}(t_k)\,,$$

and the matrices $\mathbf{\Phi}(t_k, t_{k-1})$ and $\mathbf{Q}(t_k)$ are found through numerical integration of Eq. (3.77)

$$\begin{aligned}\dot{\mathbf{\Phi}}(t, t_{k-1}) &= \mathbf{F}(\hat{\mathbf{x}}(t), t)\mathbf{\Phi}(t, t_{k-1}) \\ \dot{\mathbf{Q}}(t) &= \mathbf{F}(\hat{\mathbf{x}}(t), t)\mathbf{Q}(t) + \mathbf{Q}(t)\mathbf{F}^{\mathrm{T}}(\hat{\mathbf{x}}(t), t) + \mathbf{M}(t)\mathbf{Q}_{spec}(\tau)\mathbf{M}^{\mathrm{T}}(t)\,.\end{aligned}$$

The matrices $\mathbf{\Phi}(t_k, t_{k-1})$ and $\mathbf{Q}(t_k)$ are now square matrices with 28 rows and columns, down from 48. The reduced-order $\mathbf{\Phi}(t_k, t_{k-1})$ and $\mathbf{Q}(t_k)$ matrices have 65.97% fewer elements than the full-order $\mathbf{\Phi}(t_k, t_{k-1})$ and $\mathbf{Q}(t_k)$ matrices, which closely mirrors the reduction in run-time of the reduced-order system. This result makes intuitive sense as the number of matrix calculations is proportional to the square of the dimension of the matrices.

Chapter 5

Conclusions

5.1 Summary

An optimal navigation system with respect to the mathematical model of the physical process was developed and has been described. The mathematical models of the lunar environment, the accelerometer measurements, and the gyroscope measurements are described in Chapter 2. Also in Chapter 2 are the mathematical models of the error dynamics of the non-gravitational acceleration and vehicle angular velocity. The mathematical models of the external sensors are described in Chapter 3, along with their respective sensitivities to deviations in the state of the spacecraft. The "heart" of the navigation algorithm, the Extended Kalman Filter, is derived and the pertinent structure which utilizes the models for the inertial measurement unit, external sensors, and Lunar environment is described in Chapter 3. This results in the optimal navigation system, which is the subject of a sensitivity analysis in Chapter 4. The results of the sensitivity analysis dictate the acceptable route to simplify the navigation system without adversely affecting the estimation performance, and a reduced system is presented in Chapter 4.

The reduced order system is analyzed for important differences in the

mathematical model for non-gravitational acceleration and angular velocity. A monte carlo analysis of the full-order system and reduced system is executed, and the results are compared for estimation performance. It was found that the estimation performance of the reduced-order system closely matches that of the full-order system, and at a fraction of the computer run-time. It was found that the reduced-order system is able to execute navigation along the same nominal path as the full-order system about three times as quickly. This was accomplished by reducing the accelerometer and gyroscope scale-factor error and misalignment/nonorthogonality parameters into an expanded noise term which is not considered in estimation. To a lesser degree, the reduction of the center-of-gravity displacement from active estimation assisted in "streamlining" the system.

5.2 Future Work

The reduced-order model works with the same mathematical models of the lunar environment, sensor measurements, and sensor measurement sensitivities as the full-order system. It may still be desirable to increase the fidelity of the navigation algorithm by introducing more complex mathematical models for each of these physical systems. The navigation system currently assumes a point-mass gravitational field which may be upgraded to an interpolated gravitational field grid or a gravity potential defined by spherical harmonics. Secondly, the lunar topography may be modeled by an interpolation of values upon a digital elevation map (DEM) to provide greater fidelity with measure-

ments from the altimeter and terrain camera. The lunar topography may also be modeled with spherical harmonics, with similar results arising from measurements by an altimeter or terrain camera.

The navigation algorithm is highly-customizable, and it may be worth investigating the sensor activation scheme to find a schedule that results in higher estimation performance without sacrificing computational burden. For example, under the external sensor schedule used in this thesis the star camera is active through the entire trajectory, but the altimeter activates at an altitude of 2000 [m]. The altimeter could be activated earlier to capture the position and velocity in the "up" direction, and perhaps when coupled with a modeled topography more information could be utilized, resulting in an increase of certainty in position in all three axes.

Finally, there may be additional mathematical aids to be utilized to reinforce the robustness of the navigation system. Currently, there is thresholding and underweighting. To recap, thresholding mitigates the integration of erroneous estimated non-gravitational acceleration and angular velocity. Underweighting mitigates violating linearity constraints in a state estimate update at a time of high uncertainty when an accurate measurement becomes available. An additional mathematical aid to assist the navigation system not addressed in this thesis is residual editing. Residual editing flags measurements with exceptionally high noise contributions and omits those measurements from the state estimate update. It mitigates an erroneous update from a noisy measurement.

Appendices

Appendix A

Mathematical Notions and Notations

A.1 Mathematical Notations

There are several notations used throughout the thesis that may require some explanation. For clarity:

- Vector quantities are given in a lowercase, bold format as $\mathbf{r}$ or $\boldsymbol{\gamma}$
- Matrix quantities are given in an uppercase, bold format as $\mathbf{R}$ or $\boldsymbol{\Gamma}$
- Scalar quantities are given by either uppercase or lowercase, non-bold format as r or γ
- The quaternion is made of a scalar and vector part, written under the definitions given above. A quaternion is referred to by a bold lowercase letter with an overbar. A quaternion is therefore written by

$$\bar{\mathbf{q}} = \begin{bmatrix} q \\ \mathbf{q} \end{bmatrix}$$

A vector or matrix magnitude (taken as the two-norm) is denoted by $\|\mathbf{A}\|$ or $\|\mathbf{a}\|$. The expected value of a random variable is given by $\mathrm{E}\{x\}$. The covariance of a vector random variable is given by $\mathrm{E}\left\{\mathbf{x}\mathbf{x}^{\mathrm{T}}\right\}$.

The dimensions of matrices may be found as a superscript such as $\mathbf{M}^{n\times m}$ which means matrix $\mathbf{M}$ has n-rows and m-columns. Subscripts on a matrix refer to what the matrix is associated with, so that $\mathbf{H}_{alt}$ is the sensitivity matrix associated with the altimeter.

The Dirac Delta function is defined as

$$f(\tau) = \int_{-\infty}^{\infty} f(t)\delta(t-\tau)d\tau\,,$$

and is displayed as $\delta(t-\tau)$. The Dirac Delta function is zero for all $t \neq \tau$. It is used in the definitions of random variable covariances. Another mathematical term used heavily in this thesis is the skew-symmetric cross matrix. A three-element vector $\mathbf{a}$ is written as a skew-symmetric cross matrix as $[\mathbf{a}\times]$ and is defined by

$$[\mathbf{a}\times] = \begin{bmatrix} 0 & -a_3 & a_2 \\ a_3 & 0 & -a_1 \\ -a_2 & a_1 & 0 \end{bmatrix}\,,$$

The skew-symmetric cross matrix is used to emulate the cross-product of two vectors as

$$\mathbf{a}\times\mathbf{b} = [\mathbf{a}\times]\mathbf{b}\,.$$

The skew-symmetric cross matrix may therefore be used in absence of a vector to be crossed into. It is used particularly in defining external sensor measurement sensitivities.

More general mathematical notations may be listed as

– The transpose of a vector or matrix is denoted with a superscript "T", while the inverse is denoted as a superscript "−1" as $\mathbf{a}^{\mathrm{T}}$ or $\mathbf{a}^{-1}$.

– The *a priori* and *a posteriori* values for a given time are denoted with superscripts "-" and "+", respectively, as in state estimate values before and immediately after a state estimate update

– The hat accent and dot accent represent an estimated or expected value and the time rate of change of a value, respectively. It is displayed as $\hat{\mathbf{a}}$ for the estimated value of $\mathbf{a}$ and $\dot{\mathbf{a}}$ for the time rate of change of $\mathbf{a}$. Additionally, $\dot{\hat{a}}$ is the time rate of change of the estimated value of $\mathbf{a}$

– A value oriented in a particular reference frame will have its reference frame indicator in the subscript. A rotation matrix which transfers from one frame to another is read as rotating from the frame in the subscript to the frame in the superscript. Therefore $\mathbf{r}_i$ is a position in the inertial frame, and $\mathbf{T}_i^b\mathbf{r}_i$ is a rotation matrix which will map that position in the inertial frame to the body frame. Quaternions of rotation are read in the same way so $\bar{\mathbf{q}}_i^b$ is a quaternion which rotates the inertial frame into the body frame

A.2 Quaternion Mathematics and Attitude Representations

The quaternion of rotation is an attitude representation that is used heavily throughout this thesis in concert with the Euler rotation matrix. The

quaternion is commonly considered superior to the Euler rotation matrix because i)it is defined by four elements versus nine, which results in fewer calculations for procedures such as attitude propagation and ii) it is unable to fall victim to singularities which may exist within certain attitude orientations, colloquially known as "gimbal lock". There are many attitude representations available, more details may be found in Shuster [10], Phillips *et. al.* [17], or Altmann [16].

The quaternion of rotation is defined as

$$\bar{\mathbf{q}} = \begin{bmatrix} q \\ \mathbf{q} \end{bmatrix} ,$$

where q and $\mathbf{q}$ are the Euler-Rodriguez symmetric parameters and take the form

$$\begin{aligned} q &= \cos\frac{\theta}{2} \\ \mathbf{q} &= \sin\frac{\theta}{2}\mathbf{e} \,. \end{aligned}$$

The values θ and $\mathbf{e}$ are the angle and axis of rotation, respectively. The quaternion of rotation must conform to a unity constraint to be a pure rotation such that

$$\|\bar{\mathbf{q}}\| = \sqrt{q + \mathbf{q}^{\mathrm{T}}\mathbf{q}} = 1 \,.$$

Subsequent rotations are executed with the quaternion multiplication operator. Quaternions of rotation are multiplied via

$$\bar{\mathbf{a}} \otimes \bar{\mathbf{b}} = \begin{bmatrix} a \\ \mathbf{a} \end{bmatrix} \otimes \begin{bmatrix} b \\ \mathbf{b} \end{bmatrix} = \begin{bmatrix} ab - \mathbf{a}^{\mathrm{T}}\mathbf{b} \\ \mathbf{a}b + b\mathbf{a} - \mathbf{a} \times \mathbf{b} \end{bmatrix} ,$$

In the formulation within this thesis, the attitude estimation error is found via a multiplicative approach. The attitude estimation error may be assumed to be a small rotation so that it may be written as

$$\bar{\mathbf{q}} \otimes \hat{\bar{\mathbf{q}}}^{-1} = \delta\bar{\mathbf{q}} = \begin{bmatrix} \delta q \\ \delta\mathbf{q} \end{bmatrix} = \begin{bmatrix} 1 \\ \frac{1}{2}\delta\boldsymbol{\alpha} \end{bmatrix} ,$$

where $\delta\boldsymbol{\alpha}$ is a vector of small angles errors in roll, pitch, and yaw.

A.2.1 The Euler Rotation Matrix

Another attitude representation utilized is the Euler equation for a rotation matrix. It may be defined from the quaternion of rotation as

$$\mathbf{T}(\bar{\mathbf{q}}) = \left[\left(q^2 + \mathbf{q}^{\mathrm{T}}\mathbf{q}\right)\mathbf{I}^{3\times 3} - 2q[\mathbf{q}\times] + 2[\mathbf{q}\times]^2\right] ,$$

The rotation matrix is utilized in the calculations in this thesis primarily of equations determining sensor measurement values and measurement. Like the quaternion of rotation it must conform to a unity norm constraint to remain a pure rotation operation. We may apply the definition of $\delta\bar{\mathbf{q}}$ to the above equation to realize a rotation matrix that approximates a small rotation to first order in $\delta\boldsymbol{\alpha}$ as

$$\delta\mathbf{T} = \mathbf{I}^{3\times 3} - [\boldsymbol{\alpha}\times] .$$

The error in attitude may also be found through a multiplicative approach of the rotation matrices as

$$\delta\mathbf{T}_i^b = \mathbf{T}_i^b\hat{\mathbf{T}}_i^{b^{-1}} ,$$

so that when the previous two equation are combined we will have

$$\mathbf{T}_i^b \hat{\mathbf{T}}_i^{b^{-1}} = \mathbf{I}^{3\times 3} - [\boldsymbol{\alpha}\times]\,,$$

We may now post-multiply both sides of this equation by $\hat{\mathbf{T}}_i^b$ to acquire

$$\mathbf{T}_i^b = \hat{\mathbf{T}}_i^b - [\boldsymbol{\alpha}\times]\hat{\mathbf{T}}_i^b\,.$$

This equation is thusly inverted to arrive at the rotation from the vehicle body frame to the inertial frame in terms of the estimated rotation and the deviation in attitude as

$$\mathbf{T}_b^i = \hat{\mathbf{T}}_b^i + [\boldsymbol{\alpha}\times]\hat{\mathbf{T}}_b^i\,.$$

Appendix B

Monte Carlo Analysis Results Plots

In this appendix, the "miscellaneous" monte carlo analysis results are presented. They include all the estimated state elements outside the physical states of position, velocity, attitude, and map-tie angle error.

For the reduced system, the plots presented here are accelerometer bias, gyroscope bias, altimeter bias, star camera bias, terrain camera bias, and velocimeter bias.

In these figures, the red line represents a nominal filter estimation error covariance, and the black dots represent the sampled error variance from a 50-run monte carlo analysis.

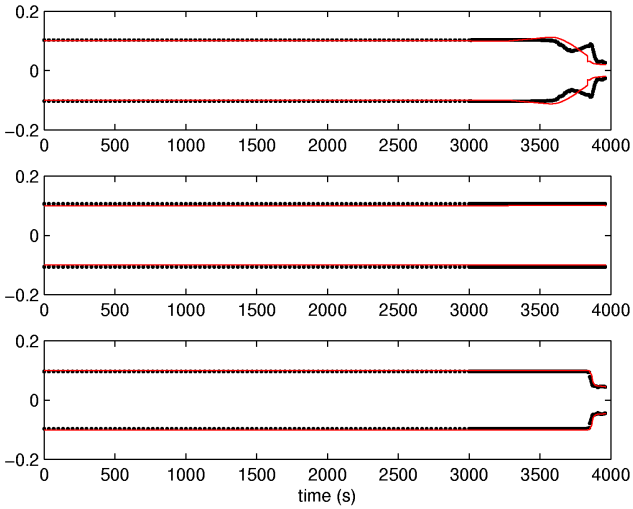

Figure B.1: accelerometer bias [mg]

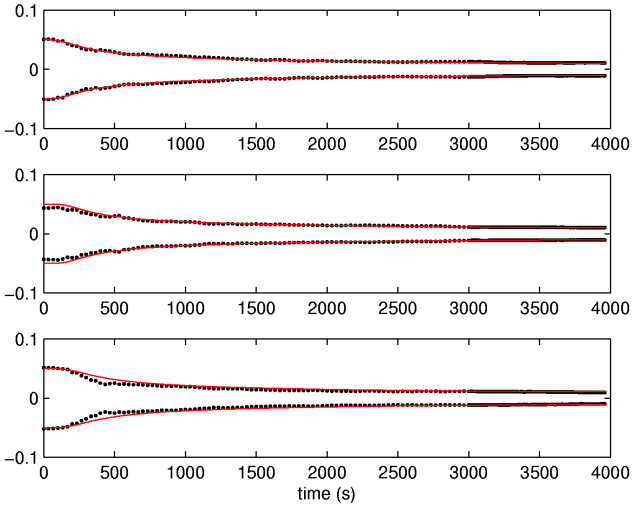

Figure B.2: gyroscope bias, [deg/hr]

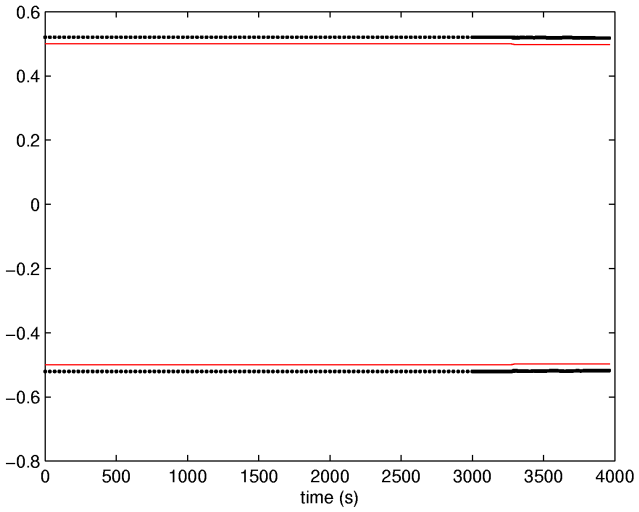

Figure B.3: altimeter bias, [m]

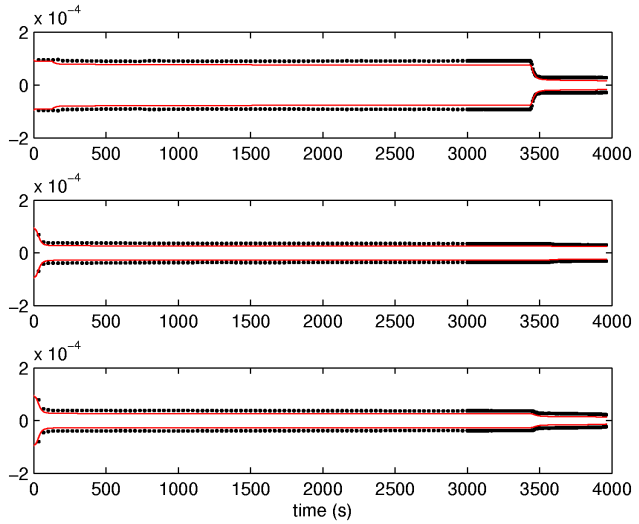

Figure B.4: star camera bias, [rad]

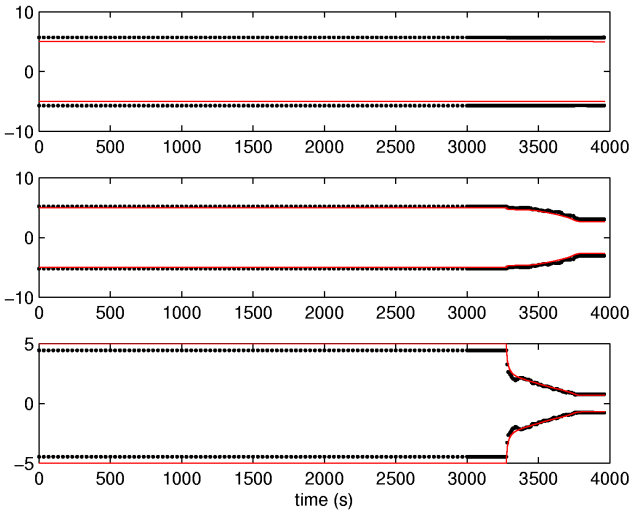

Figure B.5: terrain camera bias, [m]

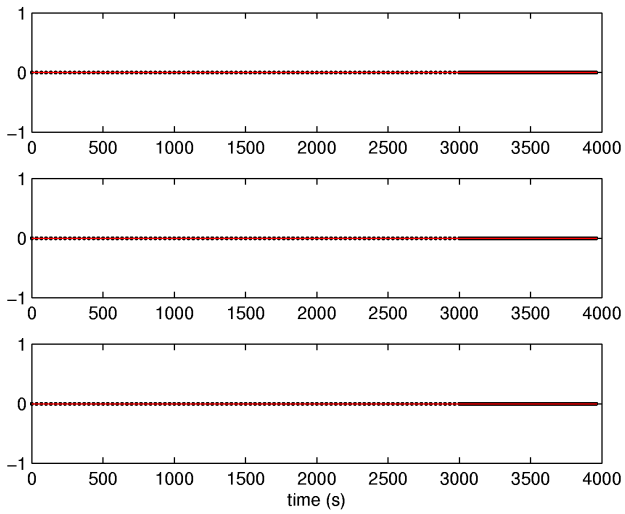

Figure B.6: velocimeter bias, [m/s]

Bibliography

[1] NASA- Exploration Systems Mission Directorate. Available at: `http://www.nasa.gov/exploration/home/index.html`.

[2] Arthur Gelb, editor. *Applied Optimal Estimation*. The MIT Press, Cambridge, MA, 1974.

[3] Byron D. Tapley, Bob E. Schutz, and George H. Born. *Statistical Orbit Determination*. Elselvier Academic Press, New York, NY, 2004.

[4] John L. Crassidis and John L. Junkins. *Optimal Estimation of Dynamic Systems*. CRC Press, New York, NY, 2004.

[5] Kenneth R. Britting. *Inertial Navigation Systems Analysis*. John Wiley & Sons, New York, NY, 1971.

[6] Kyle J. DeMars. Technical Memo: Thresholding, 2007.

[7] Kyle J. DeMars. Technical Memo: Measurement Underweighting in the Extended Kalman Filter, 2009.

[8] Kyle J. DeMars and Robert H. Bishop. Navigation Analysis to Facilitate Precision Descent Navigation for Landing at the Moon. AAS/AIAA Astrodynamics Specialist Conference, August 2007.

[9] Kyle Jordan DeMars. Precision Navigation for Lunar Descent and Landing. Master's thesis, The University of Texas at Austin, 2007.

[10] Malcolm D. Shuster. A Survey of Attitude Representations. *The Journal of the Astronautical Sciences*, 41(4):439–517, 1993.

[11] Marshall H. Kaplan. *Modern Spacecraft Dynamics & Control*. John Wiley & Sons, New York, NY, 1976.

[12] Peter C. Hughes. *Spacecraft Attitude Dynamics*. John Wiley & Sons, New York, NY, 1986.

[13] Peter Lancaster. *Theory of Matrices*. Academic Press, New York, NY, 1969.

[14] Peter S. Maybeck. *Stochastic Models, Estimation, and Control*, volume 1. Academic Press, 1979.

[15] Roger R. Bate, Donald D. Mueller, and Jerry E. White. *Fundamentals of Astrodynamics*. Dover Publications, New York, NY, 1971.

[16] Simon L. Altmann. *Rotations, Quaternions, and Double Groups*. Dover Publications, Inc., 1986.

[17] W.F. Phillips, C.E. Hailey, and G.A. Gebert. Review of Attitude Representations Used for Aircraft Kinematics. *Journal of Aircraft*, 38(4):718–737, July–August 2001.

[18] Wilson J. Rugh. *Linear System Theory.* Prentice Hall, Upper Saddle River, NJ, 2nd edition, 1996.

[19] Wolfgang Torge. *Geodesy.* Walter de Gruyter, Berlin, 3rd edition, 2001.

Vita

Clark Patrick Newman was born on July 19, 1983, the son of Kathryn Elaine Newman and Roger Clarke Newman, and raised in Houston, Texas. He graduated from Jersey Village High School in May 2002, and entered the University of Texas at Austin in the fall of 2002. From the winter through summer of 2006, Clark worked at the Satellite Development Center of Boeing, inc. in El Segundo, CA. He received his Bachelor of Science in Aerospace Engineering in May of 2007. In September of 2007 he entered Graduate School at the University of Texas at Austin for Aerospace Engineering in the fall of 2007.

Permanent address: 9606 E. Withers Way // Houston, TX 77065

This thesis was typeset with LaTeX[†] by the author.

[†]LaTeX is a document preparation system developed by Leslie Lamport as a special version of Donald Knuth's TeX Program.